



2015

JOINT FORMATION UNDER SEVERELY ALTERED BACKGROUND ATMOSPHERE IN CONTROLLED ATMOSPHERE BRAZING OF ALUMINUM

Cheng-Nien Yu

University of Kentucky, chengnien.yu@gmail.com

[Click here to let us know how access to this document benefits you.](#)

Recommended Citation

Yu, Cheng-Nien, "JOINT FORMATION UNDER SEVERELY ALTERED BACKGROUND ATMOSPHERE IN CONTROLLED ATMOSPHERE BRAZING OF ALUMINUM" (2015). *Theses and Dissertations--Mechanical Engineering*. 67.
https://uknowledge.uky.edu/me_etds/67

This Master's Thesis is brought to you for free and open access by the Mechanical Engineering at UKnowledge. It has been accepted for inclusion in Theses and Dissertations--Mechanical Engineering by an authorized administrator of UKnowledge. For more information, please contact UKnowledge@lsv.uky.edu.

STUDENT AGREEMENT:

I represent that my thesis or dissertation and abstract are my original work. Proper attribution has been given to all outside sources. I understand that I am solely responsible for obtaining any needed copyright permissions. I have obtained needed written permission statement(s) from the owner(s) of each third-party copyrighted matter to be included in my work, allowing electronic distribution (if such use is not permitted by the fair use doctrine) which will be submitted to UKnowledge as Additional File.

I hereby grant to The University of Kentucky and its agents the irrevocable, non-exclusive, and royalty-free license to archive and make accessible my work in whole or in part in all forms of media, now or hereafter known. I agree that the document mentioned above may be made available immediately for worldwide access unless an embargo applies.

I retain all other ownership rights to the copyright of my work. I also retain the right to use in future works (such as articles or books) all or part of my work. I understand that I am free to register the copyright to my work.

REVIEW, APPROVAL AND ACCEPTANCE

The document mentioned above has been reviewed and accepted by the student's advisor, on behalf of the advisory committee, and by the Director of Graduate Studies (DGS), on behalf of the program; we verify that this is the final, approved version of the student's thesis including all changes required by the advisory committee. The undersigned agree to abide by the statements above.

Cheng-Nien Yu, Student

Dr. Dusan P. Sekulic, Major Professor

Dr. Haluk E. Karaca, Director of Graduate Studies

JOINT FORMATION UNDER SEVERELY ALTERED BACKGROUND
ATMOSPHERE IN CONTROLLED ATMOSPHERE BRAZING OF ALUMINUM

THESIS

A thesis submitted in partial fulfillment of the
requirements for the degree of
Master of Science in Mechanical Engineering
in the College of Engineering at the University of Kentucky

By

Cheng-Nien Yu

Lexington, Kentucky

Director: Dr. Dusan P. Sekulic, Professor of University of Kentucky

Lexington, Kentucky

2015

Copyright © Cheng-Nien Yu 2015

ABSTRACT OF THESIS

JOINT FORMATION UNDER SEVERELY ALTERED BACKGROUND ATMOSPHERE IN CONTROLLED ATMOSPHERE BRAZING OF ALUMINUM

Adverse changes of background atmosphere in a brazing chamber cause qualitative and quantitative deterioration of joint formation in an aluminum brazing process. This study offers an insight into the adverse effects with gradually adjusted atmospheric conditions in terms of oxygen and humidity levels. Corresponding responses of the molten clad flow and the joint formation upon resolidification vs. atmospheric conditions are documented by comparative tests involving self-fluxing and surface-fluxing brazing sheets: 1) in situ and in real time study of the onset of melting, clad flow, and joint formation, and 2) inclined wedge-tee mating tests for brazeability assessment. The surface-fluxing brazing sheet in series of tests was covered with potassium fluoroaluminate flux, while the self-fluxing brazing sheet with the composite material was executed without extra flux addition. Typical outcomes of joint formation under adverse atmosphere including smaller joint size, non-uniform joint formation, in-completed joining area, and no joint formation were documented. Transitional behavior of deteriorating joint formation is observed in increasing oxygen and humidity levels. The self-fluxing material demonstrated a remarkable resilience against an adverse atmospheric impact comparing to the surface-fluxing material.

KEY WORDS: Joint Formation, Atmospheric Impact, Controlled Atmosphere Brazing,
Brazeability, Aluminum Brazing

Cheng-Nien Yu

11/16/2015

JOINT FORMATION UNDER SEVERELY ALTERED BACKGROUND
ATMOSPHERE IN CONTROLLED ATMOSPHERE BRAZING OF ALUMINUM

By

Cheng-Nien Yu

Dr. Dusan P. Sekulic

Director of Thesis

Dr. Haluk E. Karaca

Director of Graduate Studies

11/16/2015

Date

I DEDICATE THIS THESIS TO MY FAMILY

CHING-CHUAN YU

CHU-HUA HO

ANITA CHIA-LING YU

PEI-LING YU

YOUR ENDLESS LOVE AND ENCOURAGEMENT HAVE BEEN
THE GREATEST SUPPORT TO ME

ACKNOWLEDGEMENTS

I would like to express my sincere gratitude to my advisor Dr. Dusan P. Sekulic for his guidance and support with great patience throughout my graduate study. I am grateful and honored to have you as my mentor.

Additionally, I would like to thank my thesis committees: Dr. Kozo Saito and Dr. Yu Ming Zhang for your time and efforts on advising me during the defense.

Thank Dr. Doug K. Hawksworth for giving me the opportunities of research collaboration. Your suggestions and technical insights have been always instructive and helpful to me. It is a privilege and a great pleasure working with you.

I would like to express my earnest appreciation to Ms. Peizhen Li. Your continuous support and encouragement over the years have been invaluable and essential to the completion of this thesis.

I would like to thank Dr. Wen Liu and other members in the lab for your advices and assistance throughout my path on research.

Thank Mr. Charles Arvin for his professional support. He was really kind and helpful. His professional dedication and kindness had been the leading exemplar and will be always remembered.

TABLE OF CONTENTS

ACKNOWLEDGEMENTS	iii
LIST OF TABLES	vi
LIST OF FIGURES	vii
CHAPTER 1: Introduction	1
1.1 Motivation	1
1.2 Brazing	1
1.3 Aluminum Furnace Brazing	2
1.4 Surface Oxidation	4
1.5 Flux	7
1.6 Impact of Atmosphere on Brazeability	11
1.7 Self-Fluxing Material	14
1.8 Hypothesis	16
CHAPTER 2: Experimental Setup and Materials Characterization	17
2.1 Hotstage Experiments	17
2.1.1 Hotstage Microscopy Test	17
2.1.2 Sample Preparation for a Hotstage Test	20
2.1.3 Atmosphere Condition in the Hotstage Chamber	22
2.1.4 Verification of Atmosphere Condition	23
2.1.5 Brazing Temperature History	23
2.2 Furnace Experiments	25
2.2.1 Transparent Controlled Atmosphere Brazing Furnace Test	25
2.2.2 Sample Preparation for a Furnace Test	30
2.2.3 Atmosphere Condition in the Furnace Chamber	33
2.2.4 Verification of the Measurement	34
2.2.5 Brazing Temperature History	37
2.3 Material Characterization	38
2.3.1 Verification for Uniformity of Brazing Sheets	38
2.3.2 SEM/EDS Verification for Materials	41
CHAPTER 3: Result and Discussion – Hotstage Experiments	44
3.1 Results of Hotstage Experiments	44
3.2 Image Sequence for Clad Surface Features during a Brazing Process	53
3.3 Macroscopic Features of Joint Formation	64
3.4 Microscopic Features of Joint Formation	75
CHAPTER 4: Results and Discussion – Furnace Experiments	83
4.1 Brazeability Criteria	83
4.2 Results of Furnace Experiments	87
4.3 Brazeability vs. Atmospheric Conditions	115
CHAPTER 5: Conclusion and Future Work	117

5.1 Conclusion..... 117
5.2 Future Work 118
APPENDICES 119
Appendix A..... 119
Appendix B 120
Appendix C 121
Appendix D..... 123
REFERENCES 125
VITA..... 129

LIST OF TABLES

Table 2-1	Result of Calibration.....	36
Table 2-2	Clad and Sheet Thicknesses of the Traditional and Trillium™ Brazing Sheets	41
Table 2-3	Summary of the Measurement in Table 2-2.....	41
Table 3-1	Descriptive Visual Characterizations	45
Table 3-2	Summary of Hotstage Experiments.....	46
Table 4-1	Brazeability Criteria	84
Table 4-2	Test Results of Brazed Samples	87
Table 4-3	Brazeability Symbols.....	115
Table 5-1	Limits for Favorable Combined Background Atmosphere Conditions.....	118

LIST OF FIGURES

Figure 1-1	Natural Surface Layer on Aluminum Materials (Zahr et al., 2012b).....	5
Figure 1-2	SEM of Aluminum Oxide Films: 4 nm (left) and 295 nm (right) (Kawase and Yamaguchi, 1980)	5
Figure 1-3	Mechanism of the mechanical surface activation (Zahr et al., 2011)	6
Figure 1-4	Patterns of Flux Coverage (Narayanaswamy, 2006).....	10
Figure 1-5	Changes in Fillet Formability with Oxygen Content for various Flux Content (Takemoto et al., 1996)	12
Figure 1-6	Relation between Oxide Film Thickness and Wettability (Kawase and Yamaguchi, 1980)	13
Figure 1-7	Relation between Brazeability and Atmosphere Concentrations of O ₂ and H ₂ O (Stenqvist et al., 1994, Claesson et al., 1995)	14
Figure 1-8	Relation between Oxide Film Thickness and Wettability (Yu et al., 2013)	16
Figure 2-1	Hotstage Microscopy Components	18
Figure 2-2	Silver Block Module	19
Figure 2-3	Cover Lid Assembly	20
Figure 2-4	Hotstage Microscopy System.....	20
Figure 2-5	Sample Configurations for a Hotstage Experiment	22
Figure 2-6	Temperature History of the Hotstage Brazing Process	24
Figure 2-7	Brazing in Process within the Hotstage	24
Figure 2-8	Layout of Transparent CAB Furnace	25
Figure 2-9	Controlling and Monitoring Units of CAB Furnace	26
Figure 2-10	Chilled Mirror Sensor Diagram (GE, 2006)	28
Figure 2-11	Image of Chilled Mirror Unit.....	29
Figure 2-12	Hot Zone of the CAB Furnace	30
Figure 2-13	Sample Configuration of a Furnace Experiment.....	31
Figure 2-14	Trillium TM Brazing Sample.....	32
Figure 2-15	Traditional Brazing Sample	32
Figure 2-16	2 ppm Oxygen Direct Input History.....	35
Figure 2-17	200 ppm Oxygen Direct Input History.....	35
Figure 2-18	2000 ppm Oxygen Direct Input History.....	36
Figure 2-19	Temperature History of a Furnace Brazing Process	37
Figure 2-20	Brazing by CAB Furnace	38
Figure 2-21	Numbered Cross-Sections of a Traditional Brazing Sheet	39
Figure 2-22	Numbered Cross-Sections of a Trillium TM Brazing Sheet.....	39
Figure 2-23	Measurement for the Sheet and Clad Thicknesses of a Traditional Sample	40
Figure 2-24	Measurement for the Sheet and Clad Thicknesses of a Trillium TM Sample	40
Figure 2-25	SEM Image of a Traditional Brazing Sheet	42
Figure 2-26	EDS Result for a Traditional Brazing Sheet	42

Figure 2-27	SEM Image of a Trillium™ Brazing Sheet.....	43
Figure 2-28	EDS Result for a Trillium™ Brazing Sheet.....	43
Figure 3-1	Trillium™ Brazing Sheet in 20 ppm O ₂ (a) Before and (b) After the Brazing Process.....	47
Figure 3-2	Trillium™ Brazing Sheet at 200 ppm O ₂ (a) Before and (b) After the Brazing Process.....	47
Figure 3-3	Trillium™ Brazing Sheet at 500 ppm O ₂ (a) Before and (b) After the Brazing Process.....	48
Figure 3-4	Trillium™ Brazing Sheet at 2000 ppm O ₂ (a) Before and (b) After the Brazing Process.....	48
Figure 3-5	Trillium™ Brazing Sheet in Air (a) Before and (b) After the Brazing Process. Test I.....	49
Figure 3-6	Trillium™ Brazing Sheet in Air (a) Before and (b) After the Brazing Process. Test II.....	49
Figure 3-7	Traditional Brazing Sheet in 20 ppm O ₂ (a) Before and (b) After the Brazing Process.....	50
Figure 3-8	Traditional Brazing Sheet in 200 ppm O ₂ (a) Before and (b) After the Brazing Process.....	50
Figure 3-9	Traditional Brazing Sheet in 500 ppm O ₂ (a) Before and (b) After the Brazing Process.....	51
Figure 3-10	Traditional Brazing Sheet in 2000 ppm O ₂ (a) Before and (b) After the Brazing Process. Test I.....	51
Figure 3-11	Traditional Brazing Sheet in 2000 ppm O ₂ (a) Before and (b) After the Brazing Process. Test II.....	52
Figure 3-12	Traditional Brazing Sheet in Air (a) Before and (b) After the Brazing Process.....	52
Figure 3-13	Surface Features of Trillium™ Brazing Sample in a Brazing Process.....	58
Figure 3-14	Surface Features of Traditional Brazing Sample in a Brazing Process.....	63
Figure 3-15	Macroscopic Joint Features of Trillium™ Brazing Sample in 20 ppm.....	64
Figure 3-16	Macroscopic Joint Features of Trillium™ Brazing Sample in 200 ppm.....	65
Figure 3-17	Macroscopic Joint Features of Trillium™ Brazing Sample in 500 ppm.....	66
Figure 3-18	Macroscopic Joint Features of Trillium™ Brazing Sample in 2000 ppm.....	67
Figure 3-19	Macroscopic Joint Features of Trillium™ Brazing Sample in Air. Test I.....	68
Figure 3-20	Macroscopic Joint Features of Trillium™ Brazing Sample in Air. Test II.....	69
Figure 3-21	Macroscopic Joint Features of Traditional Brazing Sample in 20 ppm.....	70
Figure 3-22	Macroscopic Joint Features of Traditional Brazing Sample in 200 ppm.....	71
Figure 3-23	Macroscopic Joint Features of Traditional Brazing Sample in 500 ppm.....	72
Figure 3-24	Macroscopic Joint Features of Traditional Brazing Sample in 2000 ppm. Test I.....	73
Figure 3-25	Macroscopic Joint Features of Traditional Brazing Sample in 2000 ppm. Test II.....	74

Figure 3-26	Macroscopic Joint Features of Traditional Brazing Sample in Air.....	75
Figure 3-27	Polishing Location	76
Figure 3-28	Metallurgical Photos of Trillium™ Brazed Sample in 20 ppm (a) Left Joint and (b) Right Joint.....	76
Figure 3-29	Metallurgical Photos of Trillium™ Brazed Sample in 200 ppm (a) Left Joint and (b) Right Joint.....	77
Figure 3-30	Metallurgical Photos of Trillium™ Brazed Sample in 500 ppm (a) Left Joint and (b) Right Joint.....	77
Figure 3-31	Metallurgical Photos of Trillium™ Brazed Sample in 2000 ppm (a) Left Joint and (b) Right Joint.....	78
Figure 3-32	Metallurgical Photos of Trillium™ Brazed Sample in Air (a) Left Joint and (b) Right Joint. Test I.	78
Figure 3-33	Metallurgical Photos of Trillium™ Brazed Sample in Air (a) Left Joint and (b) Right Joint. Test II.	79
Figure 3-34	Metallurgical Photos of Traditional Brazed Sample in 20 ppm (a) Left Joint and (b) Right Joint.....	79
Figure 3-35	Metallurgical Photos of Traditional Brazed Sample in 200 ppm (a) Left Joint and (b) Right Joint.....	80
Figure 3-36	Metallurgical Photos of Traditional Brazed Sample in 500 ppm (a) Left Joint and (b) Right Joint.....	80
Figure 3-37	Metallurgical Photos of Traditional Brazed Sample in 2000 ppm (a) Left Joint and (b) Right Joint. Test I.....	81
Figure 3-38	Metallurgical Photos of Traditional Brazed Sample in 2000 ppm (a) Left Joint and (b) Right Joint. Test II.	81
Figure 3-39	Metallurgical Photos of Traditional Brazed Sample in Air (a) Left Joint and (b) Right Joint.....	82
Figure 4-1	Examples for Metric C_a (a) $L' > 0.3$ (b) $L' < 0.3$	85
Figure 4-2	Examples for Metric C_b (a) No Aggregation (b) Aggregation.....	85
Figure 4-3	Examples for Metric C_c (a) Smooth Shape (b) Irregular Shape.....	86
Figure 4-4	Examples for Metric C_d (a) Covered Tip (b) Uncovered Tip	86
Figure 4-5	Joint Formation of Traditional Brazing Samples at $T_{dp} = -48^\circ\text{C}$ and $\text{O}_2 = 20$ ppm (a) Test #1 (b) Test #2 (c) Test #3.....	91
Figure 4-6	Joint Formation of Traditional Brazing Samples at $T_{dp} = -48^\circ\text{C}$ and $\text{O}_2 = 200$ ppm (a) Test #4 (b) Test #5 (c) Test #6.....	92
Figure 4-7	Joint Formation of Traditional Brazing Samples at $T_{dp} = -48^\circ\text{C}$ and $\text{O}_2 = 2000$ ppm (a) Test #7 (b) Test #8 (c) Test #9.....	93
Figure 4-8	Joint Formation of Traditional Brazing Samples at $T_{dp} = -18^\circ\text{C}$ and $\text{O}_2 = 20$ ppm (a) Test #10 (b) Test #11 (c) Test #12.....	94
Figure 4-9	Joint Formation of Traditional Brazing Samples at $T_{dp} = -18^\circ\text{C}$ and $\text{O}_2 = 200$ ppm (a) Test #13 (b) Test #14 (c) Test #15.....	95

Figure 4-10	Joint Formation of Traditional Brazing Samples at $T_{dp} = -18^{\circ}\text{C}$ and $\text{O}_2 = 2000$ ppm (a) Test #16 (b) Test #17 (c) Test #18.....	96
Figure 4-11	Joint Formation of Traditional Brazing Samples at $T_{dp} = -7^{\circ}\text{C}$ and $\text{O}_2 = 20$ ppm (a) Test #19 (b) Test #20 (c) Test #21.....	97
Figure 4-12	Joint Formation of Traditional Brazing Samples at $T_{dp} = -7^{\circ}\text{C}$ and $\text{O}_2 = 200$ ppm (a) Test #22 (b) Test #23 (c) Test #24.....	98
Figure 4-13	Joint Formation of Traditional Brazing Samples at $T_{dp} = -7^{\circ}\text{C}$ and $\text{O}_2 = 2000$ ppm (a) Test #25 (b) Test #26 (c) Test #27.....	99
Figure 4-14	Joint Formation of Trillium TM Brazing Samples at $T_{dp} = -48^{\circ}\text{C}$ and $\text{O}_2 = 20$ ppm (a) Test #28 (b) Test #29 (c) Test #30.....	100
Figure 4-15	Joint Formation of Trillium TM Brazing Samples at $T_{dp} = -48^{\circ}\text{C}$ and $\text{O}_2 = 200$ ppm (a) Test #31 (b) Test #32 (c) Test #33.....	101
Figure 4-16	Joint Formation of Trillium TM Brazing Samples at $T_{dp} = -48^{\circ}\text{C}$ and $\text{O}_2 = 2000$ ppm (a) Test #34 (b) Test #35 (c) Test #36.....	102
Figure 4-17	Joint Formation of Trillium TM Brazing Samples at $T_{dp} = -48^{\circ}\text{C}$ and $\text{O}_2 = 20000$ ppm (a) Test #55 (b) Test #56 (c) Test #57 (d) Test #58.....	103
Figure 4-18	Joint Formation of Trillium TM Brazing Samples at $T_{dp} = -48^{\circ}\text{C}$ and $\text{O}_2 = 200000$ ppm (a) Test #65 (b) Test #66 (c) Test #67.....	104
Figure 4-19	Joint Formation of Trillium TM Brazing Samples at $T_{dp} = -18^{\circ}\text{C}$ and $\text{O}_2 = 20$ ppm (a) Test #37 (b) Test #38 (c) Test #39.....	105
Figure 4-20	Joint Formation of Trillium TM Brazing Samples at $T_{dp} = -18^{\circ}\text{C}$ and $\text{O}_2 = 200$ ppm (a) Test #40 (b) Test #41 (c) Test #42.....	106
Figure 4-21	Joint Formation of Trillium TM Brazing Samples at $T_{dp} = -18^{\circ}\text{C}$ and $\text{O}_2 = 2000$ ppm (a) Test #43 (b) Test #44 (c) Test #45.....	107
Figure 4-22	Joint Formation of Trillium TM Brazing Samples at $T_{dp} = -18^{\circ}\text{C}$ and $\text{O}_2 = 20000$ ppm (a) Test #59 (b) Test #60 (c) Test #61.....	108
Figure 4-23	Joint Formation of Trillium TM Brazing Samples at $T_{dp} = -18^{\circ}\text{C}$ and $\text{O}_2 = 200000$ ppm (a) Test #68 (b) Test #69 (c) Test #70 (d) Test #71.....	109
Figure 4-24	Joint Formation of Trillium TM Brazing Samples at $T_{dp} = -7^{\circ}\text{C}$ and $\text{O}_2 = 20$ ppm (a) Test #46 (b) Test #47 (c) Test #48.....	110
Figure 4-25	Joint Formation of Trillium TM Brazing Samples at $T_{dp} = -7^{\circ}\text{C}$ and $\text{O}_2 = 200$ ppm (a) Test #49 (b) Test #50 (c) Test #51.....	111
Figure 4-26	Joint Formation of Trillium TM Brazing Samples at $T_{dp} = -7^{\circ}\text{C}$ and $\text{O}_2 = 2000$ ppm (a) Test #52 (b) Test #53 (c) Test #54.....	112
Figure 4-27	Joint Formation of Trillium TM Brazing Samples at $T_{dp} = -7^{\circ}\text{C}$ and $\text{O}_2 = 20000$ ppm (a) Test #62 (b) Test #63.....	113
Figure 4-28	Joint Formation of Trillium TM Brazing Samples at $T_{dp} = -7^{\circ}\text{C}$ and $\text{O}_2 = 200000$ ppm (a) Test #72 (b) Test #73 (c) Test #74 (d) Test #75.....	114
Figure 4-29	Background Atmosphere Condition vs. Brazeability.....	116

CHAPTER 1: Introduction

1.1 Motivation

The motivation for the study is to understand how adverse changes of atmosphere cause qualitative and quantitative deterioration of joint formation in aluminum brazing processes. A newly developed brazing material featuring composite filler material with incorporated flux will be tested and compared with a traditional material.

For better understanding of the involved phenomena, it would be helpful to review the main segments of a sequence of steps of an aluminum brazing process. This content is presented in Section 1.2 below.

1.2 Brazing

Brazing is one of the frequently used metal joining processes. It is a technique of bonding that is using a metal with lower melting point to make permanent joints between different pieces of materials (usually metal with higher melting points). The metal with lower melting point is commonly called filler metal, while the non-melted parts joined can be called parental or mating materials (Schwartz, 1987). To maintain the integrity of non-melting parental materials during a brazing process, a larger difference of melting points between filler and parental metals is desired. As an example, a typical melting point of an aluminum filler is commonly 30°C to 40°C lower than the melting points of parental aluminum alloys (Wallace and Dewing, 1976).

Brazing and soldering represent basically the same metal joining process, but with different names, depending on the operating temperature. A well accepted convention for distinguishing brazing and soldering is assumed to be defined as a critical temperature in the neighborhood of 450°C. Bonding at higher temperatures than 450°C is called brazing while the bonding temperature lower than 450°C is named soldering (Groover, 1996). This type of a metal joining process (brazing or soldering) results in a little distortion of mating parts and features the integrity of a brazed assembly. In addition to that, it opens a possibility for joining thinner parts, up to 0.01mm (0.0005 inch) (Schwartz, 1987). Brazing is also helpful when a complex surface topography is involved. For example,

metal foam with porous structure covering round tubes (T'Joel et al., 2010), or compact heat exchanger for automobile (Zhao et al., 2009).

Joints manufactured by brazing should be sound and reliable as a consequence of the adequate metallurgical bonding process. The meniscus profile of a typical joint between mating surfaces evolves from a capillary driven flow into the clearance/proximity of the bonded, mating surfaces, occurring at the contact areas of mating parts. This, so shaped joint fillet, resists fatigue and provides a robust metallurgical bond between parental metals if the brazing process is designed adequately (Schwartz, 1987, Shapiro and Sekulic, 2008). The capillary driven flow fills the gaps between parts without a need for any localized treatment in a net-shape manufacturing fashion therefore allows a massive production. There are different types of brazing processes such as torch brazing, induction brazing, resistance brazing, dip brazing, infrared brazing, furnace brazing, etc. Among those, furnace brazing, if performed in continuous operating furnaces is suitable for high production rates (Groover, 1996).

1.3 Aluminum Furnace Brazing

Aluminum has a relatively high strength, corrosive resistance, thermal conductivity, and low density (Zahr et al., 2012b). It is commonly applied in heat exchanger manufacturing for air conditioners, oil coolers, and many other applications. Among the other brazing processes, combined with the ability of massive production, aluminum furnace brazing became the main technology suitable for heat exchanger manufacturing (Koehler and Reinhard, 2011, Takigawa and Okamoto, 1993).

Silicon particles if contained in an aluminum-silicon alloy lower the melting point of the alloy exposed to phase change. When liquidized at its melting temperature during heating, this molten alloy has the ability to flow on a solid substrate if the wetting conditions are favorable (Sekulic, 2013). Hence, the standard aluminum-silicon alloys are often used as filler metals because of their lower melting temperature compared to other types of aluminum alloys. The standard designation of this group is AA4xxx (Pan and Sekulic, 2002), with the solidus temperature at 577 °C (Humpston and Jacobson, 1993).

There are two basic types of brazing furnaces: (i) batch furnace and (ii) continuous furnace (Schwartz, 1987). Assemblies to be joined are either placed still in a chamber throughout a brazing process (batch furnace brazing), or positioned on a conveyer traveling through a series of brazing zones (continuous furnace brazing).

A typical furnace brazing process for aluminum brazing normally includes a fluxing process. A flux is a chemical compound, usually an inorganic substance or a mixture, designed for melting before a filler material. Upon melting, the flux disrupts the naturally formed surface aluminum oxide layer. Note that the complex reactions between a flux and a naturally existed aluminum oxide is yet to be fully understood, however, the fluoride ion in a fluoride based flux is believed to involve with the disruption of aluminum oxide (Sekulic, 2013). A flux is usually applied onto aluminum in the form of suspension by either brushing or dipping. It can also be electro-statically sprayed onto aluminum surfaces (Swidersky, 1999). With the aid of a flux, a filler metal can wet the substrate and spread driven by surface tension hence forming a fillet joint directly with parental metals without being hindered by a naturally always formed surface oxide layer. If an excessive oxide layers exist, the flux will be insufficient and ineffective. A protective atmosphere is a measure to prevent extreme surface oxidation during the brazing process (Schwartz, 1987, Claesson et al., 1995).

Brazing using protective atmosphere is often referred to as a controlled atmosphere brazing (CAB) process. Protective atmosphere for CAB can be an inert gas or a vacuum (Brandon and Kaplan, 1997). Several important guidelines to achieve good CAB results are as follows (Swidersky, 2001, Schwartz, 1987, Kumar and Prabhu, 2007):

- Fitted mating surfaces with a gap between 0.1 mm and 0.15 mm for non-clad parts uniform flux coating on the mating surfaces
- Adequate brazing temperature profile and its uniformity
- Brazing atmosphere control by gases such as argon, hydrogen, nitrogen, or carbon monoxide. Being chemically non-reactive, nitrogen is commonly selected. A high purity protective gas significantly reduces the content of oxygen and moisture in a chamber which are responsible for poor joint formation.

Since the main object of this study is to understand the impact caused by a modification of a background atmosphere, it would be helpful to have an insight into the mechanism of aluminum oxidation (Section 1.4), followed by flux activity (Section 1.5).

1.4 Surface Oxidation

Surface oxidation takes place whenever a bare aluminum is in contact with oxygen. Oxygen can easily infiltrate the furnace chamber from the outside atmosphere. It may be contained physically on the surfaces of a furnace before a brazing process starts (Schwartz, 1987).

The formation of an aluminum oxide is complex. It includes absorption and dissociation of O_2 , nucleation and growth of Al_2O_3 , and moving ions and electrons through oxide layers (Jeurgens et al., 2002). It is also discovered that surface oxidation will be aggravated under conditions at increased temperature (Hunter and Fowle, 1956).

Surface oxidation of aluminum happens instantaneously. In other words, before any further treatment, there already exists an oxide layer on an aluminum surface. The naturally formed surface oxidation of aluminum features good corrosive resistance because of its low electric conductivity which inhibits ion diffusion. During heating, the diffusion of aluminum and oxygen ions becomes more intense as the temperature increases and therefore creates a thicker oxidation layer (Zahr et al., 2012a, Zahr et al., 2011). It is established that the new layer of oxide is produced beneath the previously formed amorphous aluminum oxide layer after the nucleation and growth of a crystalline $\gamma-Al_2O_3$ (Field, 1989). A crystalline Al_2O_3 nucleates and grows when temperature reaches around $427^\circ C$ (Wefers and Misra, 1987, Field and Steward, 1987). When the thickness of the oxide layer builds up, the speed of oxidation decreases, because of the limited ion diffusion (Zahr et al., 2012a). There are two opposite forces competing for the formation/destruction of oxide layer, which is happening at the interface of the oxide layer and an aluminum surface (Hunter and Fowle, 1956).

The naturally occurring oxide layer consists of two sub-layers with different structures, as shown in Figure 1-1. The layer in a direct contact with aluminum is an aluminum oxide layer, Al_2O_3 , which can also be called “barrier layer”, while the other

layer in between the barrier layer and the atmosphere is mainly an aluminum hydroxide layer, $\text{Al}(\text{OH})_3$, called “surface layer”. The surface layer features pores, mixed oxides, or heterogeneous phases (Altenpohl, 1965, Zahr et al., 2012a, Hunter and Fowle, 1956). SEM images of surface oxide layers of an aluminum alloy are presented in Figure 1-2.

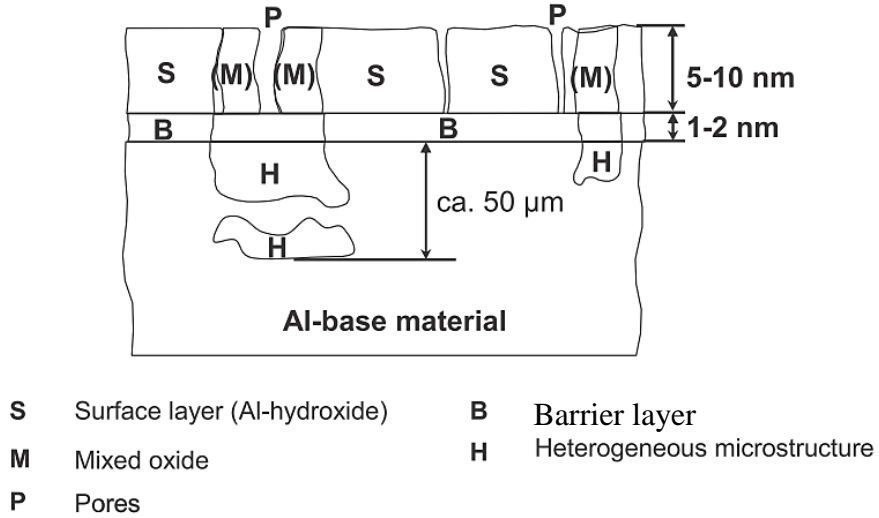


Figure 1-1 Natural Surface Layer on Aluminum Materials (Zahr et al., 2012b)

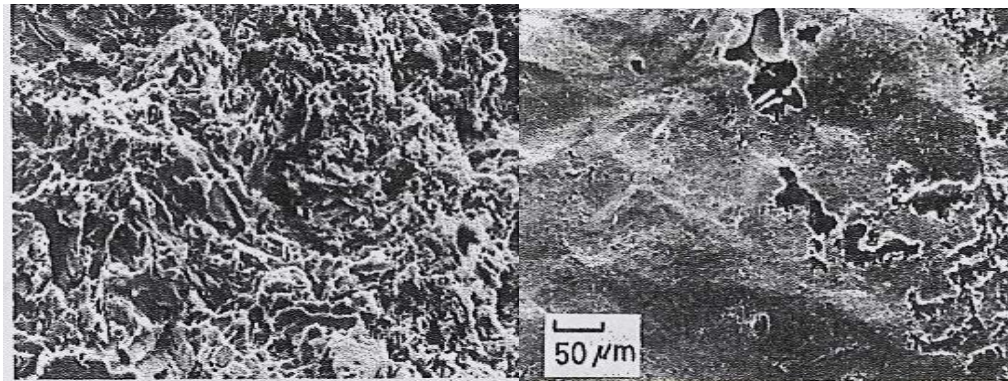


Figure 1-2 SEM of Aluminum Oxide Films: 4 nm (left) and 295 nm (right) (Kawase and Yamaguchi, 1980)

Hunter et al., 1956, suggest that the thickness of the barrier layer depends primarily on temperature. According to Hunter et al. - “It has been shown that in dry oxygen at room temperature the natural film reaches an ultimate thickness of about 10\AA in a matter of minutes.”, a bare aluminum surface forms natural oxide layer rather quickly

in environment containing oxygen (Hunter and Fowle, 1956). The structure of the natural oxide film is initially an amorphous layer and then becomes a crystalline at higher temperature. In their study, a linear relationship between temperature and barrier thickness is observed (Hunter and Fowle, 1956).

A series of study regarding the correlation between aluminum oxide layer, atmosphere conditions and brazeability, has been published by Zahr et al. in 2011 and 2012. In their studies, a series of X-Ray Photoelectron Spectroscopy (XPS), Fourier Transform Infrared Spectroscopy (FTIR) measurements, and brazeability tests have been performed. An aluminum alloy (AA3003 core with AA4045 clad) was stored under different environmental conditions with different humidity levels including:

- (i) Normal condition (23°C, 50% RH)
- (ii) Humid condition (40°C, 92% RH)
- (iii) Condensing condition (23°C, 100% RH)

Prior to brazing tests, surface oxide thicknesses of aluminum alloys in various environmental conditions were measured using XPS. The brazing tests were under the protection of a nitrogen gas. Instead of using a flux, the surface activation was provided by applying mechanical pressure, illustrated by Figure 1-3.

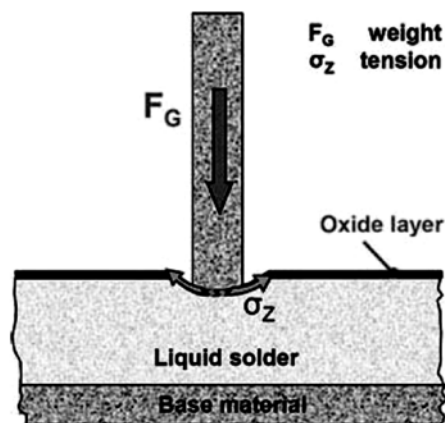


Figure 1-3 Mechanism of the mechanical surface activation (Zahr et al., 2011)*

* "Liquid solder" In Figure 1-3 stands for an aluminum braze, according to the description: "The brazing tests are done in a shielding gas lab furnace without using flux" in the article (Zahr et al., 2011).

Their results (Zahr et al., 2011, Zahr et al., 2012a) showed that the storage under (i) normal or (ii) humid conditions does not impact oxide thicknesses significantly. However, the storage in (iii) condensing condition has a strong impact on the growth of surface oxide thickness. Moreover, sample taken from the condensing condition to the normal condition for a period of days does not lower the oxide thickness but it maintains similar level of brazeability whereas the sample taken directly from the condensing environment has very poor brazeability performance. It is suggested that the main reason for deterioration of brazeability is more relevant to the contained water in pores of the hydroxide layer than the thickness of an oxide layer.

The existence of moisture increases the oxide thickness (Swidersky, 2001, Zahr et al., 2012a). Consequently, in order to prevent oxidation during a brazing process, atmosphere must be protective and hence is one of the important factors which must be taken care of. Moisture contained in the atmosphere can adhere to surfaces depending on the humidity level, temperature, and pressure conditions (Lauzon and Swidersky, 2002). Preheating before reaching the melting temperature of a filler metal during the brazing process can reduce the water contained in the flux, samples, or the brazing environment, such as the walls of the furnace. Temperature between 200°C and 250°C is usually selected as the preheating temperature (Lauzon et al., 1998).

1.5 Flux

To form successful brazed joints, non-metal substances eventually present on mating surfaces need to be eliminated so that molten filler metal can have an intimate contact with the parental materials, subsequently (after spreading and joint formation) facilitating a metallurgical bonding after cooling. From the previous section, we have learned that the non-metal surface film on an aluminum surface is consisted of aluminum oxide and aluminum hydroxide layers. These tenacious layers must be disrupted if not entirely dissolved. The task of dissolving and disrupting the surface oxide layer is achieved by a chemical called flux.

In order to dissolve the surface oxide layer of an aluminum substrate and to enable spreading, a flux requires possessing a lower melting point and better wettability

than the molten filler metal on which the flux is dispersed. It is also important for a flux to have a sufficient capability for dissolving oxides throughout heating process for preventing any additional oxidation. Flux is required to be nonreactive with metallic substances (Schwartz, 1987, Brandon and Kaplan, 1997).

Chloride salts were firstly applied for an aluminum brazing process (Hawksworth et al., 2012). A traditional composition of flux for aluminum brazing is NaCl-KCl-LiCl with a minor amount of NaF and AlF_3 (Sugiyama, 1989). However, the hygroscopic and corrosive features of the brazed parts with the flux residue are undesired and require a removal of the post-brazed residue (Cooke et al., 1978). These problems with the chloride salt have motivated the development of a non-corrosive brazing flux in a controlled atmosphere (Hawksworth et al., 2012). The flux used throughout this thesis research is a potassium fluoroaluminate salt provided by Solvay Fluor, registered as NOCOLOK™.*

Due to the non-corrosive nature and the ability for supporting a mass brazing production, the Nocolok flux is easily implemented in automotive heat exchanger manufacturing. The general composition of the Nocolok flux at the brazing temperature is the mixture of potassium tetra-fluoroaluminate (KAlF_4) and potassium hexa-fluoroaluminate (K_3AlF_6). It is sometimes denoted as $\text{K}_{1-3}\text{AlF}_{4-6}$, which can be produced by fusing AlF_3 and KF together with proper proportions. This is an inorganic fluoride salt and non-hygroscopic (Lauzon et al., 1998, Lauzon and Swidersky, 2002, Field and Steward, 1987, Wallace and Dewing, 1976). The mole fraction of KAlF_4 and K_3AlF_6 are 50% and 50%, respectively. The eutectic melting temperature of the Nocolok flux is 562 °C and it completely melts at 575°C, which is right below the eutectic temperature of an aluminum-silicon alloy, 577°C (Field and Steward, 1987). In molten state, potassium fluoroaluminate reacts and dissolves the surface oxide layer without attacking the

* In 1976, Alcan Research and Development Limited filed several patents for the development of potassium fluoroaluminates in the United States. About 65:35 and 45:55 in parts by weight of AlF_3 and KF were fused to produce K_3AlF_6 and KAlF_4 , documented in the database of the United States Patents (Wallace and Dewing, 1976, Cooke, 1976). A few other inventions of different flux compositions were filed thereafter (Kawase et al., 1986, Conn and Schrameck, 1995, Ono et al., 2000). Later, the development of controlled atmosphere brazing process using non-corrosive flux was resulted in a registration of NOCOLOK™ flux in September 1976, by Alcan Aluminium Corporation. It belonged to Alcan until the year 2001, when NOCOLOK™ was conveyed to Solvay Fluor, and the ownership has been held by Solvay till present. Nocolok brazing was widely accepted and aluminum became a primary construction material for heat exchanger manufacturing (Hawksworth et al., 2012).

adjacent molten or solid aluminum (Takigawa and Okamoto, 1993). Surface oxide film is disrupted chemically and/or shifted away physically by the wetting of flux. This will persist during a brazing process even when the filler material is melted.

The K-Al-F flux is not responsible for removing oil, lubricant, or other similar contaminants on aluminum surfaces, so it is a necessary step to degrease brazing components prior to a brazing process. Adequate cleaning process prior brazing allows better brazed joint appearance as well as a favorable corrosion behavior. Common methods for cleaning are liquid cleaning and thermal degreasing. Alkaline or alcohol based solvents are usually seen in liquid cleaning, combined with light etching when using a solution. To control liquid cleaning, several factors are needed to be considered such as time, temperature, concentration, and contact pressure. Thermal degreasing is useful when volatile substances are on aluminum surfaces. The suggested temperature for thermal degreasing is around 200°C to 250 °C but no more than 300°C, to prevent serious oxidation in a high temperature environment (Swidersky, 2001).

Common methods for applying flux on brazing surfaces are i) dipping into a salt bath, ii) brushing by a slurry paste, or iii) electrostatic spraying (Hawksworth et al., 2012, Eisenbeis, 2011, Swidersky, 2001). Since the moisture physically attached to flux powder may cause localized aggregation, non-uniformity of flux deposition exists when powder flux is applied in a humid environment. Narayanaswamy (Narayanaswamy, 2006) did a series of experiments to verify whether the localized aggregation of flux deteriorates the spreading of molten aluminum. In his research, a tiny coin-shaped AA4343 test specimen was placed on top of a substrate made of AA3003 and brazed using a hotstage microscopy system. Nocolok flux was selected with the loading density of 10 g/m². The selected flux was loaded in four different geometric patterns (Figure 1-4):

- (i) Full flux coverage
- (ii) Half flux coverage
- (iii) Quarter flux coverage
- (iv) No flux coverage

Results showed that, the wetting behavior of filler metal is slightly changed because of the irregular distribution of flux coverage. The flow speed of filler metal in all directions is not the same for the cases of (ii) half flux coverage and (iii) quarter flux coverage. However, the amount of spreading of filler metal is still appreciable for those cases loaded with flux, i.e. patterns (i), (ii), and (iii). This implies that the good wetting ability of flux helps alleviate the issue of non-uniform flux deposition.

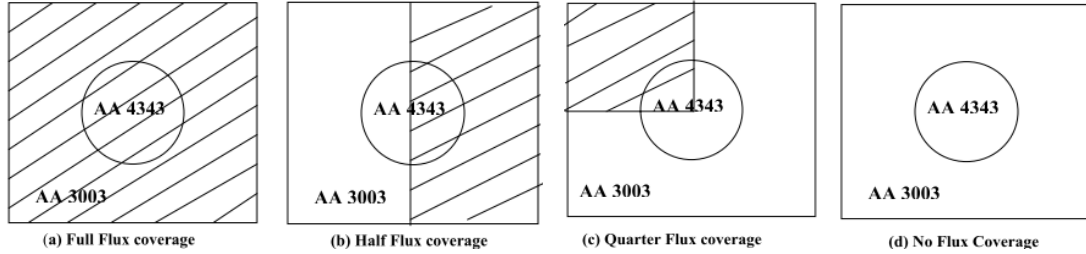
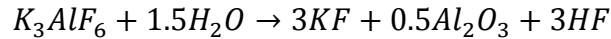
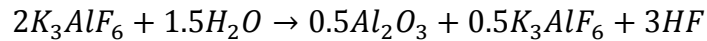
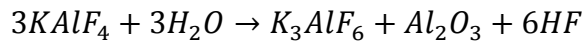
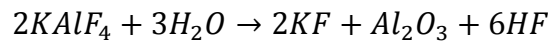


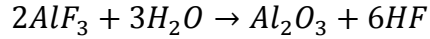
Figure 1-4 Patterns of Flux Coverage (Narayanaswamy, 2006)

Atmosphere is one of the major influences which affect a brazing process. The atmosphere not only affects the wetting behavior of a filler metal, but also influences the efficiency of flux action, which may lead to a failure of brazing process in some cases. Mentioned by Field et al (Field and Steward, 1987), “Water vapour, a common though variable constituent of furnace atmospheres, reduces the efficiency of all aluminium fluxes.” A number of consulted references offers a group of possible reactions between moisture and flux as follows:



Above reactions were proposed by Field and Steward (Field and Steward, 1987) for the interaction between moisture and the Nocolok flux. Additional possible reactions for the K-Al-F flux were proposed as follows (Lauzon et al., 1998, Thompson and Goad, 1976):





These reactions indicate a change of composition of flux and result in a change of melting temperature (Field and Steward, 1987), i.e. the melting temperature shifts away from the eutectic temperature 562°C of $KAlF_4$ and K_3AlF_6 (Cooke et al., 1978), and the ability of flux is therefore limited.

It is worth to note that the formation of hydrogen fluoride (HF) in the above reactions is hazardous. HF may cause pulmonary and dermal irritations (Zimmer and Biswas, 2000, Baskin and Bemis, 2003). It can also cause corrosion of furnace sealing (Lauzon et al., 1998). Hence, it is critical to reduce the moisture content in the brazing atmosphere.

Now, let us review some previous works focused specifically on the impact of atmosphere on brazeability.

1.6 Impact of Atmosphere on Brazeability

Studies regarding the alternation of the oxygen content of a brazing process have been published. Suggestions for oxygen levels and humidity levels are provided accordingly.

Takemoto (Takemoto et al., 1996) suggested that the oxygen content of a powder aluminum braze filler metal is a good criterion for brazeability. They produced three groups of atomized powder filler metals by different sets of atomizing atmosphere (inert, semi-inert, and air), and thus had powder filler metals with different oxygen contents. Repeatedly applying them under a typical brazing cycle, brazeability was measured and presented in Figure 1-5. According to their result, filler powders produced under inert atomizing gas tend to have better brazeability than powders produced in semi-inert or air environment when flux loading is low.

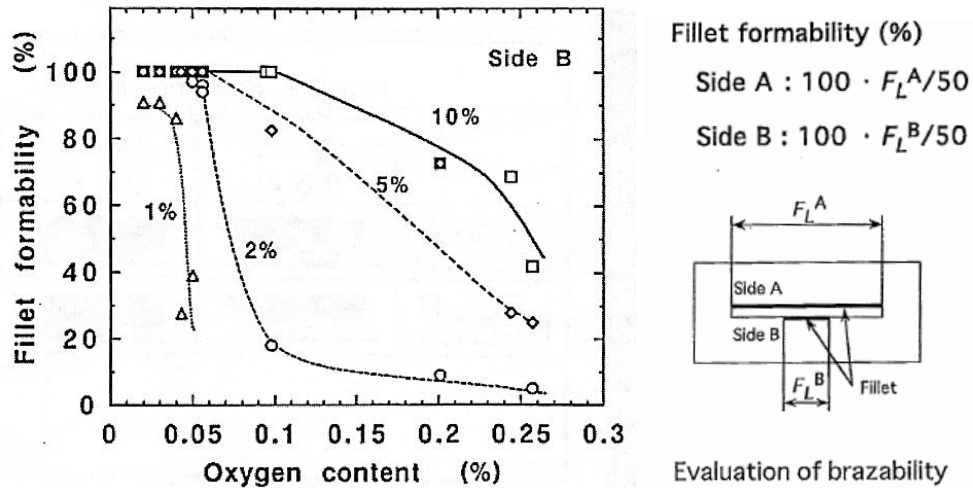


Figure 1-5 Changes in Fillet Formability with Oxygen Content for various Flux Content (Takemoto et al., 1996)

Kawase and Yamaguchi (Kawase and Yamaguchi, 1980) studied the effect of oxide film thickness on aluminum brazeability in vacuum, which showed that the thicker oxide film leads to worse wettability of the filler metal, as shown in Figure 1-6. Approximately 30 nm of oxide layer thickness was established as the tolerable oxide thickness which allows sufficient wettability of the filler metal.

For a non-corrosive Nocolok flux brazing process, Swidersky (Swidersky, 2001) suggested a density of 5 g/m^2 flux coating for a successful brazing result. When the oxide layer increases from 4 nm to 22 nm, the brazeability is not significantly deteriorated with flux loading at 5 g/m^2 , however a worsened braze happens when the flux coating reduces to 2 g/m^2 .

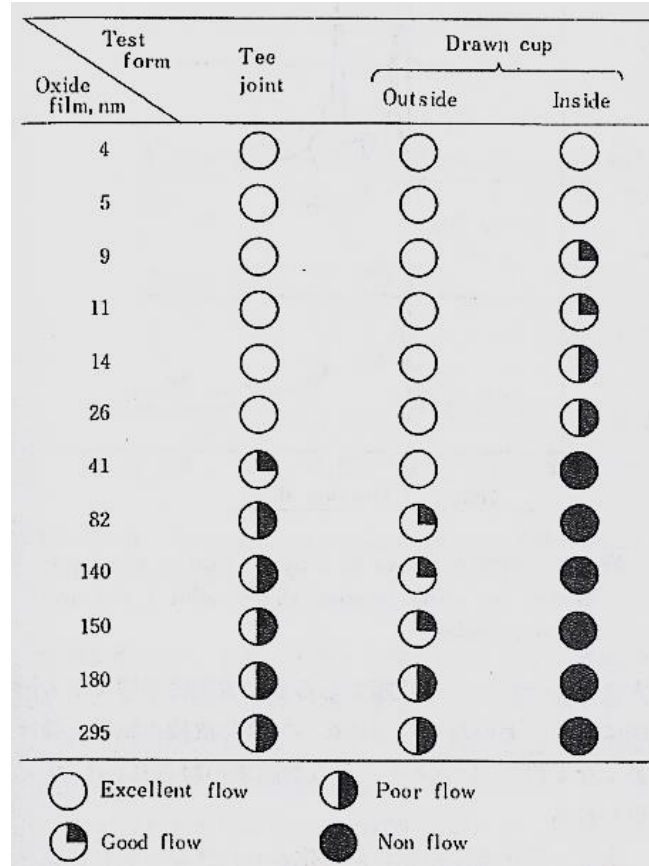


Figure 1-6 Relation between Oxide Film Thickness and Wettability (Kawase and Yamaguchi, 1980)

A relation between brazeability and concentrations of oxygen and moisture in the atmosphere has been studied by Stenqvist (Stenqvist et al., 1994) according to Claesson's report (Claesson et al., 1995). Results showed that in a controlled atmosphere brazing process at low oxygen levels (less than 50 ppm), low humidity (-45°C), and flux loading more than 1.1 g/m², a metallurgical joint can be formed. However, joint formation will be worsened if dew point temperature goes up to -35°C or -30°C. The deteriorating situation appears if the oxygen level in the atmosphere is increased, e.g. 400 ppm. Most of the samples with the same settings in the < 50 ppm O₂ cannot accomplish a joint formation when tested in the 400 ppm O₂ environment except for a poor joint registered at a higher flux loading level (3.2 g/m²), see Figure 1-7.

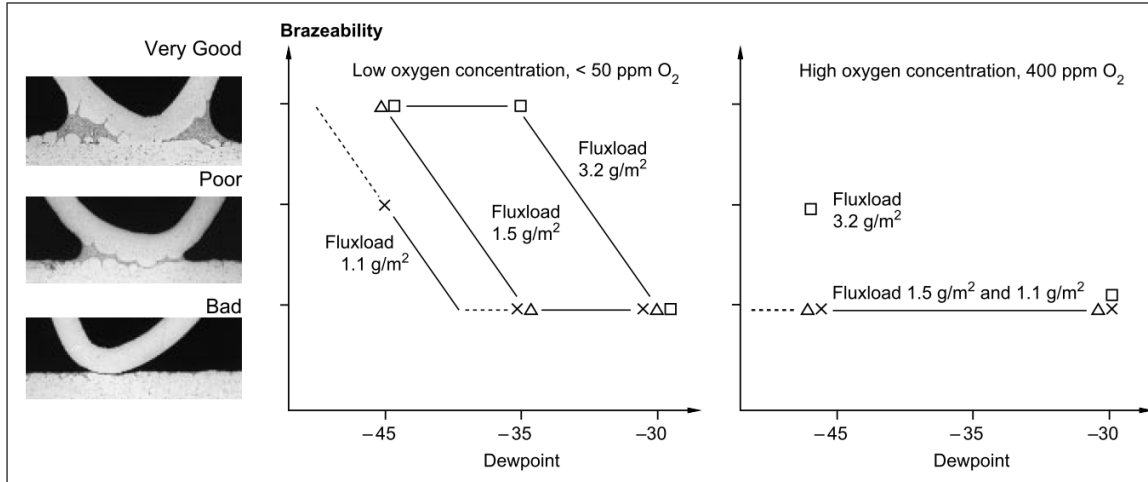


Figure 1-7 Relation between Brazeability and Atmosphere Concentrations of O_2 and H_2O (Stenqvist et al., 1994, Claesson et al., 1995)

A commonly accepted standard for a well-protective brazing environment is a combination of oxygen level, humidity level, and flux loading at 100 ppm, -40°C , and 5 g/m^2 , respectively (Swidersky, 2001, Field and Steward, 1987, Liu, 1996, Cooke et al., 1978). From the documented works shown above, it is obvious that flux loading, oxygen level, and humidity level are the factors which lead to poor joint formation; however, there is yet to be established a more elaborated correlation between poor brazeability and the atmosphere in a controlled atmosphere brazing process.

1.7 Self-Fluxing Material

Motivated by the intention of simplifying a brazing process, self-fluxing (or pre-fluxed) and flux-free systems have been developed over the years such as flux pre-coating techniques (Kilmer and Eye, 2002, Wittebrood, 2004). The benefits for self-fluxing systems are (i) precise control of flux loading without waste and (ii) a simplified brazing process without steps of adding flux (Swidersky, 2001). Fluoride coating and blended flux with filler metal are examples for self-fluxing brazing (Van Evans et al., 2000). Nickel thin film coating provides a way for brazing without a flux (Dockus, 1978).

The self-fluxing material TrilliumTM has been developed featuring an aluminum clad with pre-incorporated flux (Ogilvy et al., 2010, Ogilvy et al., 2008, Hawksworth et

al., 2012). Yu et al. offers a study of the impact of atmosphere deterioration impact on brazeability of both traditional and Trillium™ brazes (Yu et al., 2012). By the pre-incorporated flux in a filler metal, the clad can be self-fluxed during a CAB process and would form the joint fillet when aluminum mating surfaces are present. This self-fluxing mechanism reduces the effort of precisely fluxing and drying before brazing. The ingredients of the Trillium™ filler are aluminum silicon alloy and potassium fluoroaluminate, with the melting point at around 550°C or higher for the flux.

For a typical traditional brazing process with a K-Al-F flux, the flux is added on the surfaces of aluminum components. During a heating process, the flux disrupts the surface oxide layer of an aluminum alloy upon melting and comes into contact with filler metal. The flux coverage protects the filler metal from oxygen traces in the atmosphere. Hence, the function of flux might be degraded if the disruption of oxide layer is not as expected under an increase of the oxide layer thickness or insufficient flux amount, etc. On the other hand, the flux activity of a Trillium™ clad starts between the oxide layer and the filler. That is, the flux has a contact with the filler metal during a heating process before an interaction with the surface aluminum oxide. Then it disrupts the surface oxide layer from the clad-oxide interface, without contacting the chamber atmosphere. Figure 1-8 illustrates the difference between traditional and Trillium™ brazing sheets in terms of types of fluxing activities. This mechanism is expected to have better protection of severe background atmosphere during brazing (Sekulic, 2013).

To identify the efficiency of this self-fluxing material, a series of experiments on the impact of the background atmosphere is to be carried out with a precise brazing process control in this study. Traditional fluxing materials were also tested in parallel. All test samples were prepared and brazed in a controlled atmosphere brazing furnace. Detailed descriptions of the experimental setup will be given in Chapter 2.

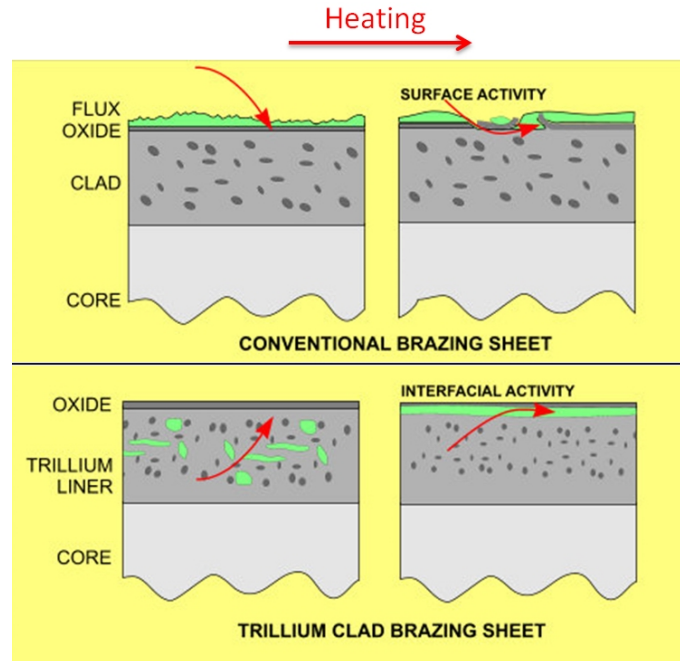


Figure 1-8 Relation between Oxide Film Thickness and Wettability (Yu et al., 2013)*

1.8 Hypothesis

Based on the difference of fluxing mechanism as stated in Section 1.7, a self-fluxing clad brazing sheet (Hawksworth et al., 2012) exposed to an adverse atmosphere condition is presumed to perform better than a surface-fluxing traditional sheet in a controlled brazing process. Adverse atmosphere conditions assume oxygen concentration higher than 100 ppm and dew point temperature higher than -40°C . The performance is defined as a set of topographical metrics characterizing joint fillet formation, referred to a method established in 1989 (Kawase et al., 1989).

* The figure was presented in the NSF Student Poster Competition Session in November 20, 2013, ASME-IMECE Conference, San Diego, USA. A prior version of this figure was presented by Dr. Hawksworth in the 5th IBSC Conference, Nevada, USA, 2012 (Yu et al., 2012).

CHAPTER 2: Experimental Setup and Materials Characterization

In this chapter, two systems assembled to accommodate the required experiments. Procedures for the sample preparation will be discussed. The first system involves a testing facility for the hotstage experiments (Section 2.1). The second one is the transparent brazing furnace (Section 2.2). The material characterization is discussed in Section 2.3.

2.1 Hotstage Experiments

2.1.1 Hotstage Microscopy Test

The Linkam THMS 600 hot stage has been installed on an Olympus BX51M optical microscope (Linkam, 2015, Olympus, 2015). Heating and cooling processes are controlled by the module of CI-94 controller via LNP liquid nitrogen pump. These devices are integrated within the microscope observation system. An in-house designed control software with the CI-94 controller provides a precise temperature control throughout the brazing process. A PAXcam video camera is installed on the Olympus microscope for monitoring the brazing process in real time. Fiber-lite illuminator is installed as an auxiliary lightening source to improve the limited illumination from the microscope. An outline of the hotstage microscopy system is offered in Figure 2-1. Detailed discussion will be given next.

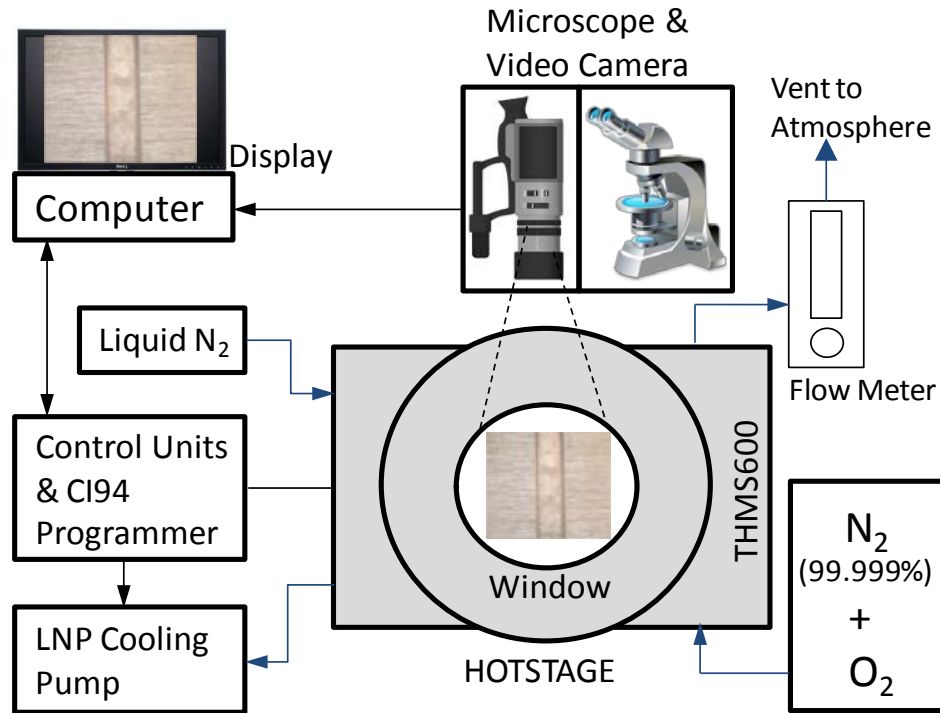


Figure 2-1 Hotstage Microscopy Components

The hotstage offers controlled heating and cooling in a range between 600°C and -196°C, with the heating and cooling rates both up to 150°C per minute with stability of 0.1°C. The stage body size is 137 x 92 x 22 mm³. In the middle of the chamber, a silver block is installed and used as a heating/cooling substrate. Heating element is embedded in the silver block as well as the temperature sensor. The high thermal conductivity of silver allows a uniform heating rate across the silver block surface facing the chamber quartz glass window. The silver block module is shown in Figure 2-2. A crucible carrier is connected to an outside located displacement system capable of manipulating X-axis and Y-axis locations. This manipulation is capable of slightly adjusting the location of sample versus the silver block. Before placing any sample in the hot zone chamber, a thin quartz glass substrate sheet is positioned on top of the silver block in order to protect it from possible contamination during a brazing process. The quartz glass substrate is surrounded by a stainless steel ring, which works as a sample holder as well as a radiation shield. A sample can be placed on top of the quartz glass substrate sheet. The sample is heated by conduction from the bottom (a dominant heat transfer mode), and radiation from the ring

(an auxiliary heat transfer mode). The sample area is 22 mm in diameter, same as the quartz glass substrate.



Figure 2-2 Silver Block Module

A gas-tight cover lid features a quartz glass window which allows observation in real time, as shown in Figure 2-3. The dimension of this glass window is 22 mm in diameter with thickness of 0.5 mm. Silicon rubber ring is installed around the cover lid for sufficient segregation of the outside atmosphere. The dimension of the inner chamber is approximately 70 mm in diameter and 17 mm in height. With the installation of the cover lid, chamber environment is separated from the outside atmosphere. Flow control and atmosphere condition will be discussed in Section 2.1.3. A picture of the hotstage microscopy system is presented in Figure 2-4.



Figure 2-3 Cover Lid Assembly



Figure 2-4 Hotstage Microscopy System

2.1.2 Sample Preparation for a Hotstage Test

Two different aluminum brazing sheets were used for making test samples, provided by Sapa Heat Transfer.

One of the brazing sheets was aluminum alloy AA3003 core with AA4045 (with ~10% Silicon) clad. The thickness of the sheet, consisted of both clad and core, was 0.53 mm thick. Clad was on single side with the clad ratio of 6%. See Figure 2-23 in Section 2.3. Another brazing sheet was made by using the same substrate material, with a new clad material named Trillium™ (Ogilvy et al., 2010, Hawksworth et al., 2012). Total thickness of Trillium™ brazing sheet was about 0.31 mm with 9% clad ratio, single clad, shown in Figure 2-24.

Both types of brazing sheets have about 29~30 µm clad thickness, what is imposed as a required condition for comparing experimental results. For clarity, throughout the whole text, the brazing sheet which has no flux content will be termed “traditional brazing sheet”, for which an addition of a flux is required for a brazing test; whereas the brazing sheet with the new material will be termed “Trillium™ brazing sheet”. Note that no additional flux for Trillium™ brazing sheet is needed since flux has been incorporated during the production of the Trillium™ brazing sheet. Details of material characterization are provided in Section 2.3.

Both brazing sheets were cut to shape to form small square pieces in the dimensions of 10 x 10 mm², to serve as the mating components. Aluminum alloy AA3003 sheets were selected to make 1 x 10 mm² aluminum strips. The thickness of the AA3003 sheet was 0.4 mm. For each brazing experiment, AA3003 strip was placed on top of a brazing sheet with the clad side facing upward. The margin of error of the sample dimensions was kept within ± 0.2 mm.

Brazing parts were first cleaned in an ultrasonic cleaner, soaked in a 190 proof ethanol for 1 minute, rinsed by water, and then cleaned by SF-1 degreaser (L&R Ultrasonics). SF-1 is a biodegradable water based (70-90%) degreaser, consisting of sodium metasilicate (1-5%), sodium xylene sulfonate solution (1-10%), quaternary ammonium compound (1-5%), and ethoxylated propoxylated alcohols (1-5%). After the ultrasonic cleaning procedures, the parts were manually cleaned using a tissue paper wetted by a 190 proof ethanol.

Before assembling brazing components, for the traditional material, an additional step was needed. To be applied onto the brazing parts, Nocolok potassium fluoroaluminate flux (Solvay International Chemical Group) was measured so that ~1 mg flux was mixed with a 190 proof ethanol to form a slurry paste, and then the flux solution was brushed onto the mating pieces. Flux loading was kept ~10g/m² for each sample*. Samples were prepared and placed in the chamber of hotstage microscopy for two-hour purging in an ultra-high purity nitrogen (99.999% N₂) before brazing. A sketch of the sample formation is presented in Figure 2-5.

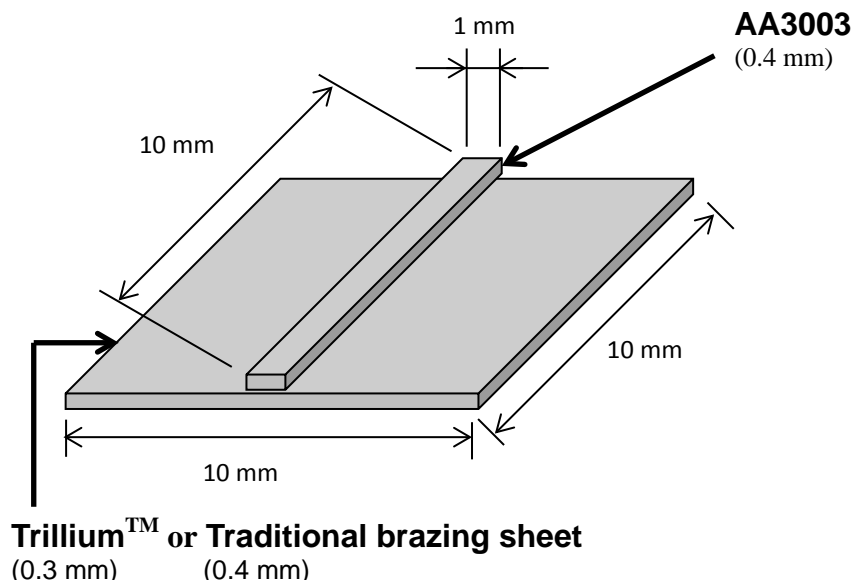


Figure 2-5 Sample Configurations for a Hotstage Experiment

2.1.3 Atmosphere Condition in the Hotstage Chamber

Chamber environment was protected by continuous inert gas input. Certified grade nitrogen and oxygen balanced nitrogen gases were obtained through a commercial supplier (Scott-Gross) with explicitly specified concentrations. In this research, gas sources for oxygen mixed nitrogen range from 2 ppm, 2×10^2 ppm, 5×10^2 ppm, 2×10^3 ppm, and 2×10^5 ppm oxygen levels. Note that 2 ppm oxygen concentration in nitrogen is equal to 99.999% pure N₂. For the level of 2×10^5 ppm, the test chamber was opened to

* This value was higher than the typical flux loading: 5 g/m² as a conservative approach (Swidersky, 2001).

the atmosphere and closed without any further purging process. Also, the gas tubes were disconnected from the hotstage.

To establish a desired chamber atmosphere condition, one of these external gas sources was connected and the gas was introduced into the chamber. The gas flow was controlled by a flowmeter manufactured by Concoa Precision Gas Controls. The Concoa 560 Series 150 mm Flowmeter provides a range of flow from 0 to 50 ccm (cubic centimeters per minute) with the accuracy between $\pm 3\%$ of the full scale. Based on the suggestion of the manufacturer (Linkam), a flowrate equal or less than 50 ccm ensures a better temperature control in the hotstage. Therefore, throughout the hotstage experiments, fixed volumetric flow rate of 50 ccm was always maintained at the atmospheric pressure of 1 atm and room temperature of 23°C. At the fixed volumetric flow rate of 50 ccm, the mass flow rate is estimated 10^{-6} kg/s.

2.1.4 Verification of Atmosphere Condition

To secure the same brazing atmosphere as supplied by the gas source, brazing chamber was purged for 2 hours before a brazing cycle. Measured dimensions of the inner chamber gave an approximate value of the volume of the chamber, equal to 65 cm³. With the mass flow rate of 10^{-6} kg/s (50 ccm), a calculated filling rate for supplying the chamber atmosphere is 46 times per hour. Therefore, after purging for two hours, the gas chamber was exposed to 92 replacements, so an identical oxygen level compared to the gas source was presumed to be valid. The result of 2 hours purging was later confirmed by a Teledyne 316RA Oxygen Analyzer and it has shown identical concentration as featured by the gas source.

2.1.5 Brazing Temperature History

After two hours purging, samples were heated by the ramp of up to 100°C/min, asymptotically approaching peak temperature at 600°C. The dwell time at the peak was 2 minutes. The cooling rate during the quench was 100°C/min until 40°C. The entire process was well controlled by an in-house designed computer program via the control unit. The brazing temperature profile of each experiment was the same. The profile of the

temperature history during a hotstage brazing test is shown in Figure 2-6. A picture captured in the middle of a brazing process is shown in Figure 2-7.

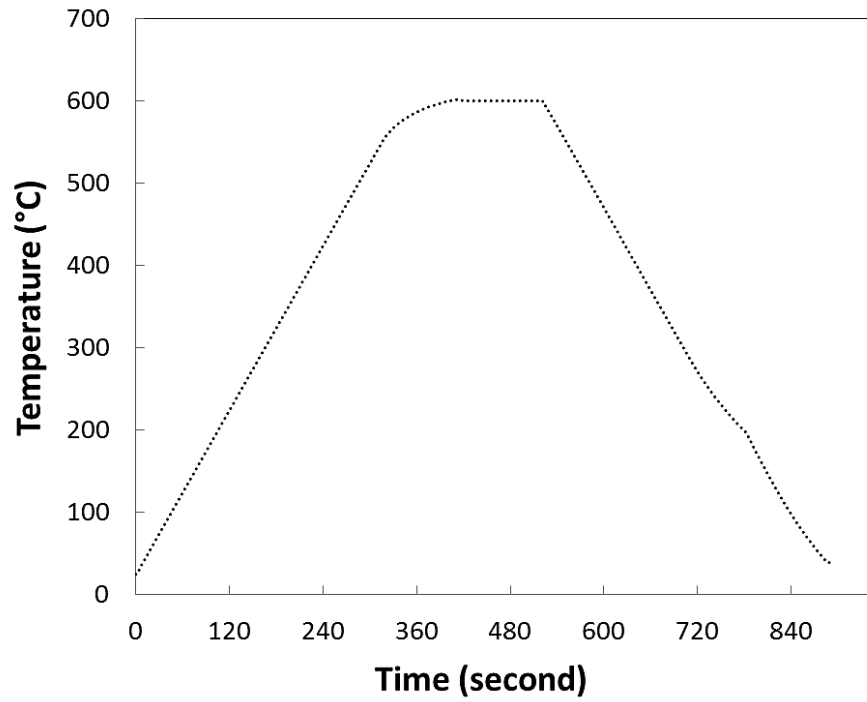


Figure 2-6 Temperature History of the Hotstage Brazing Process



Figure 2-7 Brazing in Process within the Hotstage

2.2 Furnace Experiments

2.2.1 Transparent Controlled Atmosphere Brazing Furnace Test

A transparent controlled atmosphere brazing (CAB) furnace system (Centorr Vacuum Industries) was installed in the Brazing, Soldering, and Heat Exchangers Research Laboratory in the University of Kentucky and used in this study for CAB tests. Major components included in this brazing facility are: (i) gas supply system, (ii) vacuum pump system, (iii) gas humidifier center, (iv) transparent furnace hot zone, (v) dew point monitor system, (vi) oxygen analyzer, and (vii) data acquisition system. A schematic of the CAB furnace system is presented in Figure 2-8. Detailed description for each component will be given next.

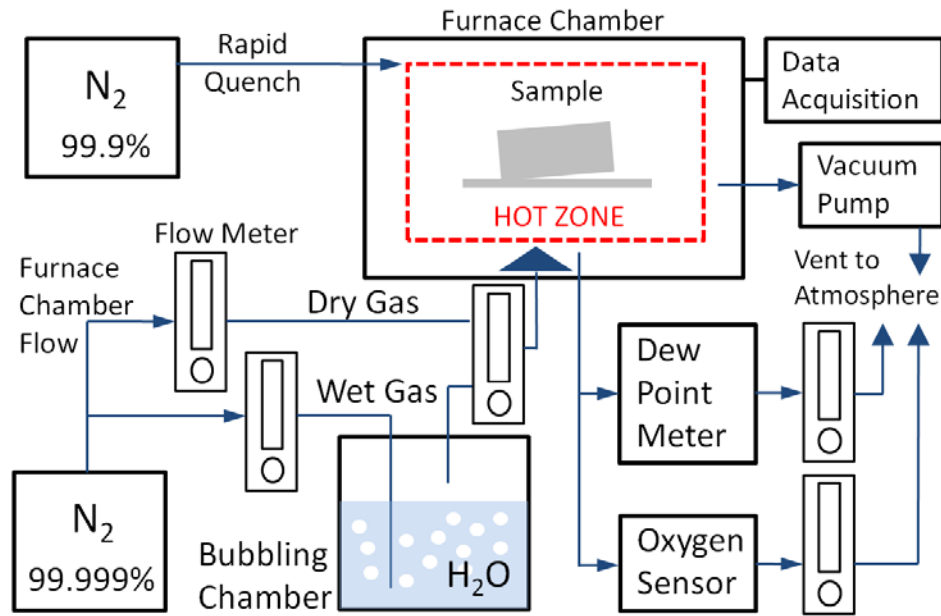


Figure 2-8 Layout of Transparent CAB Furnace

The gas supply system consists of pressured gas cylinders supplied by a commercial provider (Scott-Gross). The company provides ultra-high purity nitrogen (99.999% grade) as well as modified with various oxygen concentrations. In the furnace CAB study, the following O₂ concentrations were used: 2 ppm, 2 x 10² ppm, 2 x 10³ ppm, 2 x 10⁴ ppm, and 2x10⁵ ppm (dry air). The 99.9% pure nitrogen gas was applied during the rapid quench process after completion of the dwell at the peak temperature level. The

gas supplied was certified by the supplier (Scott-Gross), see Appendix A. An E2M1.5 Rotary Vacuum Pump (BOC Edwards) was used for evacuating the hot zone before pumping source gas into the chamber. This mechanical pump provides a negative pressure for the chamber down to the level of 10^{-1} mbar (10^{-1} Torr). A gas pressure valve (MDC In-Line Vacuum Valve KIV-200-PAA) was installed for switching on/off the pumping function.

The gas supply offers a specific concentration of O_2 in N_2 . To achieve the target dew point temperature, the supply line was split into two routes. One of which went through the humidifier, bubbled through the H_2O chamber, while the other one bypassed the humidifier. Both routes (dry and wetted gases) merged in a regulator before entering the chamber. The flow rate was controlled by a flowmeter, manufacturing by Dwyer (Model#RMA-6-BV). The accuracy for dew point measurement was $\pm 2^\circ C$. For every CAB experiment in this research, the chamber flow rate was kept at $944 \text{ cm}^3/\text{min}$ ($2 \text{ ft}^3/\text{hr}$). A photo of the gas humidifier and monitoring system is shown in Figure 2-9.

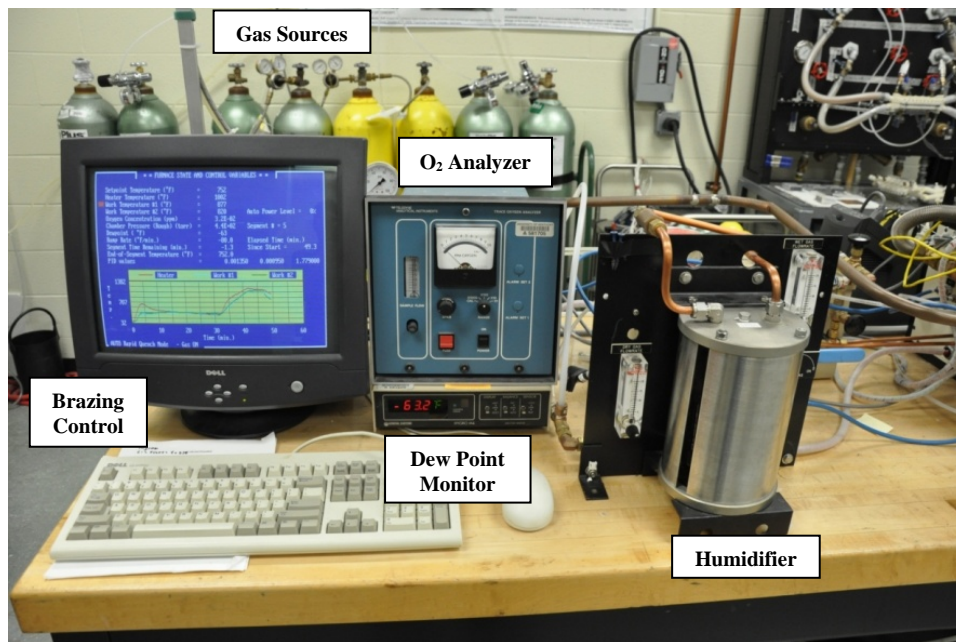
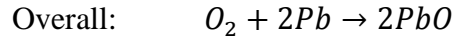
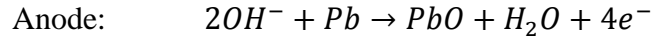
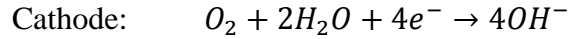


Figure 2-9 Controlling and Monitoring Units of CAB Furnace

The Teledyne Model 316RA Oxygen Analyzer was installed for monitoring the outlet gas from the chamber. The electro-chemical transducer, B2-C, used for detecting

trace oxygen was made of potassium hydroxide (KOH) and pure lead (Pb). The chemical reactions involved with electrochemical process responsible for sensor operation are as follows (Teledyne, 2014):



The above reactions given from the manual are interpreted, to the author's understanding, as follows: the oxygen from the sampling gas diffuses through a Teflon membrane of the sensor and reacts with the existing water molecular and electron at the cathode. A reactive product hydroxide ion oxidizes the existing lead at the anode and results in lead monoxide, water, and electrons. In this matter, oxygen serves as a fuel to the fuel cell (i.e. Model#B2-C sensor) and thus creates a resulting output current.

According to the manual (Teledyne, 1995), the produced current is proportional to the level of oxygen adjacent to the sensor. By monitoring the produced current, the oxygen concentration within the sampling gas is therefore acquired. The oxygen analyzer (Model# 316RA) installed with a B2-C sensor can measure trace oxygen by different scales, ranging 0-10 ppm, 0-100 ppm, 0-1000 ppm, or 0-10000 ppm. The accuracy is $\pm 2\%$ of the selected scale. Response time at 25°C is in average 45 seconds at 0-10 ppm. The higher the oxygen concentration, the shorter time is needed for a stable reading.

The oxygen reading was compared with the gas cylinder specification by measuring a direct input from the gas source. Detailed calibration process will be discussed in Section 2.2.4. A flow meter was integrated in the analyzer which controls the sample gas flow at the volumetric rate of 472 ccm (1 scfh) for each experiment. An estimated equivalent mass flow rate is 9×10^{-6} kg/s. A picture of the oxygen analyzer is shown in Figure 2-9.

The dew point monitor module includes two units: (i) 1311DR Chilled Mirror Sensor and (ii) M4 Hygrometer. Both of them were manufactured by General Eastern which is now a part of General Electric. Figure 2-10 obtained from the manual (GE, 2006)

illustrates the operating diagram of the chilled mirror sensor. A set of LED and a photodetector were integrated within the sensor. These were used for illuminating the condensate mirror, on which a sample gas is impinging, and for collecting the reflection signal. The photodetector will be fully illuminated if the mirror surface is clean with no dew formed. On the contrary, a less illumination will be detected if condensation occurs at the mirror. Another set of LED and photodetector was used as a reference. Signal received is monitored by the M4 Hygrometer (GE, 2006). An image was taken for a view of the chilled mirror unit in Figure 2-11.

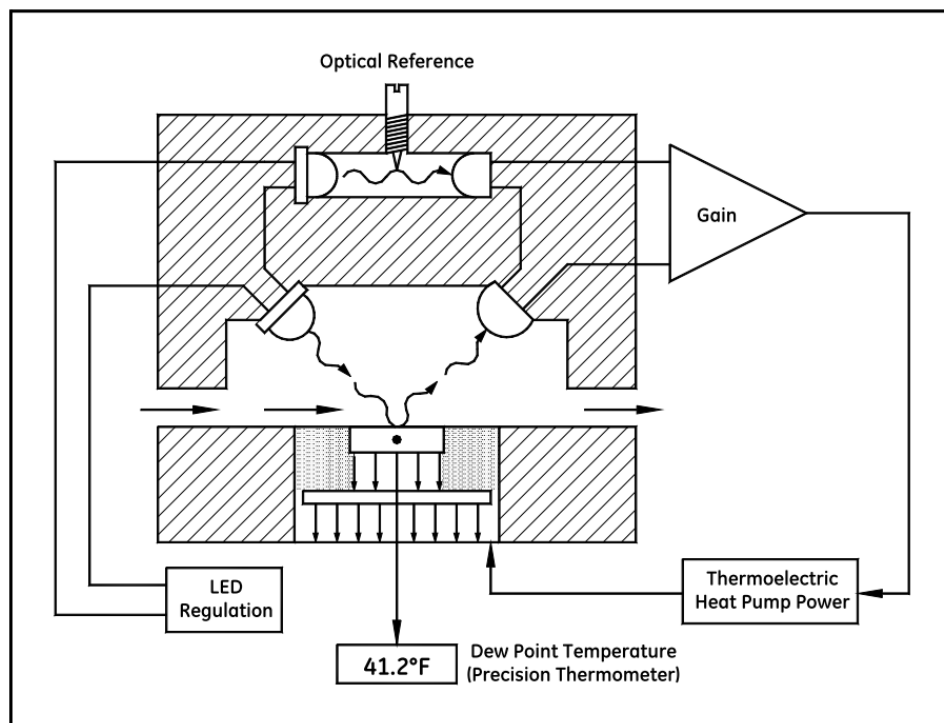


Figure 2-10 Chilled Mirror Sensor Diagram (GE, 2006)

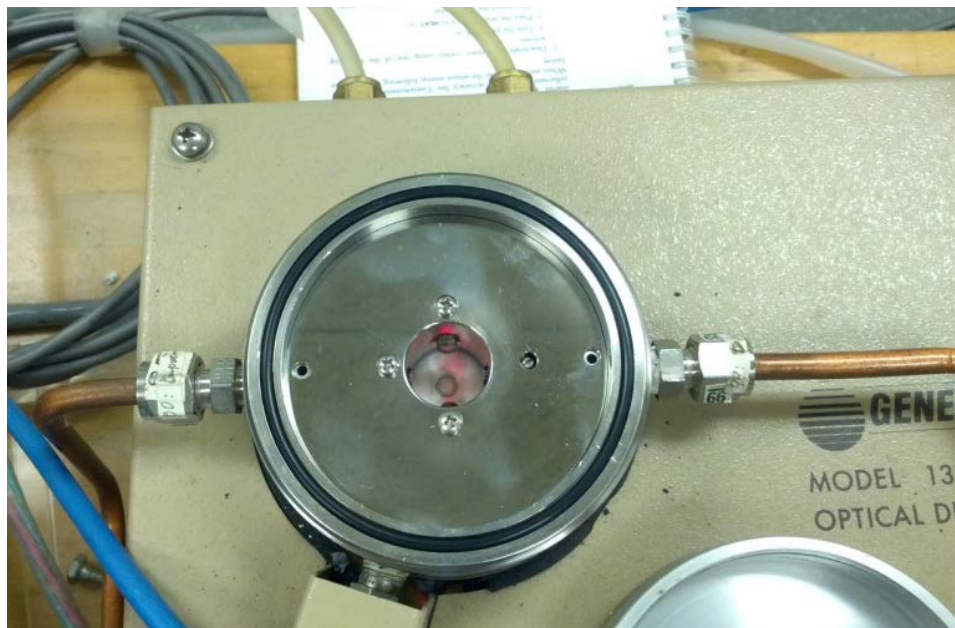


Figure 2-11 Image of Chilled Mirror Unit

The range of operating temperature for dew point sensor is between -80°C and 20°C (-112°F and 68°F). Accuracy of the dew point measurement is $\pm 0.2^{\circ}\text{C}$ ($\pm 0.36^{\circ}\text{F}$) by the factory setting. Response rate is $1.5^{\circ}\text{C}/\text{sec}$. The volumetric flow rate of the sample gas ranges 236 to 2360 ccm (0.5 to 5 scfh). The corresponding mass flow rate ranges $5 \times 10^{-6} \sim 5 \times 10^{-5} \text{ kg/s}$. Calibration results will be given in Section 2.2.4.

Transparent hot zone was assembled out of several layers of clear fused quartz glass tubes. Samples were placed on a SS304 isothermal work platform, which located in the middle of the inner quartz glass hot zone. The inner glass is surrounded by the Joule heating coil which delivers thermal energy to the sample through radiation. A layer of glass with an advanced semi-permeable coating covers the heating coils and reflects thermal radiation portion of the spectrum back into the hot zone, with almost no blockage of the visual light portion of the spectrum. The hot zone system is shown in Figure 2-12.



Figure 2-12 Hot Zone of the CAB Furnace

The brazing process is controlled by a Centorr designed program – “Focus”. Temperature of the sample is registered by Watlow K-type thermocouples and the signal is sent to the control unit (Honeywell UDC 3500). The highest operating temperature that can be reached is 950°C (1742°F). Maximum available heating rate is 35°C/min (63°F/min).

2.2.2 Sample Preparation for a Furnace Test

The source materials are the same as in the hotstage experiments. Specifications and characterization of materials are documented in Section 2.1.2 and Section 2.3. A layout of a furnace sample is presented in Figure 2-13.

The furnace brazing sample has three components: (a) a rectangular substrate was prepared from a brazing sheet in the size of 70 x 39.3 mm², with the clad side facing upward. (b) AA3003 sheet was cut in the size of 50 x 20 mm², served as a mating component for a wedge-tee joint. (c) A 20 mm SS303 stainless steel bar, with 1.6 mm in diameter, was used for creating a variable clearance between the AA3003 sheet and the substrate.

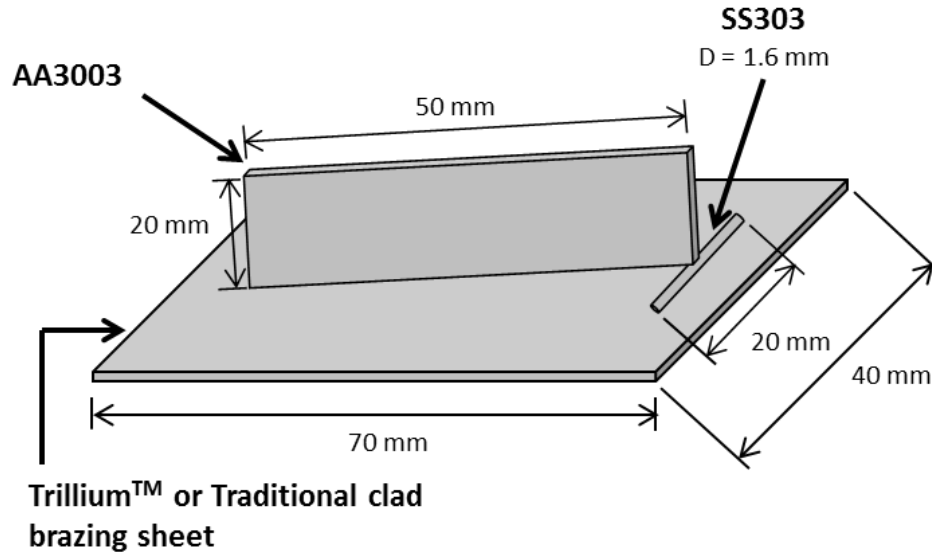


Figure 2-13 Sample Configuration of a Furnace Experiment

The contact point of AA3003 and the substrate located 10 mm away from the sample edge (on the 40 mm side). Stainless steel wire SS304 (0.4 mm in diameter) was used for fixing AA3003 mating plate to the substrate. Since the thickness of a substrate was small, a carbon steel 1018 plate was used as a supporting base below the brazing sheet so that mating components were securely fastened. The bottom surface of the AA3003 plate was manually grinded using a SiC#320 sand paper, in the longitudinal direction (the 50 mm side) in order to secure the same surface condition between tests. The deviation in linear dimensions for each of the components was kept within ± 0.2 mm.

The cleaning procedures were the same as for the hotstage samples (See Section 2.1.2). Both Trillium™ and traditional materials were assembled after a cleaning process, wiped using a tissue wetted by a 190 proof ethanol, and then dried. At this point, Trillium™ brazing sample was ready for a test, shown in Figure 2-14. The traditional brazing sample requires an additional flux addition. In order to keep the same flux loading for each traditional sample, a brazing assembly was weighted before and after the flux addition. A Scientech analytical scale was used for measurement (Model#SA310). The readability is 0.0001 g with the standard deviation of 0.00015 g (Scientech, 2015).

Areas for calculating flux loading were measured by two faces of AA3003 sheet ($2 \times 50 \times 20 \text{ mm}^2$), and the top face of the substrate ($70 \times 39.3 \text{ mm}^2$). For each sample, the measured flux loading was kept as $5\sim 10 \text{ g/m}^2$. Note that an industrial standard for flux loading is 5 g/m^2 (Swidersky, 2001). Flux powders were carefully deposited onto sample surfaces. Then ethanol was added onto the flux powder for brushing, which distributed the flux slurry evenly on mating surfaces. Traditional sample was considered ready for a brazing test when the ethanol has fully evaporated. A traditional sample photo is given in Figure 2-15.

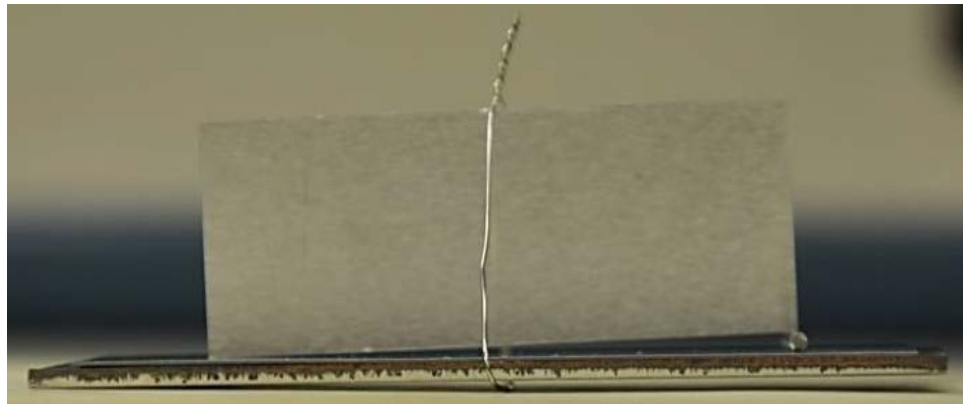


Figure 2-14 Trillium™ Brazing Sample

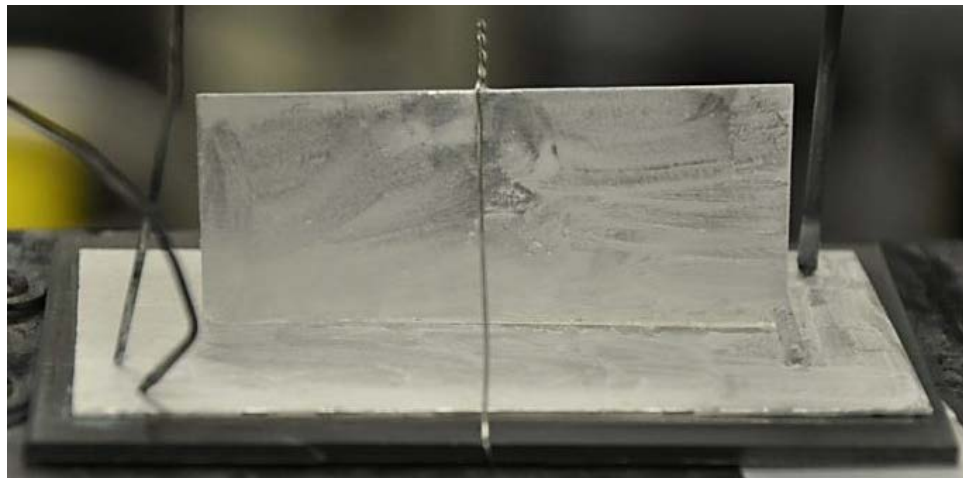


Figure 2-15 Traditional Brazing Sample

During heating in the hot zone, when sample temperature has reached $\sim 577^{\circ}\text{C}$ (the eutectic temperature of Al-Si alloy), the clad started to melt and became liquidized. The molten metal was driven into the gap due to capillary action and the joint fillet was formed after solidification. The length of the joint along the gap was used as a criterion of brazeability assessment.

2.2.3 Atmosphere Condition in the Furnace Chamber

Chamber environment was facilitated by a continuous input of a desired concentration of O_2 mixed N_2 gas source depending on experimental requirement, as explained earlier (Section 2.2.1). Among furnace brazing experiments, the target oxygen concentrations mixed 99.999% nitrogen gas were selected at 2 ppm, 2×10^2 ppm, 2×10^3 ppm, 2×10^4 ppm, and 2×10^5 ppm (the last one is an approximate O_2 concentration to air, without the presence of moisture, i.e. dry air). To ensure the oxygen level in the furnace chamber, the Teledyne 316RA oxygen analyzer was used for monitoring the concentration at the outlet of the hot zone chamber.

Base on the setup provided in Section 2.2.1, different levels of humidity were established by properly adjusting the proportion of dry gas and wet gas steams. The targeted dew point temperature was secured by the dew point monitor system at the outlet of the chamber. Selected target humidity levels were -48°C (-54°F), -18°C (0°F), and -7°C (20°F). The readings were verified by a professional calibration provided by General Eastern, a sub-division of General Electrics, refer to Section 2.2.4 for details.

Both the oxygen analyzer and the dew point sensor were used for monitoring the entire brazing cycle. The volumetric flow rate entering to the furnace chamber was kept at 944 ccm (2 scfh), equivalent to 2×10^{-5} kg/s mass flow rate. Purging process was around 4 to 6 hours depending on whether the dew point and oxygen readings were at targeted levels. Each combination of above conditions (5 different oxygen levels and 3 different dew point levels) was tested with TrilliumTM and traditional materials, and repeated at least three times for securing sufficient statistical confidence.

2.2.4 Verification of the Measurement

The oxygen analyzer and the dew point monitor were used during CAB furnace tests in order to monitor two major variables: (i) humidity level and (ii) oxygen concentration. This section presents the calibration processes for the oxygen analyzer and the dew point monitor system.

To establish a difference in the composition between readings from the oxygen analyzer and a supplied gas source, an on-site calibration process was performed based on the user's manual by Teledyne (Teledyne, 1995). A certified gas source with 500 ppm oxygen mixed 99.999% nitrogen provided by Scott-Gross was directly measured by the oxygen analyzer for the calibrating process. The volumetric flow rate was kept at 472 ccm (1 scfh). The potentiometer was unlocked and adjusted until the reading of O₂ concentration reached 500 ppm, the same concentration as the calibration gas source. Subsequently, the potentiometer was locked and the analyzer was used to measure the other gas source with various oxygen concentrations in individual experiments. Readings of O₂ vs. time for 2 ppm, 200 ppm, and 2000 ppm O₂ gas sources were presented in Figure 2-16, 2-17, and 2-18, respectively.

In Figure 2-16, four repeated runs for a 2 ppm oxygen source are presented. It shows that the oxygen level reads less than 20 ppm and higher than 11 ppm after 2 hours. Range of O₂ level between 10 and 16 ppm was found after 8 hours. Note that the lowest reading was 10 ppm even though it was obtained from a 2 ppm certified gas source for a prolonged period of time. Figure 2-17 for a 200 ppm source shows that oxygen readings reached 210 ppm after 30 minutes. In Figure 2-18, the reading of a 2000 ppm oxygen source was 2000 ppm after 5 minutes, and it was stable afterward with an error within 100 ppm. From the data above, it can be seen that the oxygen analyzer shows a good agreement with the certified concentrations of oxygen sources (with 2% error of selected measuring scales, i.e. 0-10 ppm, 0-100 ppm, 0-1000 ppm, or 0-10000 ppm) except for the 2 ppm level. Throughout the whole sequence of tests, a value of 20 ppm oxygen concentration is conservatively selected to represent the 2 ppm gas source due to the limitation of the oxygen analyzer. The certified information for gas sources was given in Appendix A.

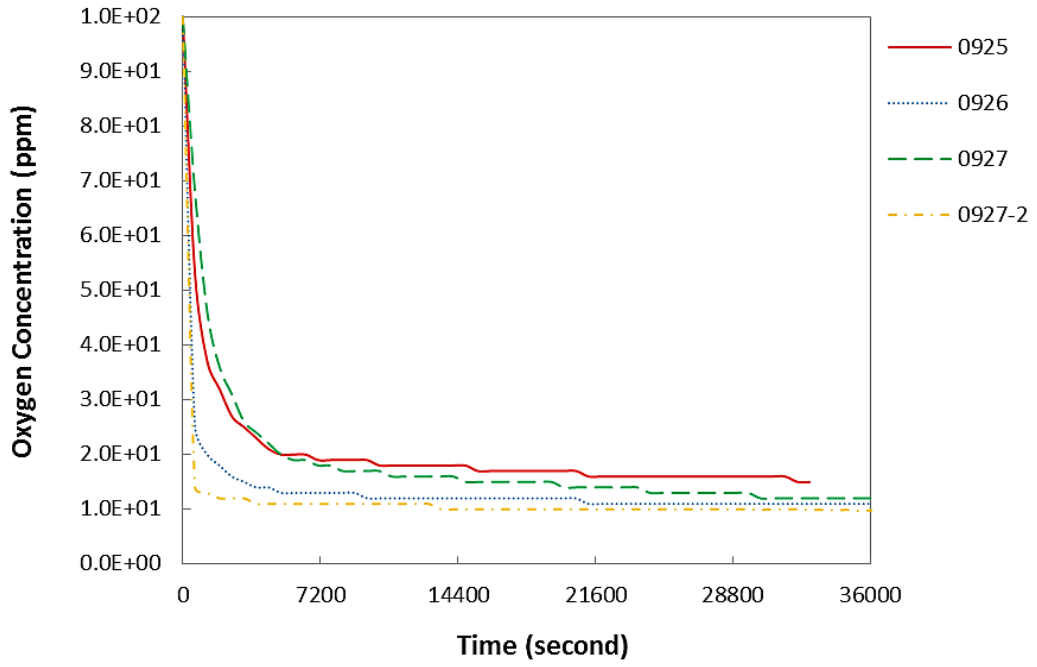


Figure 2-16 2 ppm Oxygen Direct Input History

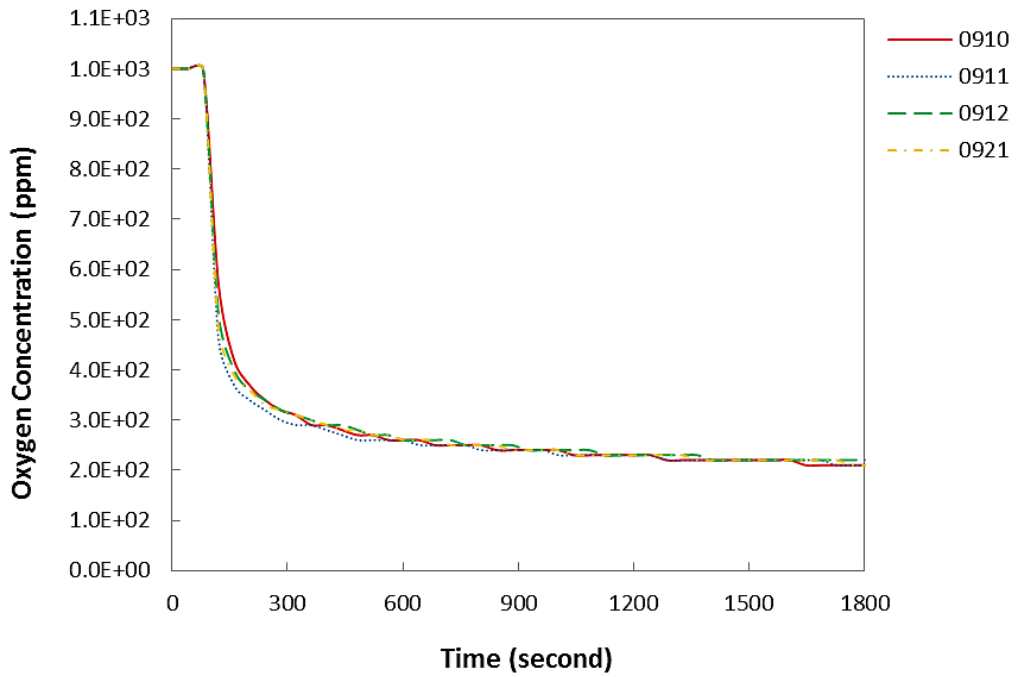


Figure 2-17 200 ppm Oxygen Direct Input History

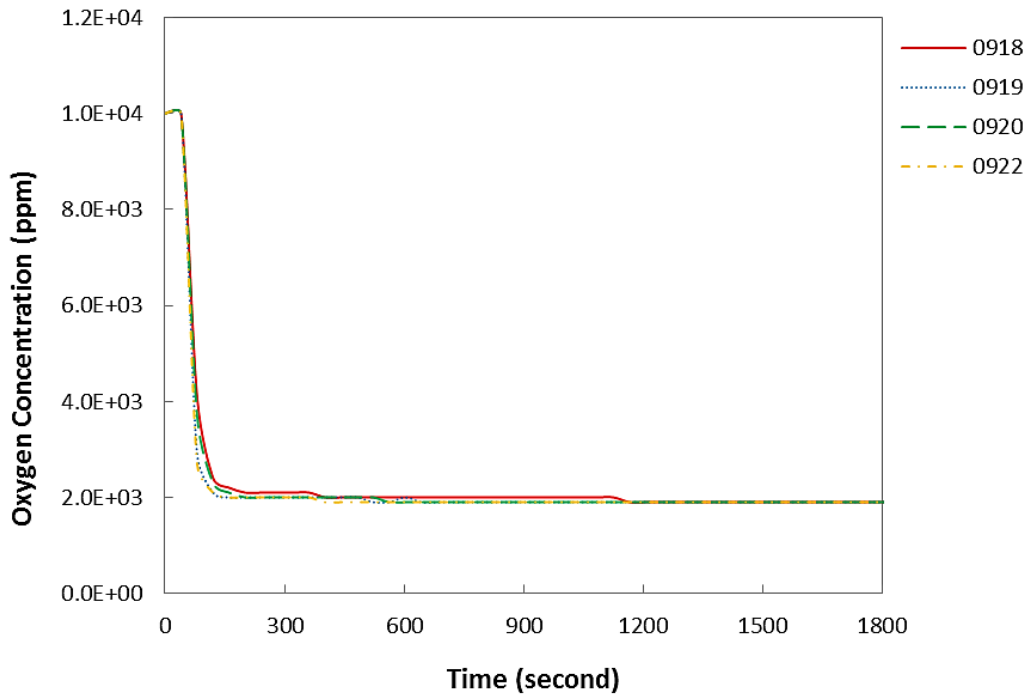


Figure 2-18 2000 ppm Oxygen Direct Input History

The dew point monitor system was sent to General Electric Sensing (GE Sensing) for a professional calibration. Measured values between the dew point monitor system (un-adjusted) and GE’s calibrating instrument are given in Table 2-1. Details of the calibration report are presented in Appendix B. The result shows good agreement between the dew point monitor system and the professional calibration instrument from GE Sensing. Therefore, the dew point data of the atmosphere obtained from the dew point monitor are verified with a great accuracy, an error within 0.2°F.

Table 2-1 Result of Calibration

GE Standard Dew Point (°F)	Customer Unit Dew Point (°F)	Difference (°F)
-55.48	-55.68	0.20
-0.63	-0.78	0.15
19.24	19.10	0.14
32.02	31.89	0.13
42.00	41.80	0.20

2.2.5 Brazing Temperature History

When the oxygen and dew point reached the desired levels, a brazing process was initiated. The heating started with 35°C/min, followed by a dwell around 200°C for 30 minutes, subsequent heating (35°C/min) to 600°C followed by a dwell of 2 minutes, and rapid quenched to 400°C. The same temperature profile was achieved and fixed for each of the experiments. A plot of the temperature profile is offered in Figure 2-19. A photo taken during a brazing process of the CAB transparent furnace is shown in Figure 2-20.

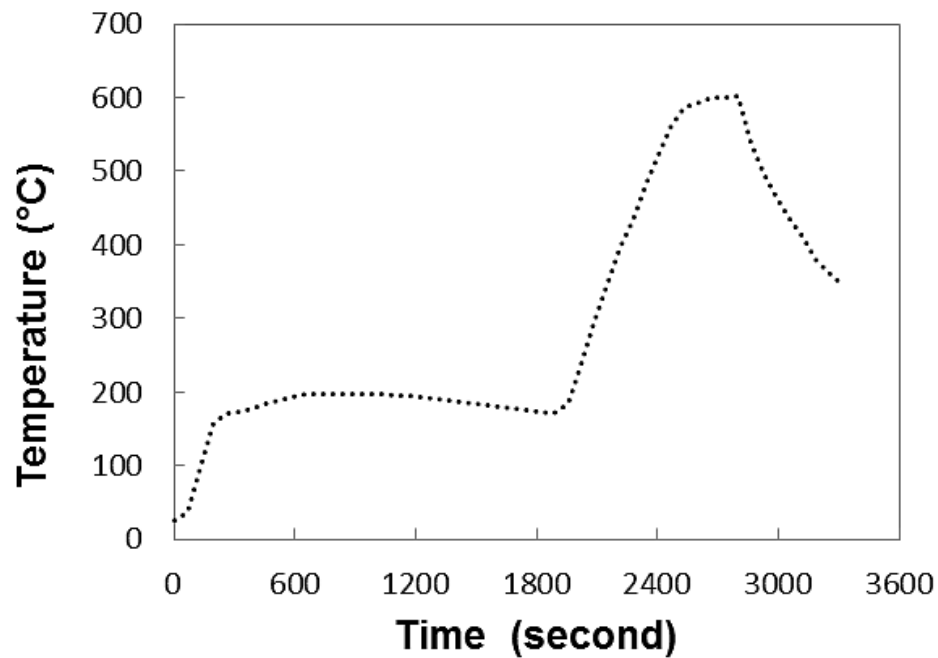


Figure 2-19 Temperature History of a Furnace Brazing Process

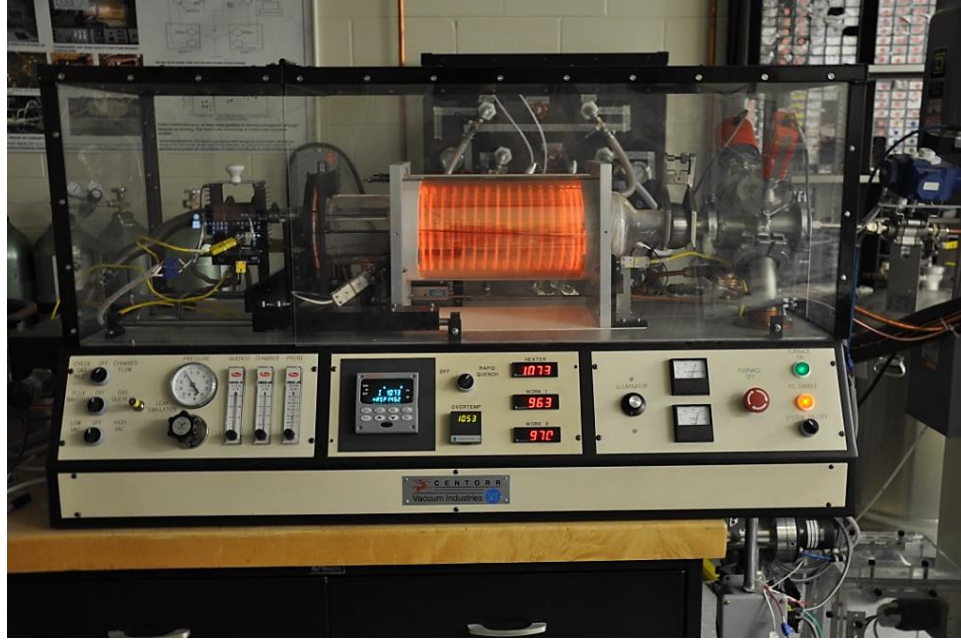


Figure 2-20 Brazing by CAB Furnace

2.3 Material Characterization

The clad layer uniformity with respect to the given brazing sheet gauge will be addressed in this section, including the brazing sheet thickness and the clad thickness all before brazing – i.e., material as received. Subsequently, a series of SEM/EDS studies will be provided to characterize the materials.

2.3.1 Verification for Uniformity of Brazing Sheets

Both Trillium™ and traditional brazing sheets before brazing were partitioned and polished for a verification of the given specification data including

- (1) Sheet thickness
- (2) Clad thickness
- (3) Clad alloy (silicon expected)
- (4) Core alloy (manganese expected)

These auxiliary tests have been performed using an optical microscope, SEM, and EDS. The traditional brazing sheet was partitioned into 10 segments and numbered from 1 to 10. Each partitioned specimen was 10 mm in width except for the last piece (10th

specimen), see Figure 2-21. The width of the source Trillium™ brazing sheet was narrower (~39 mm) than the provided traditional sheet (~97 mm). In Figure 2-22, total of 4 segments were cut with 10 mm in width for each Trillium™ material specimen except for the last one (4th). These specimens were mounted, polished, and micro-photographed for further measurement. Figure 2-23 ~ 2-24 demonstrate the measured thicknesses of the brazing sheet and the clad, using the Image Pro Plus software. As shown in Figure 2-23, three spatially distinct horizontal control lines (marked in red) were used to identify the characteristic interfaces between the clad layer and the core zone. The average values of the sheet thickness and the clad thickness for each numbered cross-section were obtained and tabulated in Table 2-2. The statistics of measured data is presented in Table 2-3. According to the measurement, Trillium™ brazing sheet shows uniform thicknesses for sheet and clad among the numbered specimen, whereas the traditional brazing sheet has an irregularity at the edge (located at 10th). Based on this nature, traditional test samples were produced only from locations between #1 and #9 from the source sheet of the traditional material.

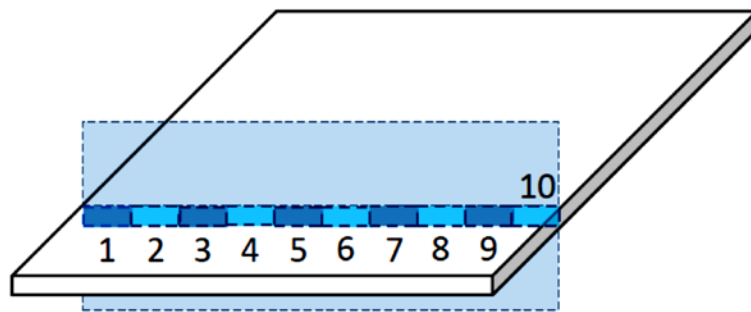


Figure 2-21 Numbered Cross-Sections of a Traditional Brazing Sheet

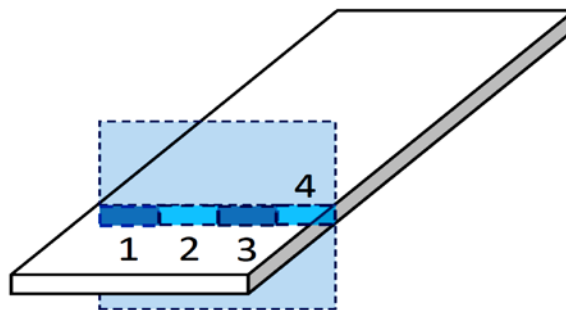


Figure 2-22 Numbered Cross-Sections of a Trillium™ Brazing Sheet

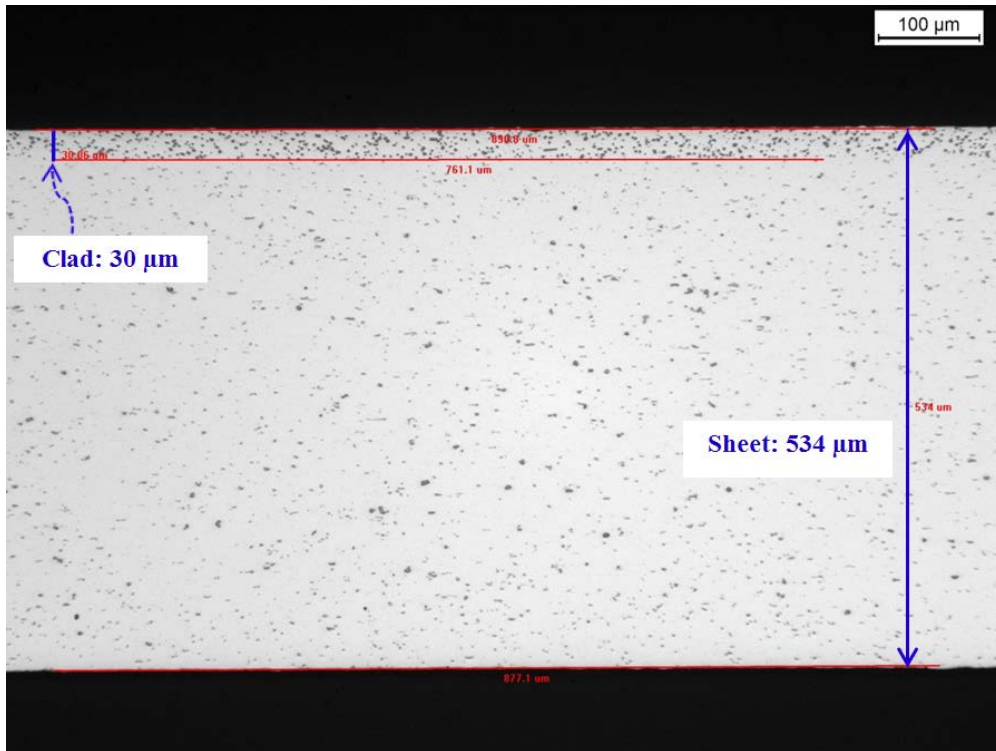


Figure 2-23 Measurement for the Sheet and Clad Thicknesses of a Traditional Sample

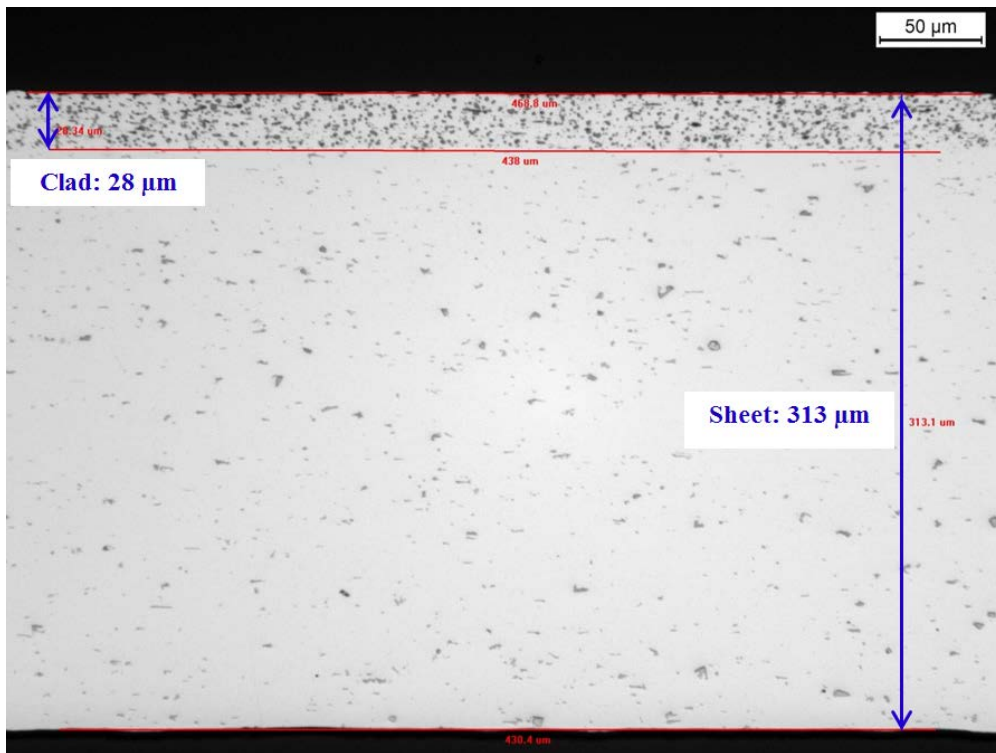


Figure 2-24 Measurement for the Sheet and Clad Thicknesses of a Trillium™ Sample

Table 2-2 Clad and Sheet Thicknesses of the Traditional and Trillium™ Brazing Sheets

Specimen #	1	2	3	4	5	6	7	8	9	10
Traditional Sheet Thickness (μm)	526	535	534	533	532	536	532	533	532	504
Trillium™ Sheet Thickness (μm)	311	311	314	312						
Traditional Clad Thickness (μm)	28	30	33	31	31	30	31	29	29	21
Trillium™ Clad Thickness (μm)	28	28	30	28						

Table 2-3 Summary of the Measurement in Table 2-2

	Avg	Max	Min	Standard Deviation	+Error	-Error	Avg Error
Traditional Sheet Thickness (μm)	533	536	526	2.9	3	7	
Trillium™ Sheet Thickness (μm)	312	314	311	1.3	2	3	
Traditional Clad Thickness (μm)	30	33	28	1.5	3	2	±3
Trillium™ Clad Thickness (μm)	29	30	28	1.0	1	1	±1

2.3.2 SEM/EDS Verification for Materials

Trillium™ and traditional source sheets (prior to brazing processes) were polished and the Si and Mn contents have been traced at two locations: (1) clad domain and (2) core zone. Instruments involved were Hitachi S-3200 Scanning Electron Microscopy (SEM) with Energy Dispersive X-ray Spectroscopy (EDS) detector. Results were illustrated by Figures 2-25 ~ 2-28. The Si contents at selected locations of the clad area for both samples were around 10%, similar to the feature of a typical AA4045 aluminum alloy. Areas deep into the core have no Si content detected for both brazing sheets, as expected. 1.8 wt.% and 2.5 wt.% of Mn (manganese) were identified for Trillium™ and traditional cores, respectively, as expected for an aluminum alloy AA3003).

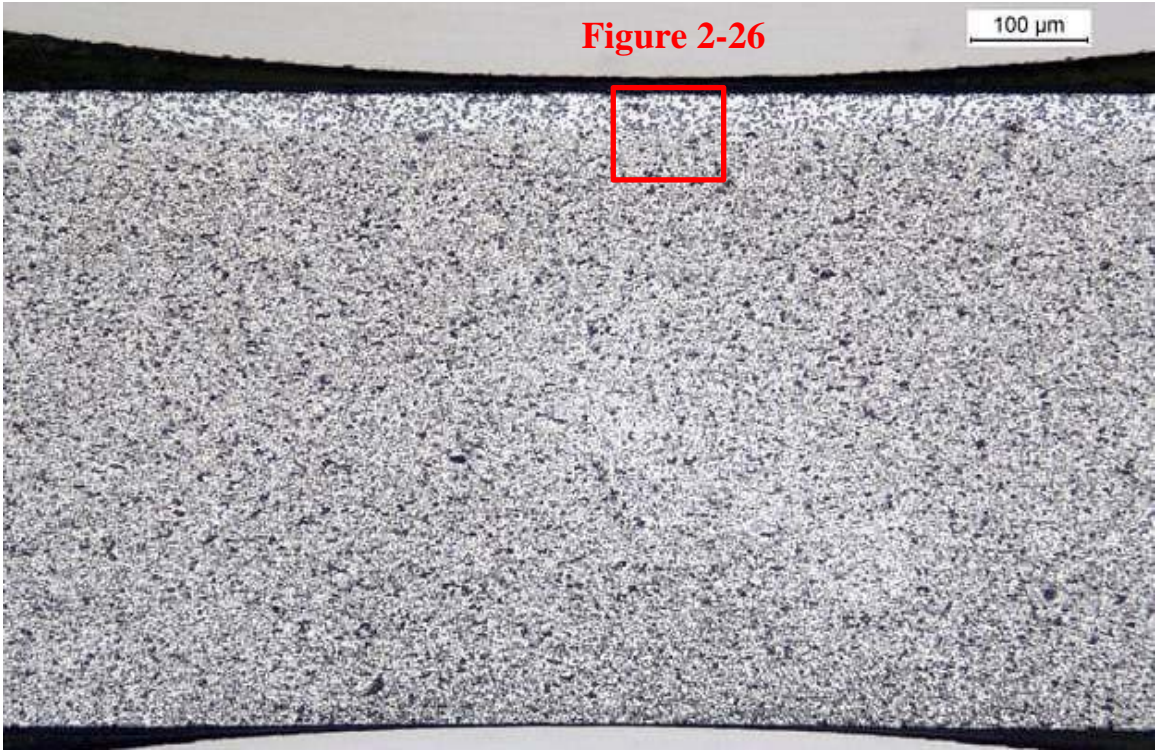
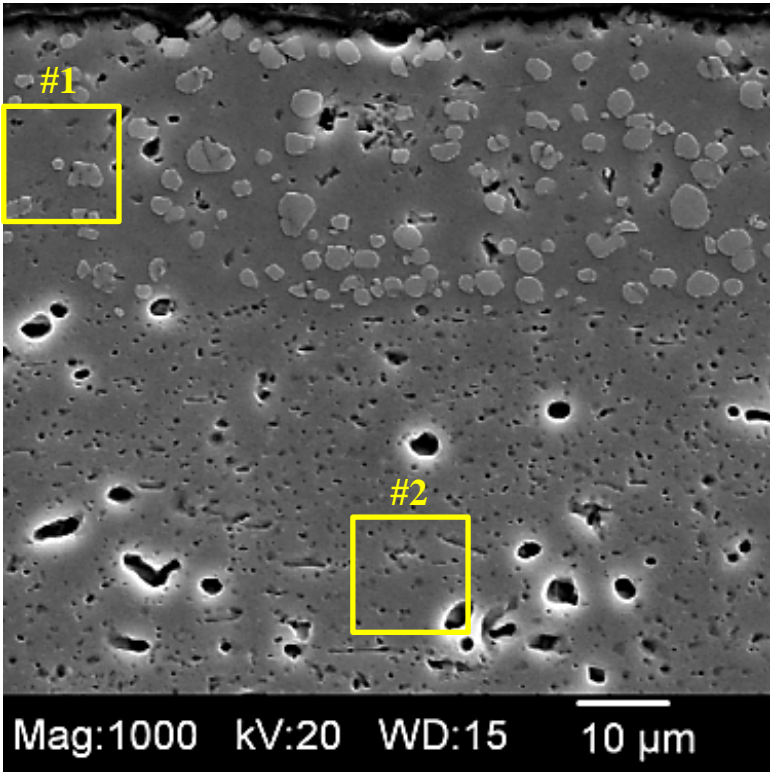


Figure 2-25 SEM Image of a Traditional Brazing Sheet



#1 – Clad Area

Elements:	WT%	AT%
AlK	90.5	90.83
SiK	9.5	9.17
MnK	0	0

#2 – Core Area

Elements:	WT%	AT%
AlK	97.5	98.76
SiK	0	0
MnK	2.5	1.24

Figure 2-26 EDS Result for a Traditional Brazing Sheet

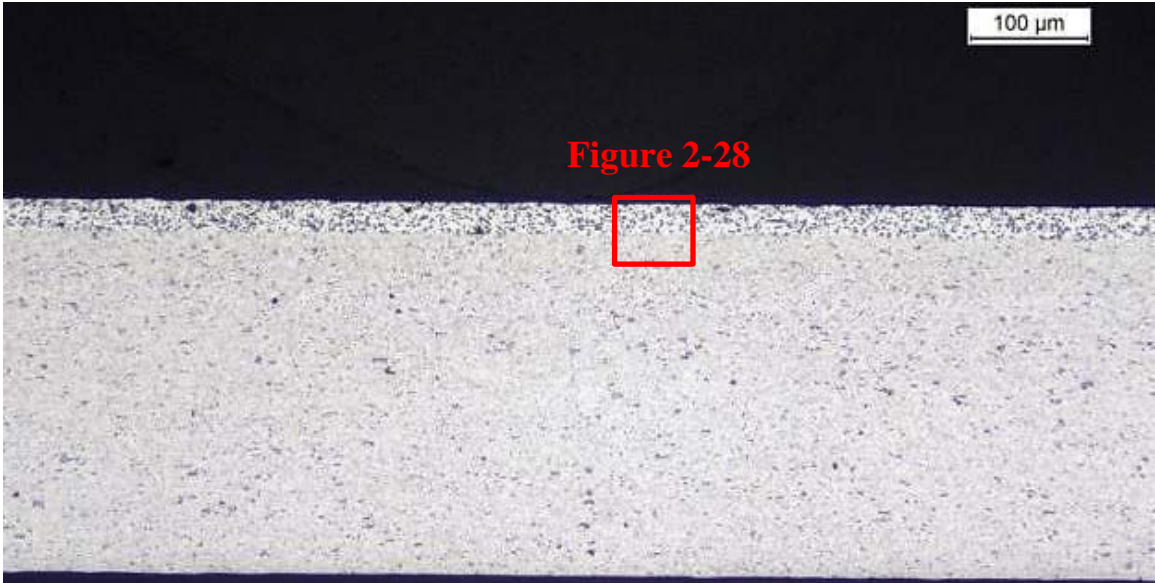
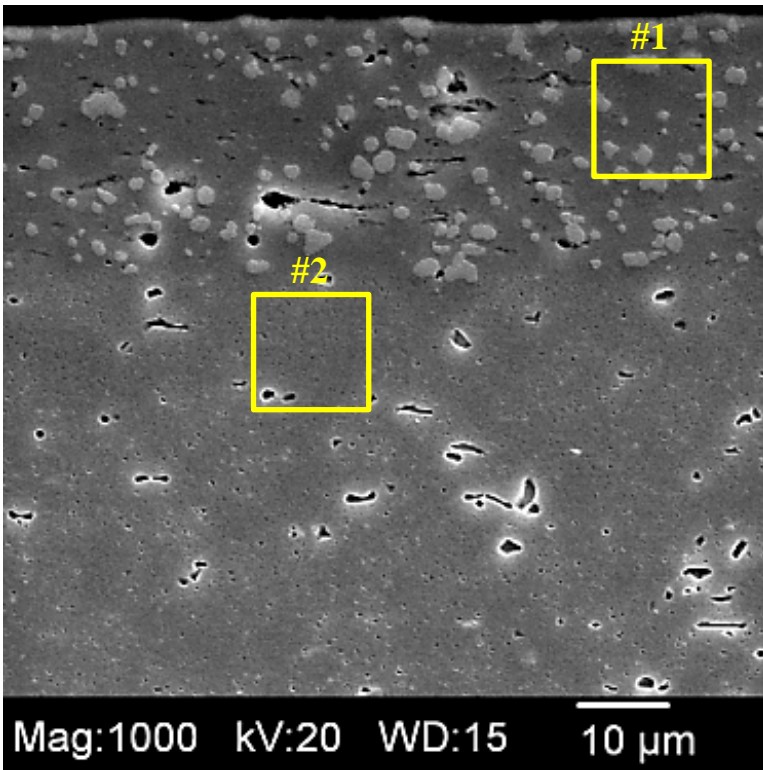


Figure 2-27 SEM Image of a Trillium™ Brazing Sheet



#1 – Clad Area

Elements:	WT%	AT%
AlK	89.96	90.32
SiK	10.04	9.68
MnK	0	0

#2 – Core Area

Elements:	WT%	AT%
AlK	98.25	99.13
SiK	0	0
MnK	1.75	0.87

Figure 2-28 EDS Result for a Trillium™ Brazing Sheet

CHAPTER 3: Result and Discussion – Hotstage Experiments

In this chapter, the summary of the experimental work aimed at a study of the brazing performance of both (i) Trillium™ and (ii) traditional brazing material under different atmosphere conditions is presented and discussed. Each test under a given oxygen concentration was repeated three times. Additional experimental data are presented in Appendix C. The experiments were performed using hotstage microscopy.

3.1 Results of Hotstage Experiments

In all experiments the variable parameter is oxygen concentration. The description of the experimental facility and experimental procedures are given in Sections 2.1.1 ~ Section 2.1.3. Other controlled parameters are:

- dew point temperature ($< -48^{\circ}\text{C}$)*,
- heating ramp rate ($+100^{\circ}\text{C}/\text{min} \pm 0.1^{\circ}\text{C}$)[†],
- peak temperature ($600^{\circ}\text{C} \pm 0.1^{\circ}\text{C}$),
- dwel time (2 min), and
- cooling ramp rate ($-100^{\circ}\text{C} \pm 0.1^{\circ}\text{C}$).

Pictures in Table 3-1 taken with a microscope offer the top view of samples as a visual representation of in situ brazing for corresponding descriptive characterizations given in Table 3-2. Table 3-2 offers a descriptive summary of the result. Figures 3-1 ~ 3-6 and Figures 3-7 ~ 3-12 provide two sets of pictures, before and after brazing processes for Trillium™ and traditional brazing sheets, respectively. Figure 3-13 (a) ~ (j) and Figure 3-14 (a) ~ (j) in Section 3.2 demonstrate clad surface features during the brazing process for both materials. In section 3.3, Figures 3-15 ~ 3-26 present the visual joint appearance of both materials taken for a macroscopic study.

Various brazed results are presented in Table 3-1. It is the top view through the window of the hotstage chamber. One can see that in the middle of a photo, there is a

* This is an estimated value. By measuring the oxygen level in the hotstage, it is believed that when oxygen level reaches the level from the sourcing gas, the humidity will be also close to the condition of the sourcing gas. As measured by transparent furnace system, the measured humidity value for the sourcing gas is $< -54^{\circ}\text{F}$ (-48°C). Note that the dew point measurement system was not connected to the exhaust of the hotstage.

[†] Temperature stability 0.1°C is provided by the hotstage manufacturer. See Section 2.1.1.

rectangular profile which represents the AA3003 strip, refer to Figure 2-5. The areas outside the rectangular are surfaces with either Trillium™ or traditional clad. The bright domains on two sides of the AA3003 strip, see the photo in the first row, are reflecting the auxiliary lights illuminated onto the meniscus joints. Irregular joint fillets feature less bright domains.

Table 3-1 Descriptive Visual Characterizations

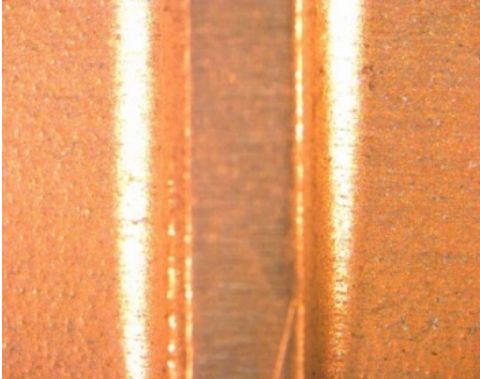


Category	Description	Brazen Sample
Uniform spreading	<ul style="list-style-type: none"> • Spreading is uniform • Joint between the mating surfaces is consistent 	
Partially uniform/non-uniform spreading	<ul style="list-style-type: none"> • Spreading is not uniform • Irregular joint formation appeared 	
Poor spreading or no spreading	<ul style="list-style-type: none"> • Only a localized spreading occurred 	

Table 3-2 Summary of Hotstage Experiments

Oxygen (ppm)	Trillium™ Brazing Sheet	Traditional Brazing Sheet
2×10^1	<ul style="list-style-type: none"> • Consistent joint formation • Uniform spreading & fillet formation 	<ul style="list-style-type: none"> • One out of three samples features somewhat less uniform spreading • Other samples feature uniform spreading
2×10^2	<ul style="list-style-type: none"> • Consistent joint formation • Uniform spreading & fillet formation 	<ul style="list-style-type: none"> • Consistent joint formation • Smooth spreading & fillet formation
5×10^2	<ul style="list-style-type: none"> • Consistent joint formation • Uniform spreading & fillet formation 	<ul style="list-style-type: none"> • Two of samples feature non-uniform spreading • One sample features uniform spreading
2×10^3	<ul style="list-style-type: none"> • Consistent joint formation • Uniform spreading & fillet formation 	<ul style="list-style-type: none"> • Inconsistent • Two samples with no spreading but poor joint formation exists • One sample features marginal spreading
2×10^5 (in air)	<ul style="list-style-type: none"> • Inconsistent joint formation • One observed case with a partial bonding but no visible molten clad spreading • One observed case with no bonding 	<ul style="list-style-type: none"> • No bonding • The melting of clad was not visible • Two samples feature visible re-solidification • One sample does not feature re-solidification

For each oxygen concentration, one representative sample was selected out of three repeated tests and presented. Microscopic views of Trillium™ material at different oxygen levels before and after brazing are presented in Figures 3-1 ~ 3-6. Traditional samples are presented in Figures 3-7 ~ 3-12. The same samples as given in Figures 3-1 ~ 3-12 were also photographed by a digital camera and presented by three different angles of macroscopic views, as shown in Figures 3-15 ~ 3-26.

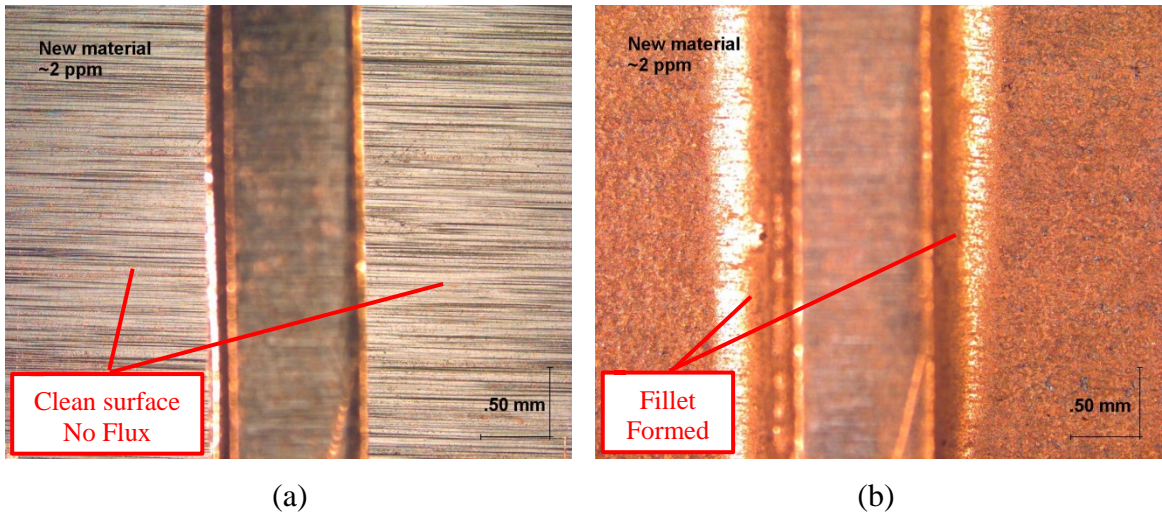


Figure 3-1 Trillium™ Brazing Sheet in 20 ppm* O₂ (a) Before and (b) After the Brazing Process

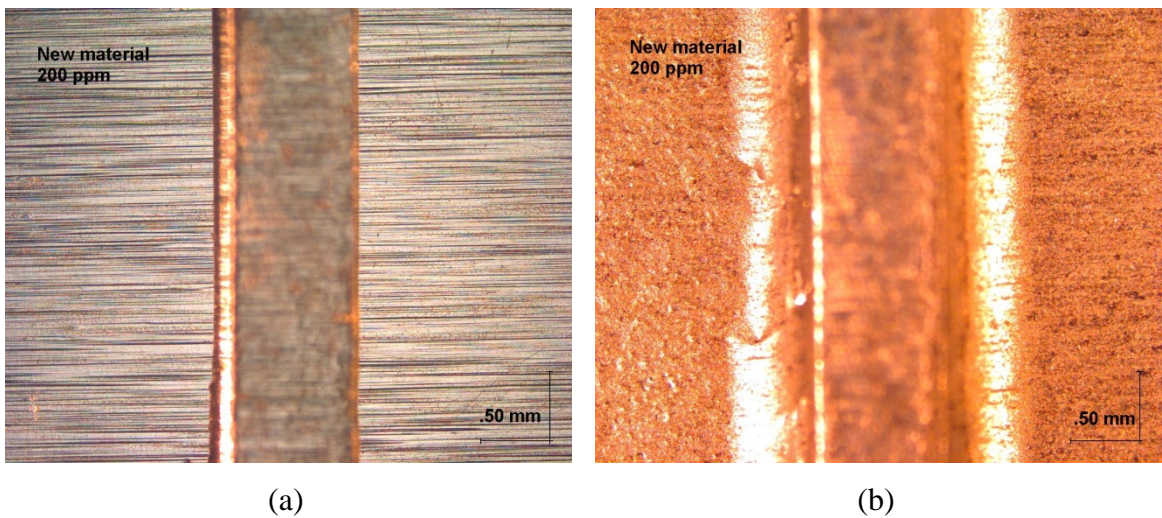
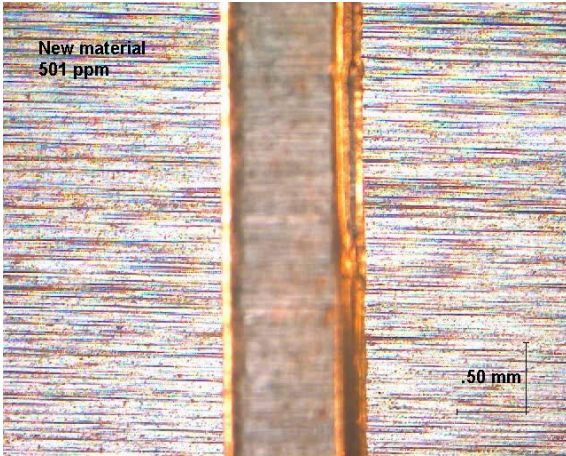
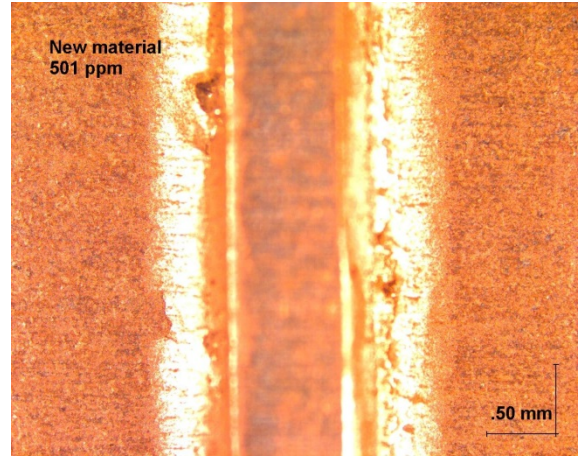


Figure 3-2 Trillium™ Brazing Sheet at 200 ppm O₂ (a) Before and (b) After the Brazing Process

* As stated in Section 2.2.4, the value of 20 ppm O₂ is a conservatively selected value representing a 2 ppm gas source.

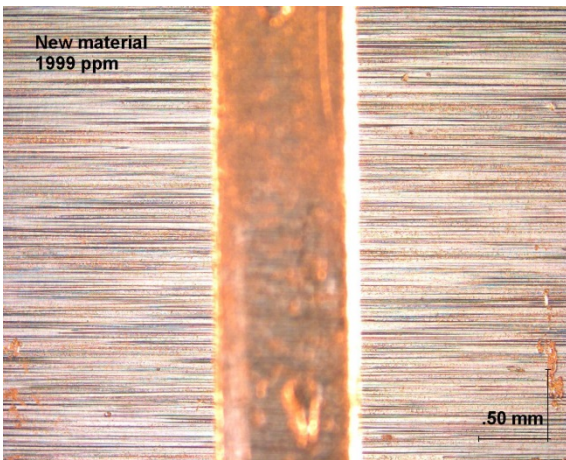


(a)

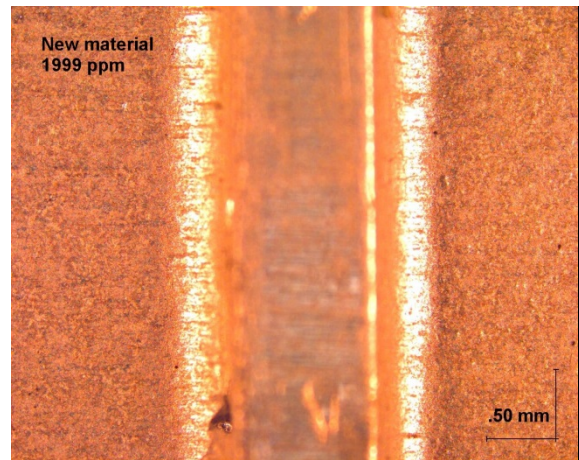


(b)

Figure 3-3 Trillium™ Brazing Sheet at 500 ppm O₂ (a) Before and (b) After the Brazing Process



(a)



(b)

Figure 3-4 Trillium™ Brazing Sheet at 2000 ppm O₂ (a) Before and (b) After the Brazing Process

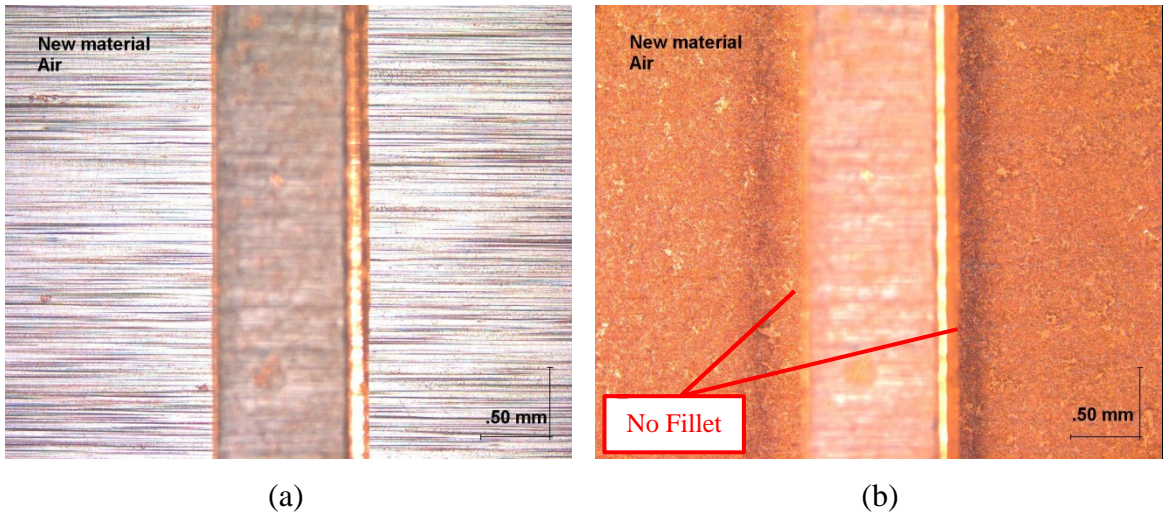


Figure 3-5 Trillium™ Brazing Sheet in Air (a) Before and (b) After the Brazing Process. Test I.

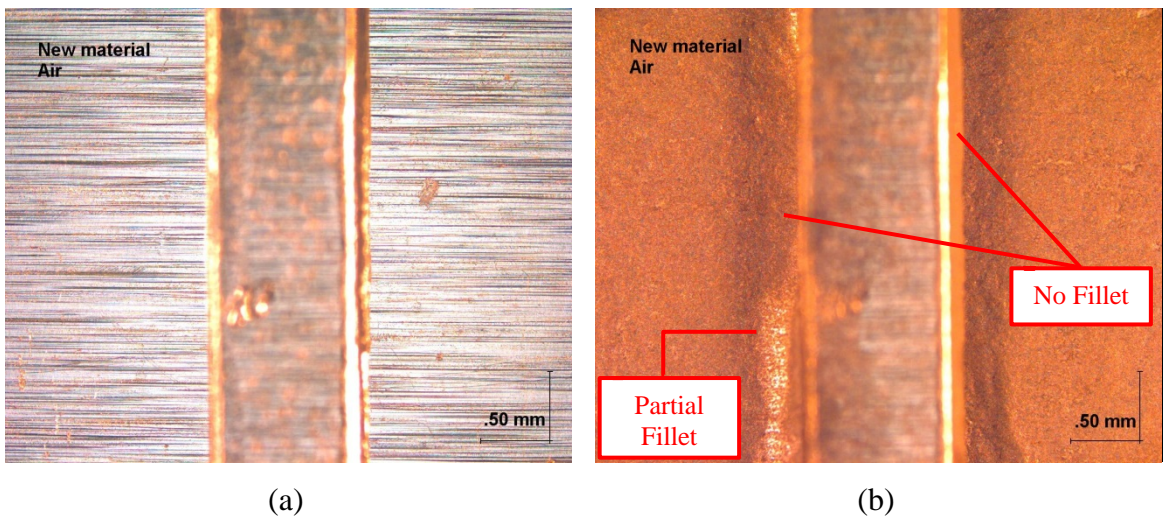


Figure 3-6 Trillium™ Brazing Sheet in Air (a) Before and (b) After the Brazing Process. Test II.

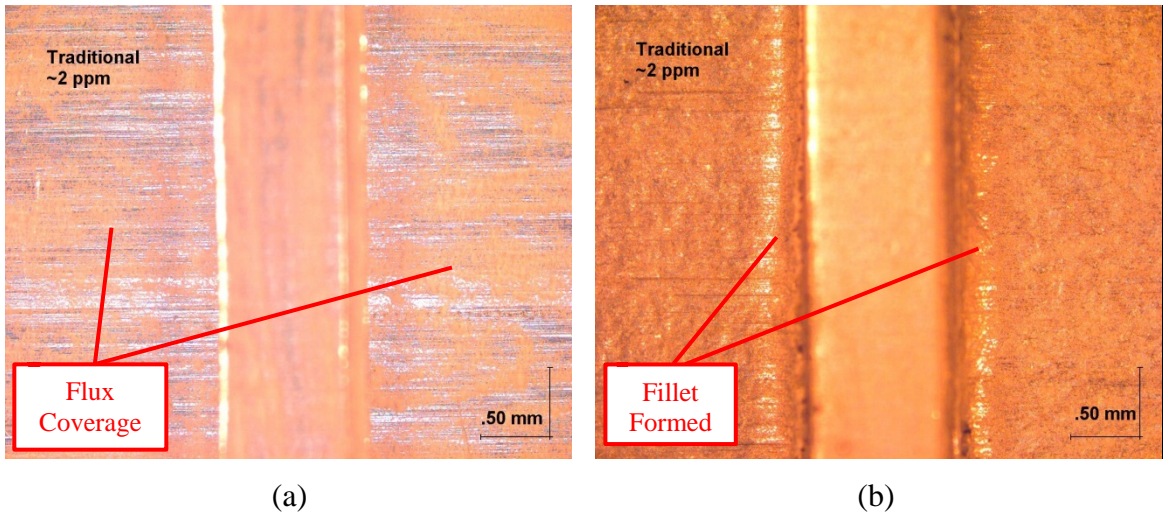


Figure 3-7 Traditional Brazing Sheet in 20 ppm O₂ (a) Before and (b) After the Brazing Process

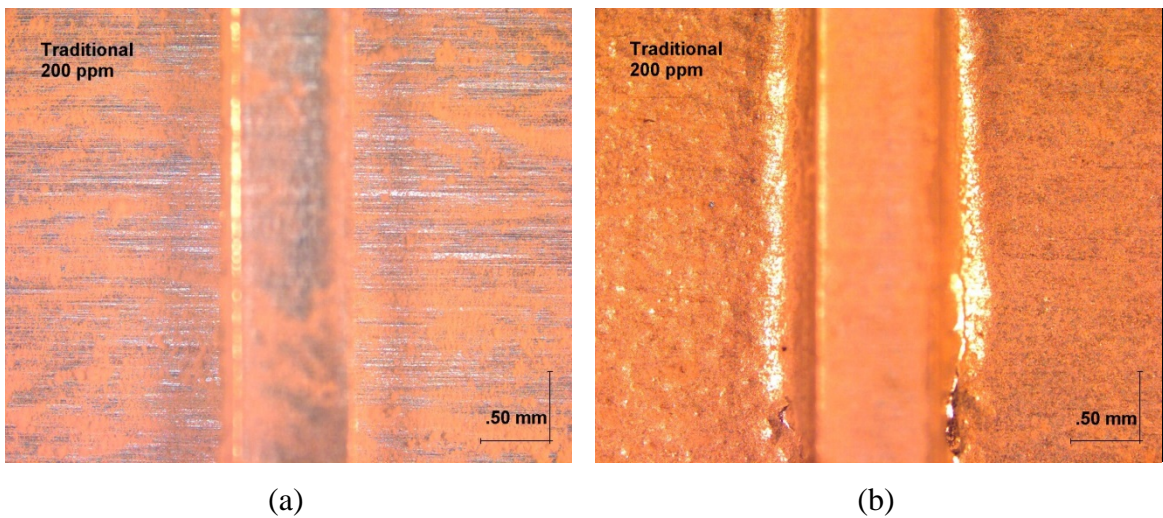


Figure 3-8 Traditional Brazing Sheet in 200 ppm O₂ (a) Before and (b) After the Brazing Process

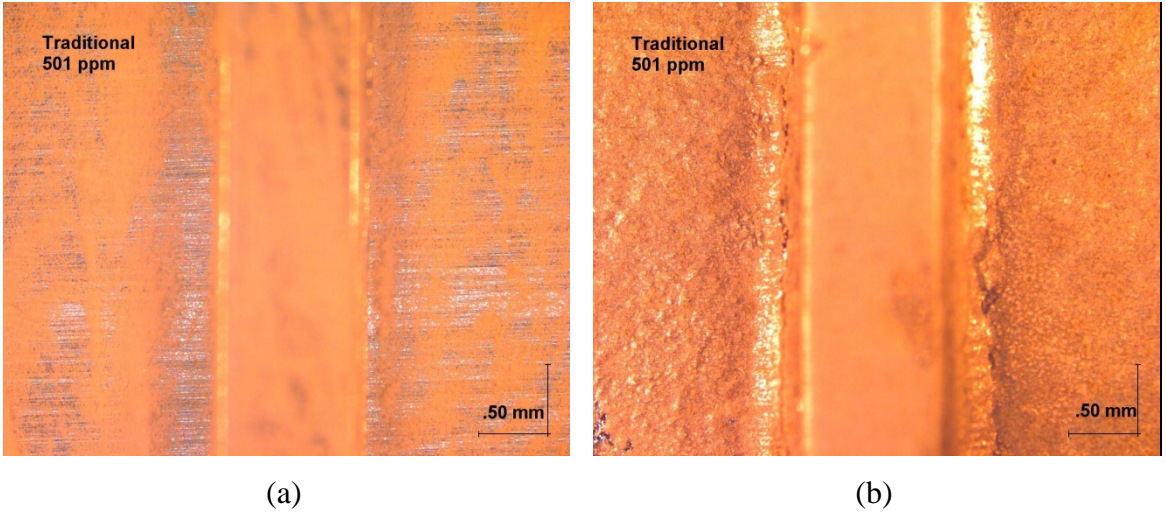


Figure 3-9 Traditional Brazing Sheet in 500 ppm O₂ (a) Before and (b) After the Brazing Process

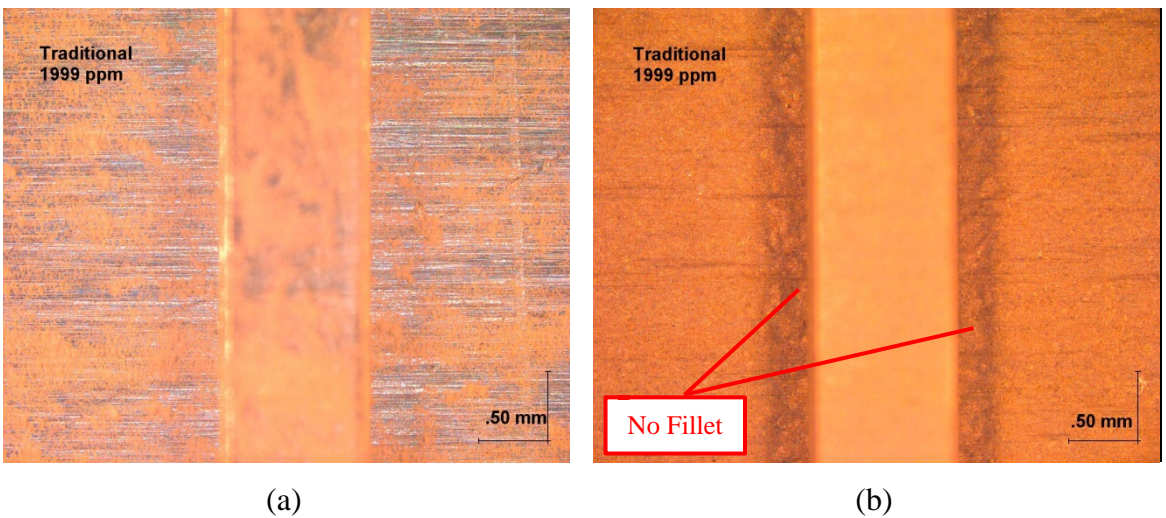


Figure 3-10 Traditional Brazing Sheet in 2000 ppm O₂ (a) Before and (b) After the Brazing Process. Test I.

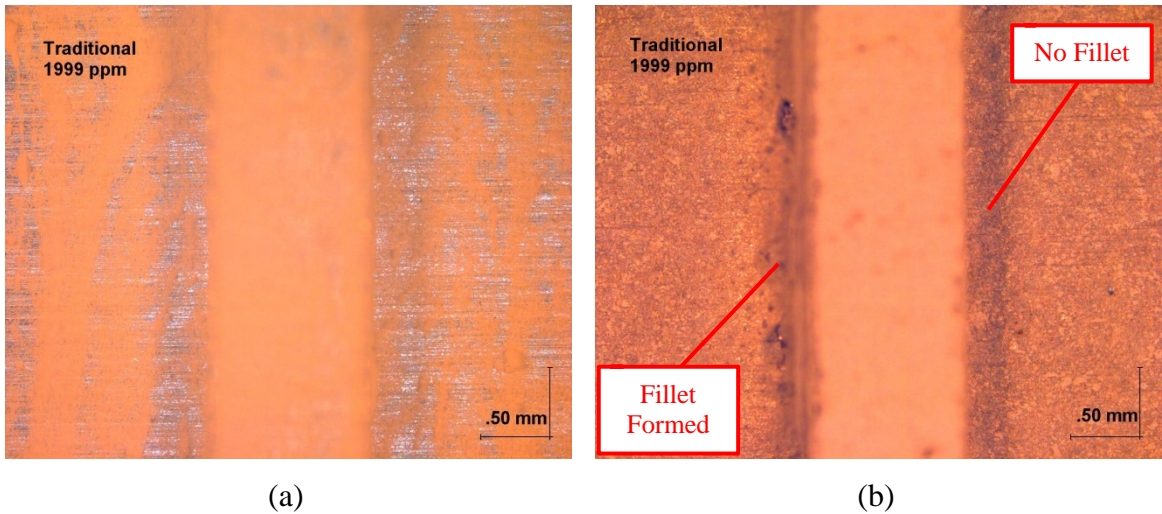


Figure 3-11 Traditional Brazing Sheet in 2000 ppm O₂ (a) Before and (b) After the Brazing Process. Test II.

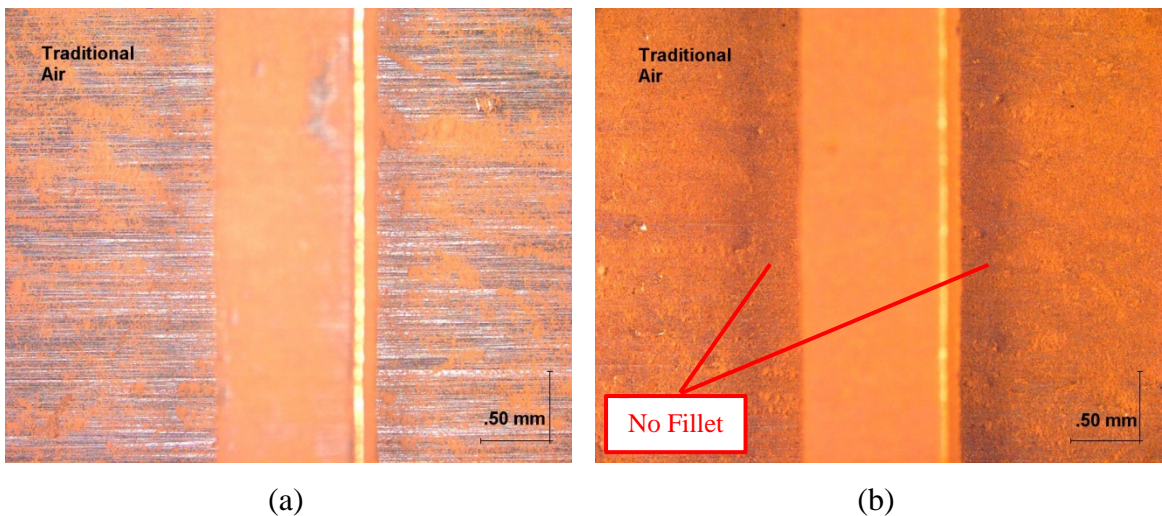


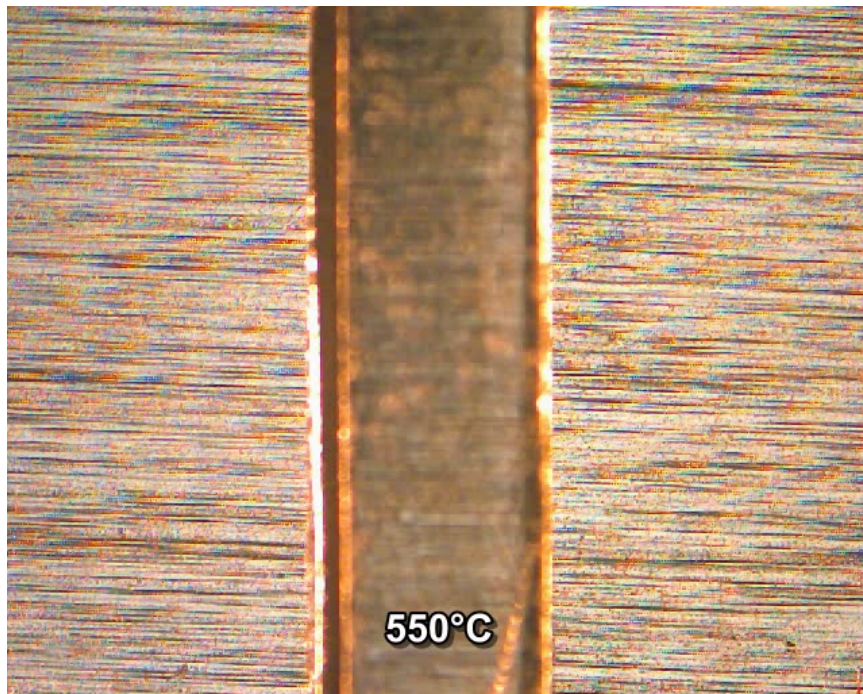
Figure 3-12 Traditional Brazing Sheet in Air (a) Before and (b) After the Brazing Process.

According to Figures 3-1 (b), 3-2 (b), 3-3 (b), and 3-4 (b), we may see that Trillium™ brazing sheet has successful and consistent joint fillet formation up to 2000 ppm oxygen. The traditional material has successful and consistent joint fillet formation up to 500 ppm O₂ (Figures 3-7 (b), 3-8 (b), and 3-9 (b)), however, the traditional sample has either irregular partial joint formation (Figure 3-11 (b)) or no joint formation (Figure 3-10 (b)) in the environment of 2000 ppm oxygen. Neither one of both

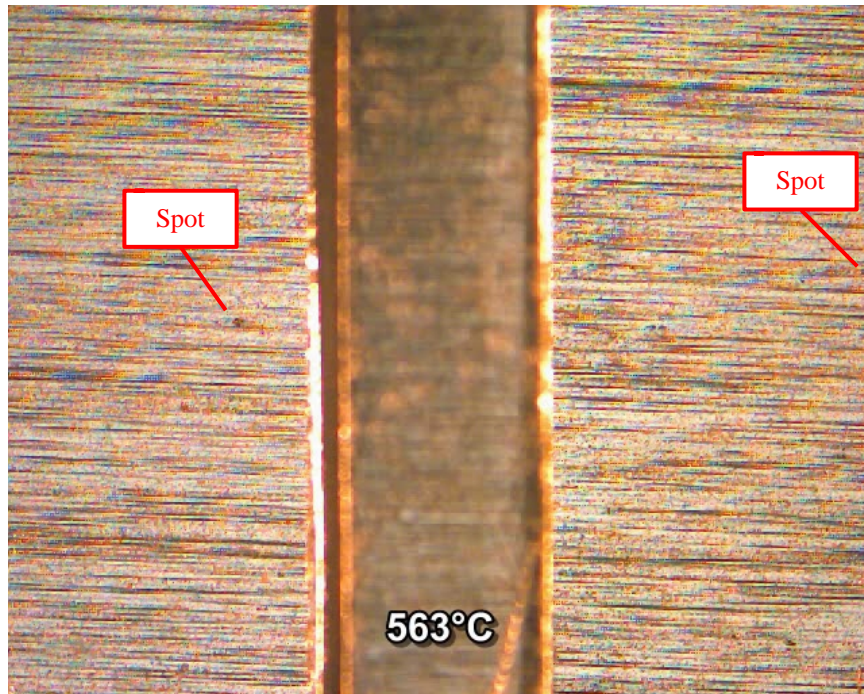
materials has joint formation in an air environment (Figure 3-5 (b) and Figure 3-12 (b)) except for one case with partial formation (Figure 3-6 (b)). These series of experiments have clearly suggested the limits of acceptable oxygen level for both materials are between 2000 ppm O₂ and an air environment. Trillium™ brazing sheet has consistent fillet formation up to 2000 ppm (Figure 3-4 (b)) but the traditional brazing sheet features poor or none fillet formation in 2000 ppm (Figures 3-10 (b) and 3-11 (b)). This indicates that Trillium™ brazing sheet tolerates an order of magnitude of ppm oxygen higher than the traditional material, i.e. more resilient in an adverse brazing background atmosphere.

3.2 Image Sequence for Clad Surface Features during a Brazing Process

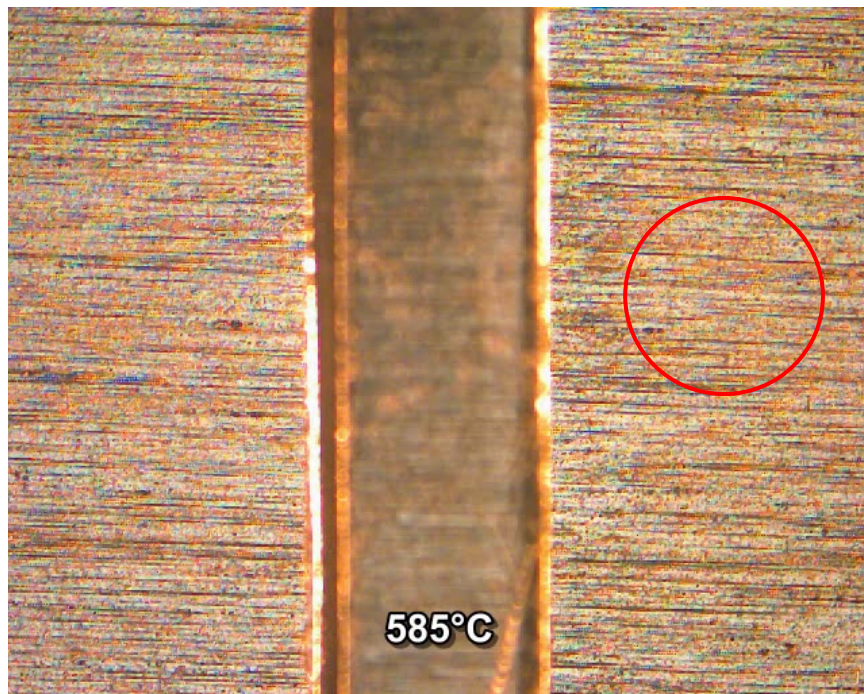
Series of frames from recorded brazing videos under the microscope are selected for presenting joining features. Comments are given frame by frame. The first set of photos is for Trillium™ brazing sheet under 99.999% pure nitrogen gas, in Figures 3-13 (a) ~ (j). The second set of frames is from the test of a traditional brazing sheet under the same background atmosphere conditions, presenting in Figures 3-14 (a) ~ (j). The temperature reading is provided as a subtitle in each frame. For a whole temperature history with time, refer to Figure 2-6.



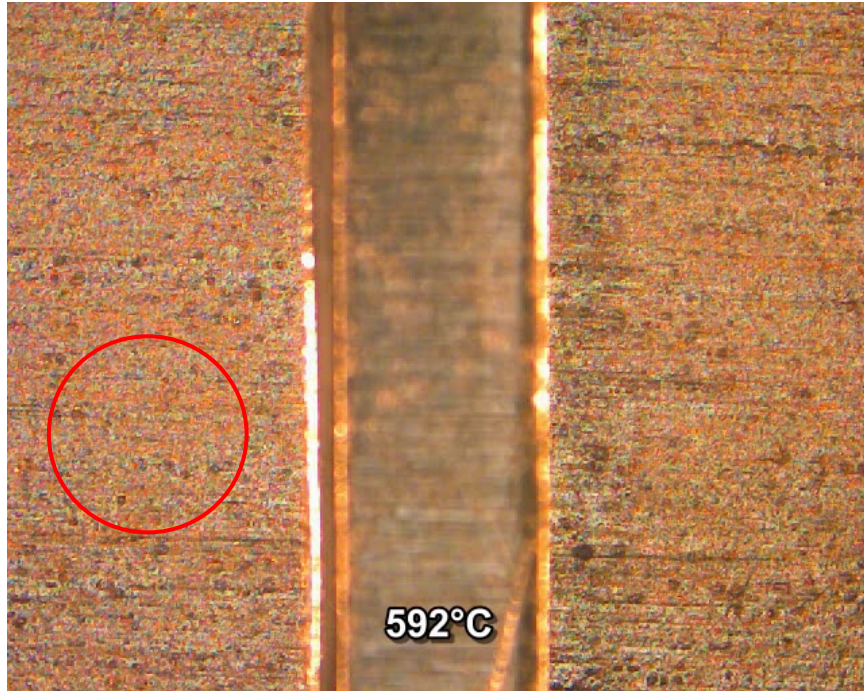
(a) The initiation of video at 550°C. No surface change registered before this temperature.



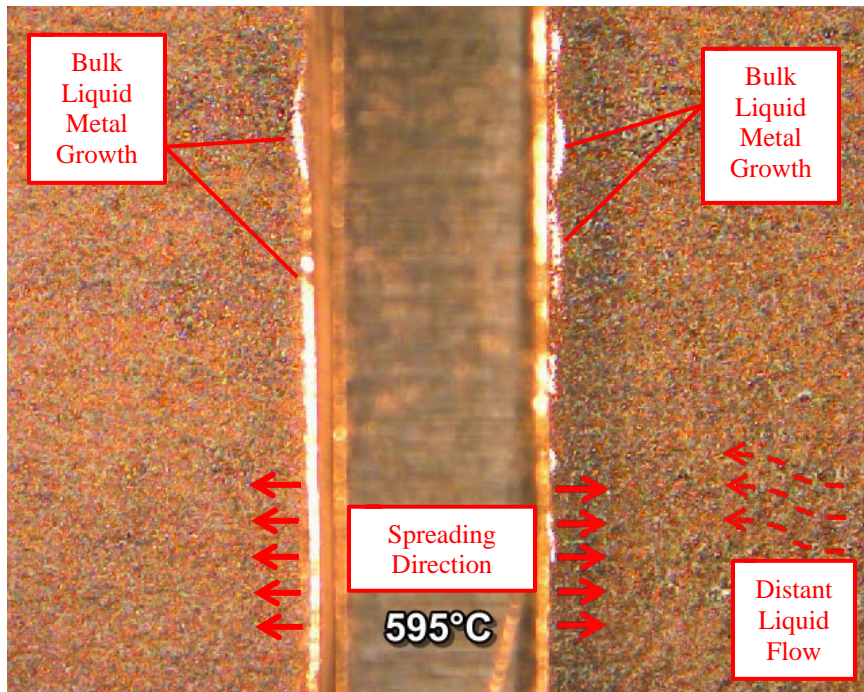
(b) At 563°C, spots begin to appear which implies the flux activity.



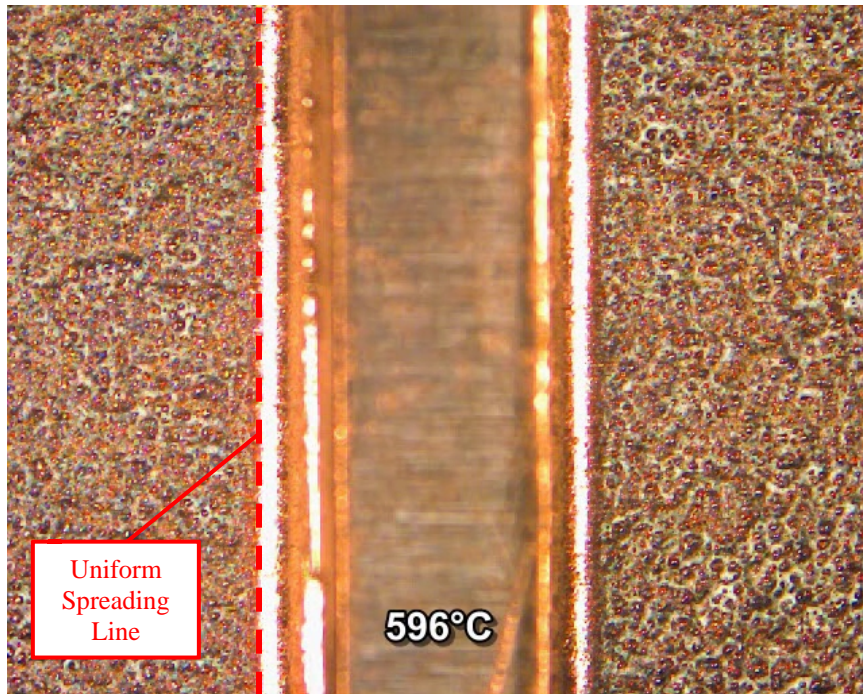
(c) At 585°C, more spots and flecks presented widely on the clad surface (see marked area as an example). It is believed as an indication of an ongoing flux activity.



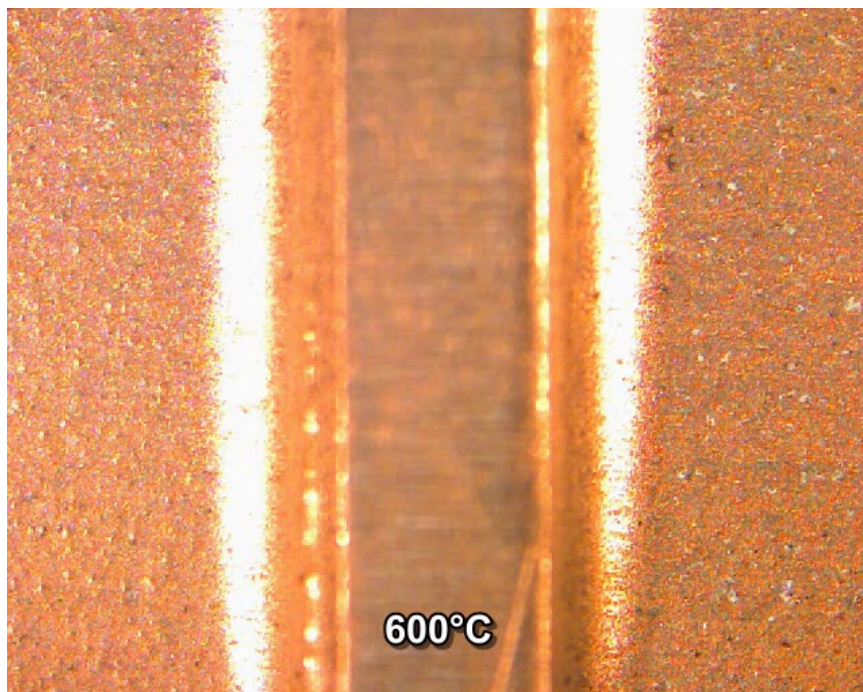
(d) At 592°C, severe flux interaction and clad melting are expected. Surface becomes rough and active bubbling behavior registered, an example area marked in the circle.



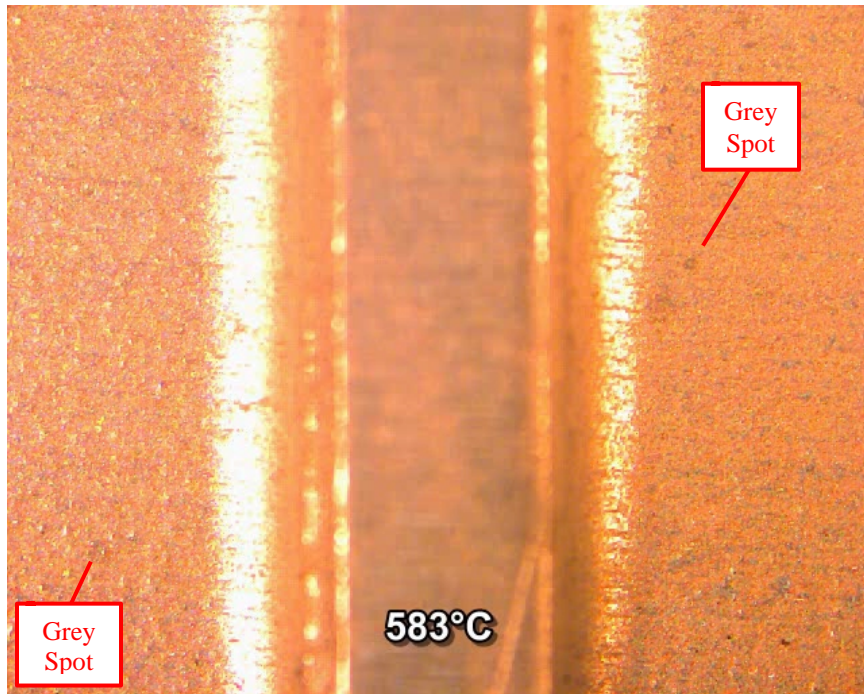
(e) At 595°C, the initiation of growth of liquid metal domains is registered. It is growing outward from the gap between the strip and the substrate. Distant liquid metal is flowing toward the bulk liquid metal.



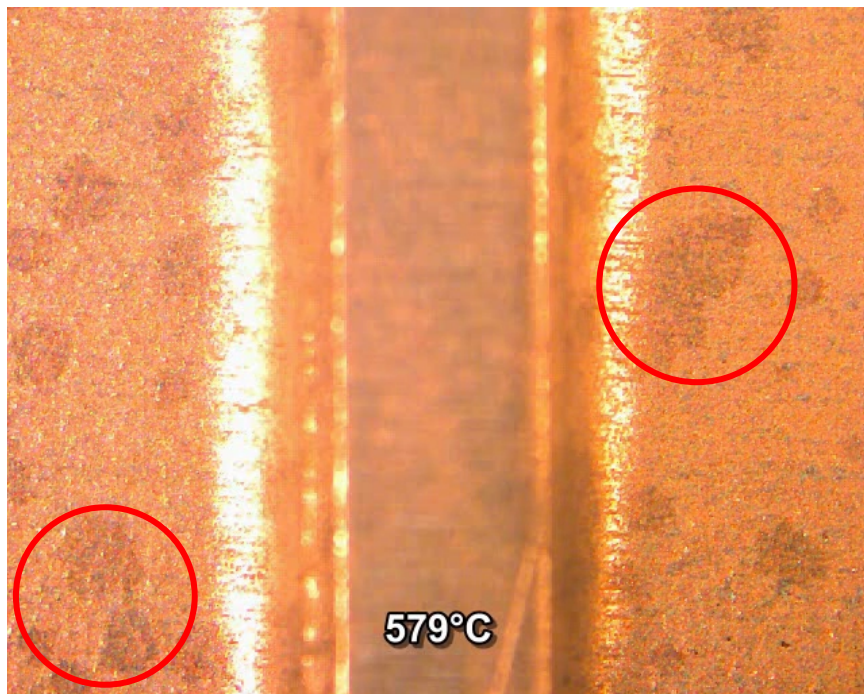
(f) The growth of joint fillet formation reaches its equilibrium. A uniform front line of the spreading indicates a good brazing performance, marked by the dashed line.



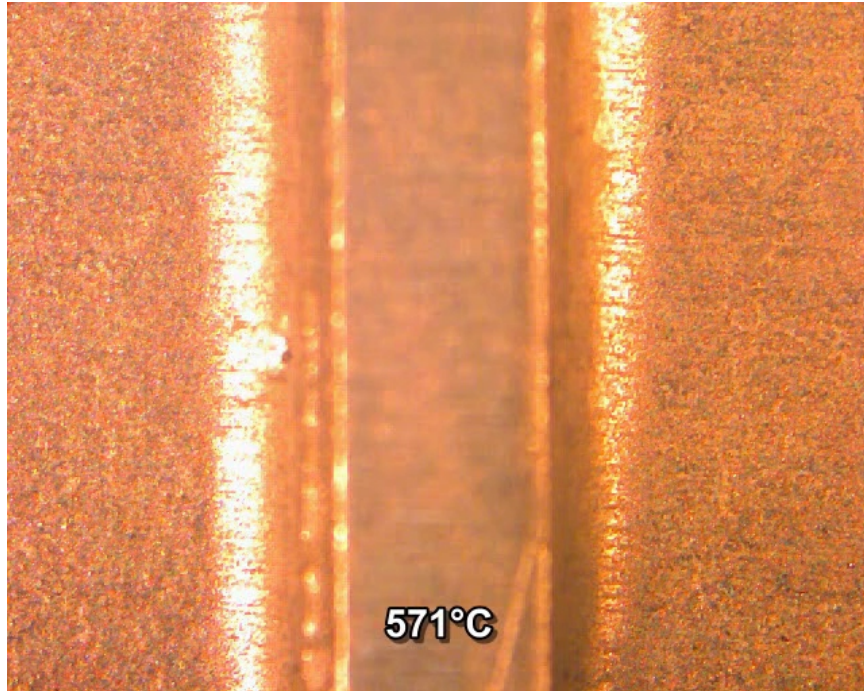
(g) Dwell at the peak temperature 600°C for 2 minutes. No change of surface feature during the dwell.



(h) The initiation of resolidification happens at 583°C. Multiple grey spots present.

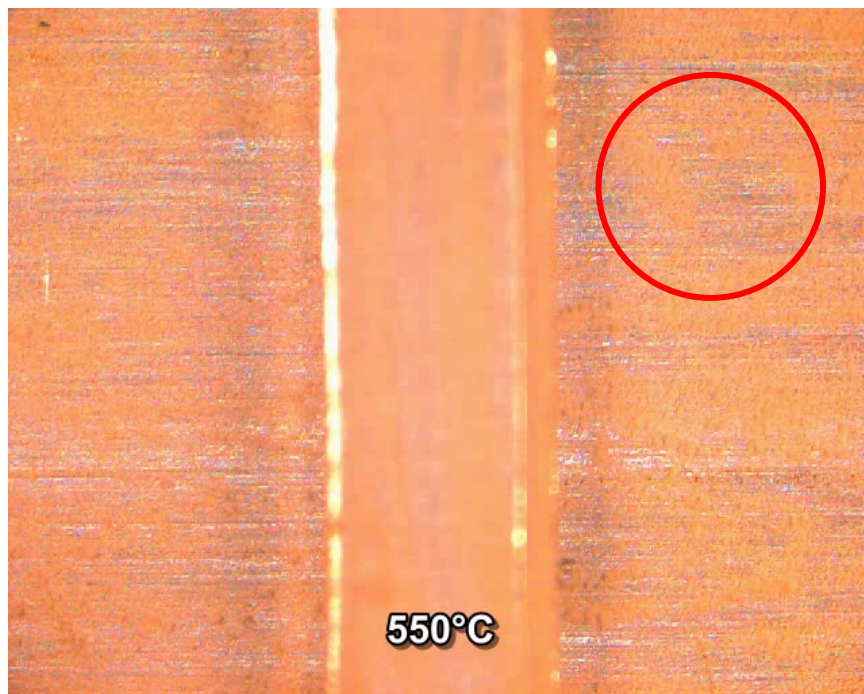


(i) Severe action of resolidification. Grey spots are growing and coalescing, see marked areas.

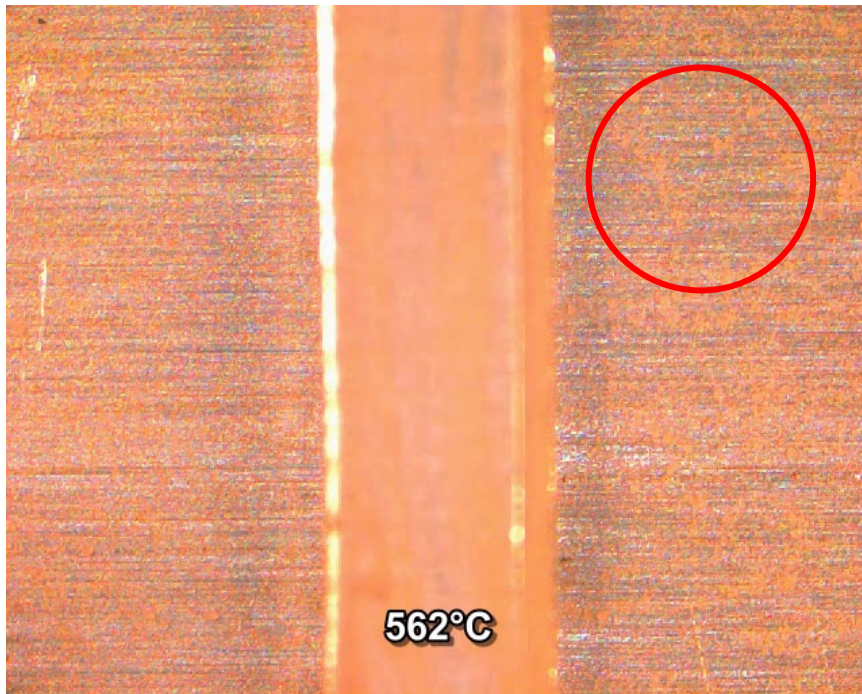


(j) Termination of resolidification at 571°C. Solid joint fillet formed. No further surface change later than this frame.

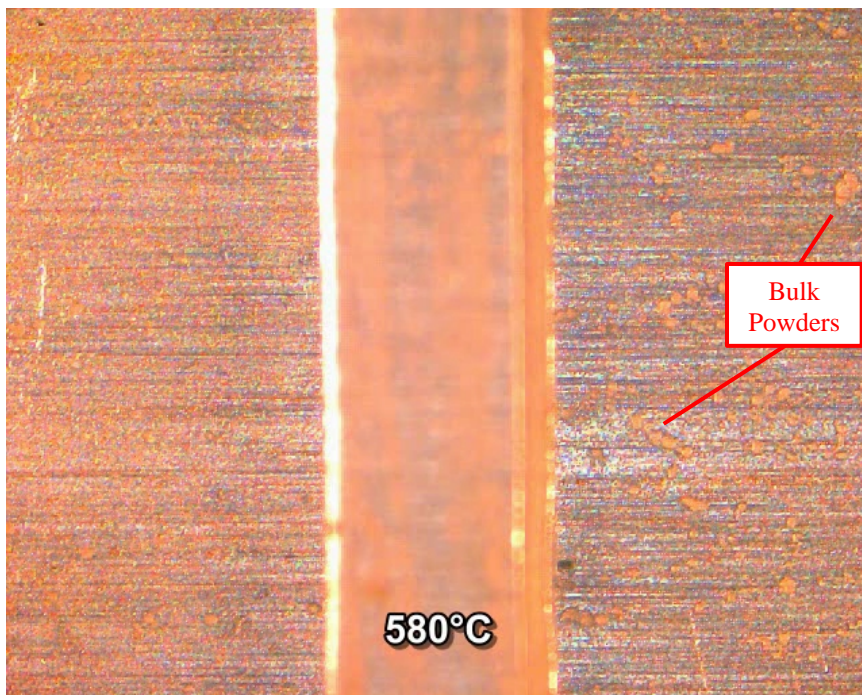
Figure 3-13 Surface Features of Trillium™ Brazing Sample in a Brazing Process



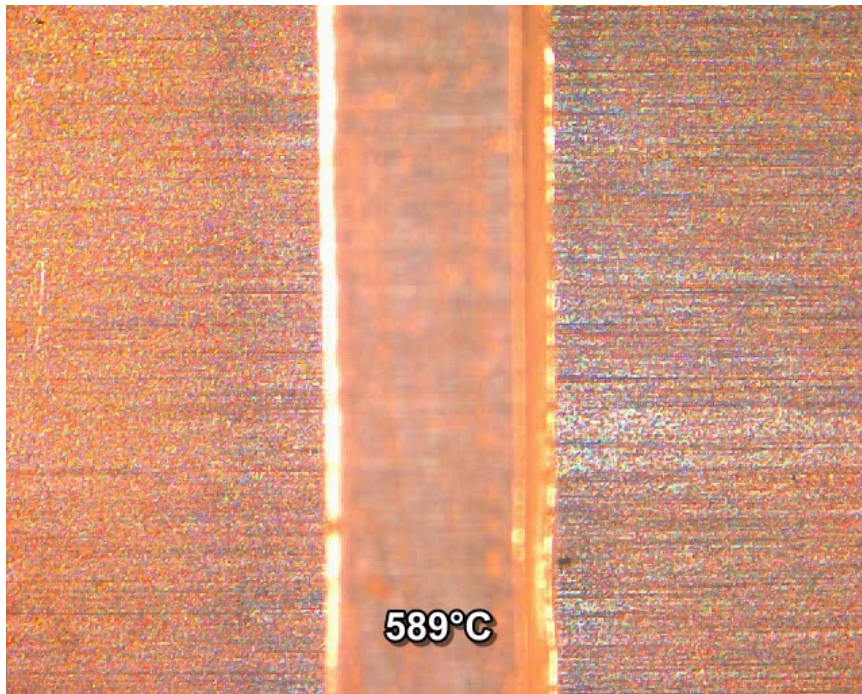
(a) The initiation of video at 550°C. No surface activity registered before this temperature. As an example, in the marked area the powder flux is uniformly covering the substrate.



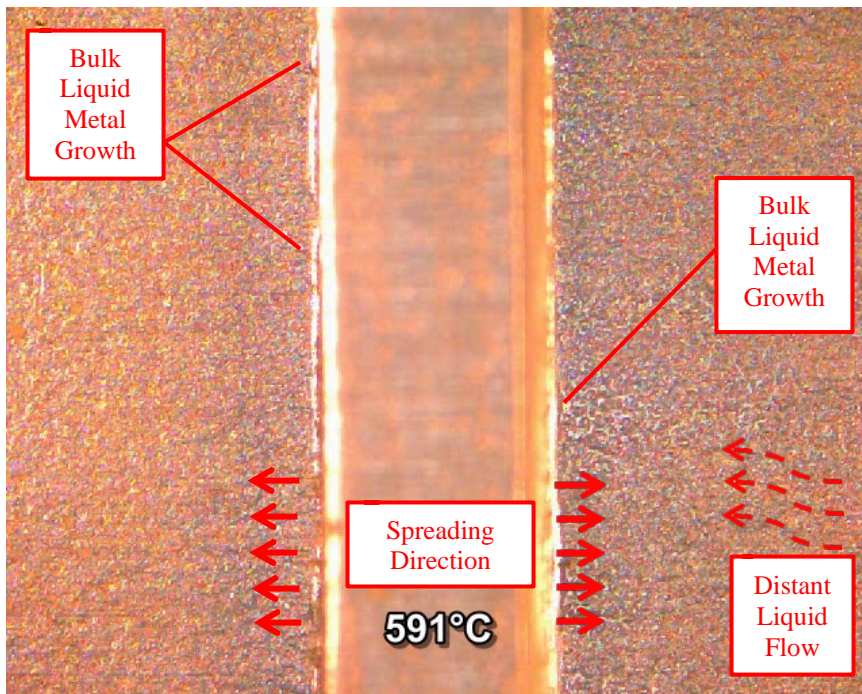
(b) At 562°C, a portion of flux on the surface begins to melt. The aluminum surface is revealing due to the transparency of molten flux. Compare with the marked area in previous figure (Figure 3-14 (a)).



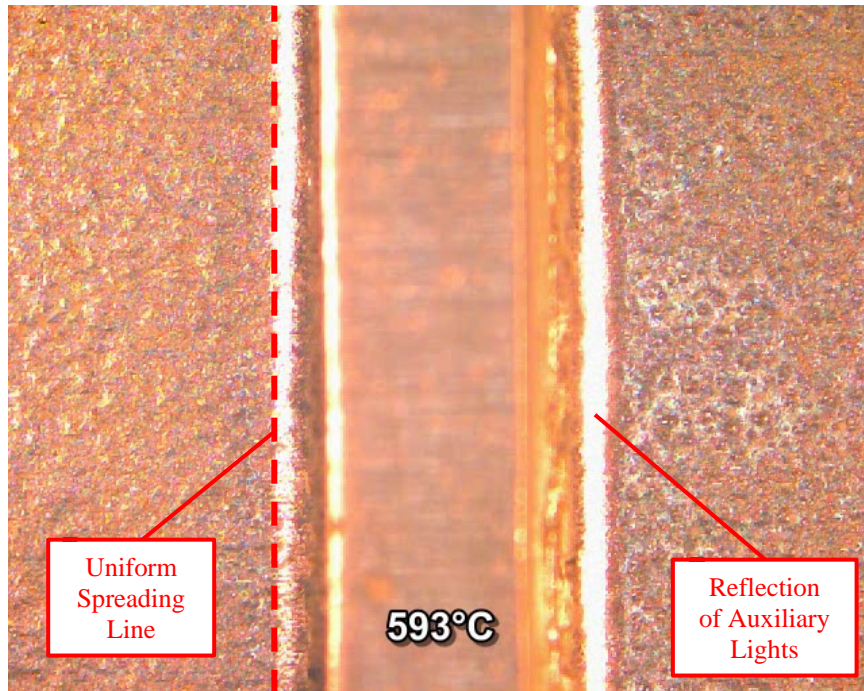
(c) Flux is melting successfully on most of the aluminum surface except for some bulk powders, as indicated in the figure.



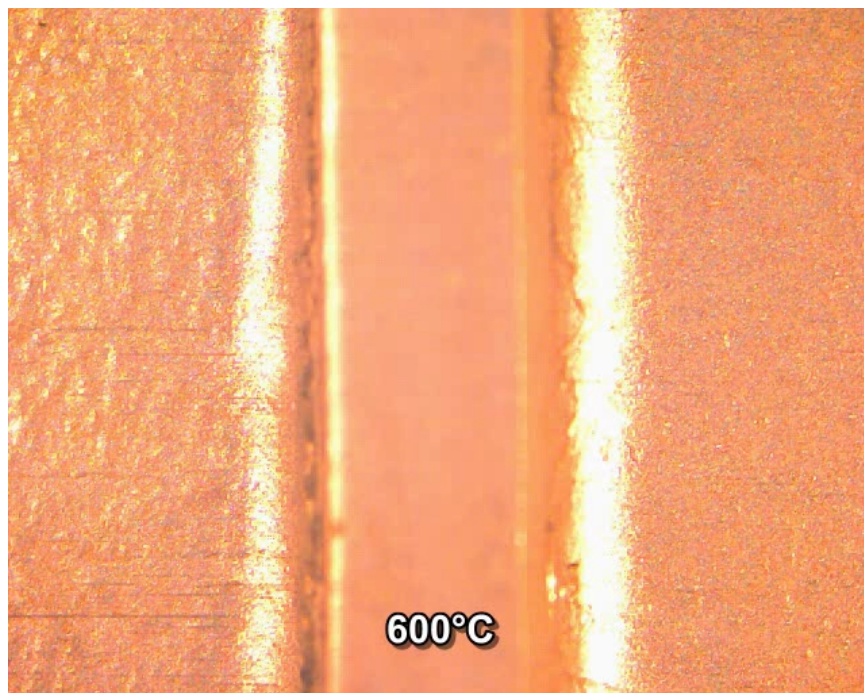
(d) Severe flux interaction and clad melting are expected. Surface becomes rough.



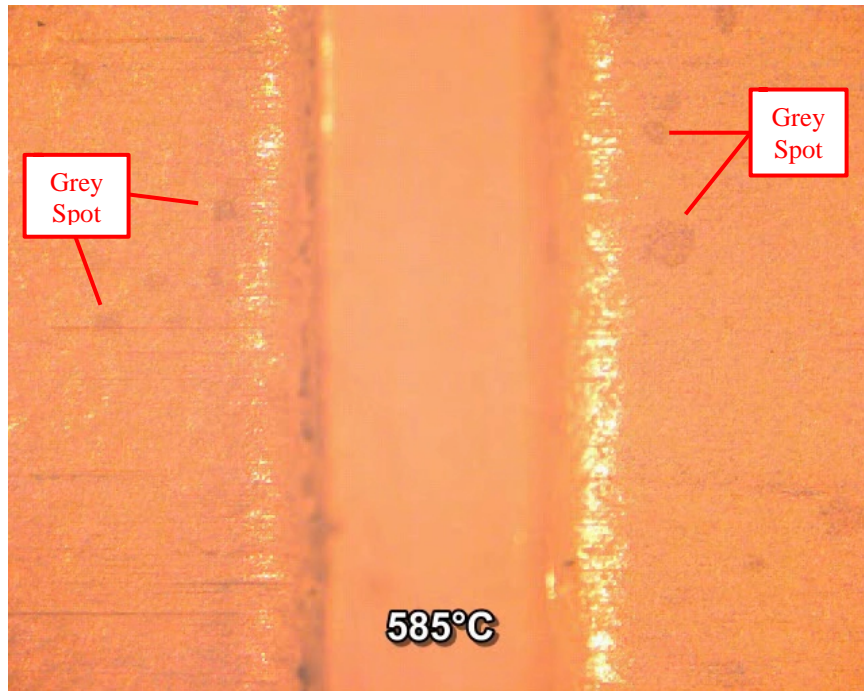
(e) At 591°C, the initiation of growth of bulk liquid metal observed. It is growing outward from the gap between the strip and the substrate. Distant liquid metal on the substrate flows toward the joint.



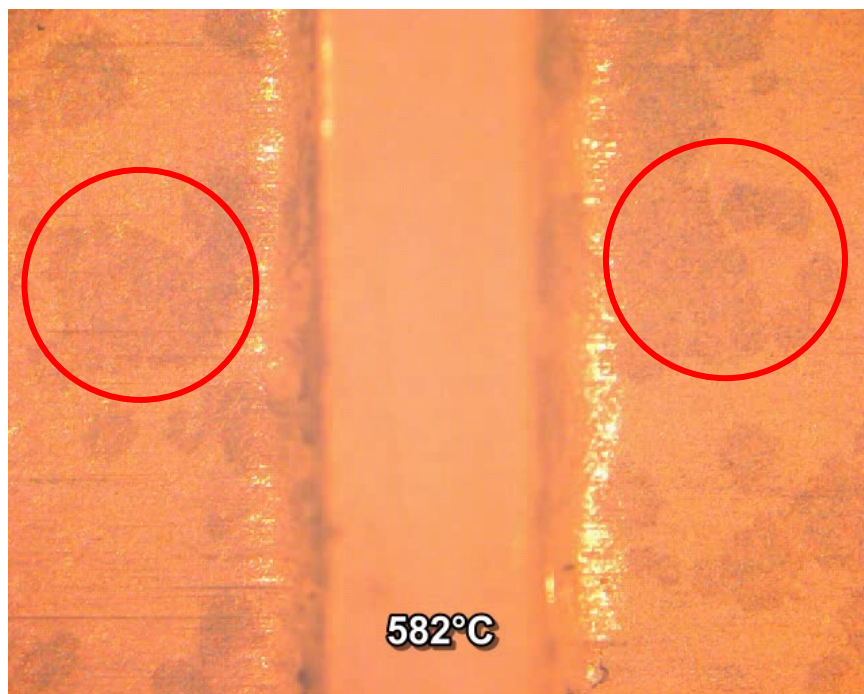
(f) The growth of joint fillet formation reaches its equilibrium. A uniform front line of spreading indicates good wetting. The forming meniscus fillet reflects the auxiliary lights from two sides which also indicate the triple line locations over time.



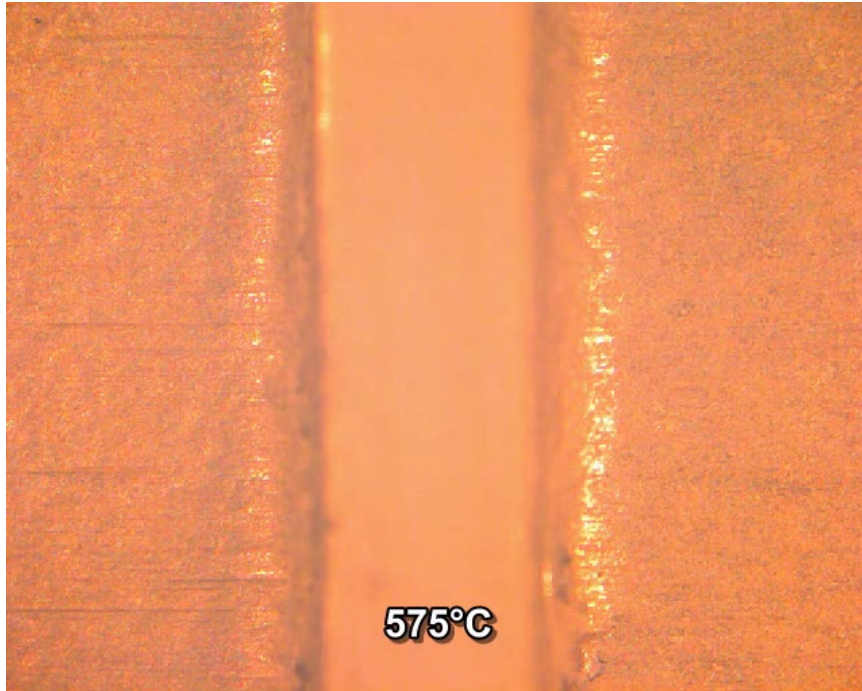
(g) Dwell at peak temperature 600°C for 2 minutes. No change on the surface monitored during the dwell.



(h) The initiation of resolidification happens at 585°C. Series of small grey spots present.



(i) Severe activity of resolidification. Grey spots are growing and coalescing.



(j) Termination of resolidification. Solid joint fillet formed. No further surface change observed later than this frame.

Figure 3-14 Surface Features of Traditional Brazing Sample in a Brazing Process

Figures 3-13 and 3-14 have highlighted the surface events during a brazing process of a clad brazing sheet. The events include the following:

- (i) Melting of a flux
- (ii) Melting of a clad material
- (iii) Spreading of a molten clad and accumulation in the joint domain
- (iv) Resolidification of a molten clad

The temperature levels of the melting of flux, melting of clad, spreading, and resolidification are within a few degrees difference for both materials. Figures 3-13 and 3-14 also suggest similar behavior in terms of joint fillet formation for both materials when the background atmosphere has low oxygen content ($< 20\text{ppm}$).

3.3 Macroscopic Features of Joint Formation

Two groups of macro images, Figures 3-15 ~ 3-20 and Figures 3-21 ~ 3-26 were taken using a digital camera and presented correspondingly for Figures 3-1 ~ 3-6 (Trillium™ brazing sheet) and Figures 3-7 ~ 3-12 (traditional brazing sheet), respectively.

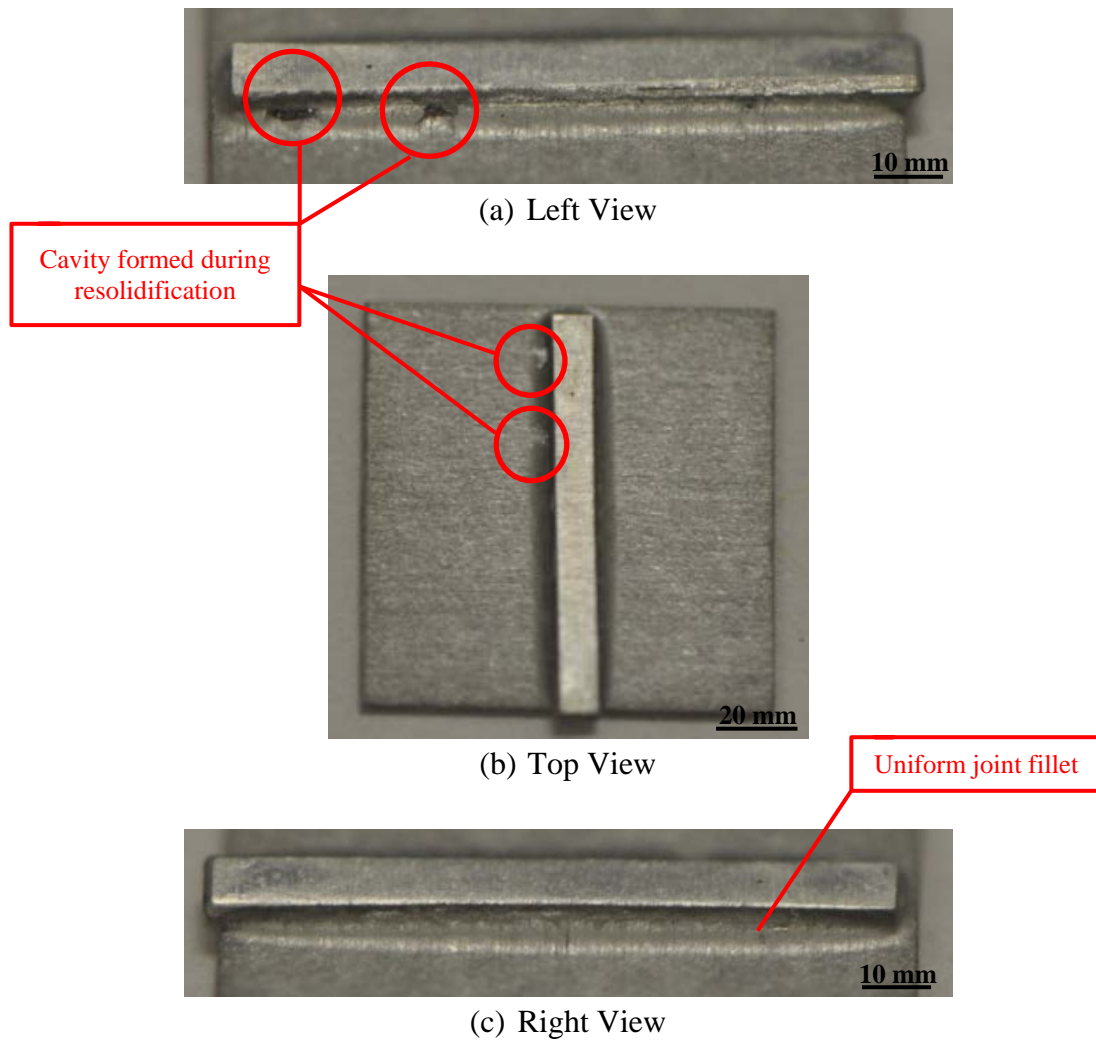


Figure 3-15 Macroscopic Joint Features of Trillium™ Brazing Sample in 20 ppm

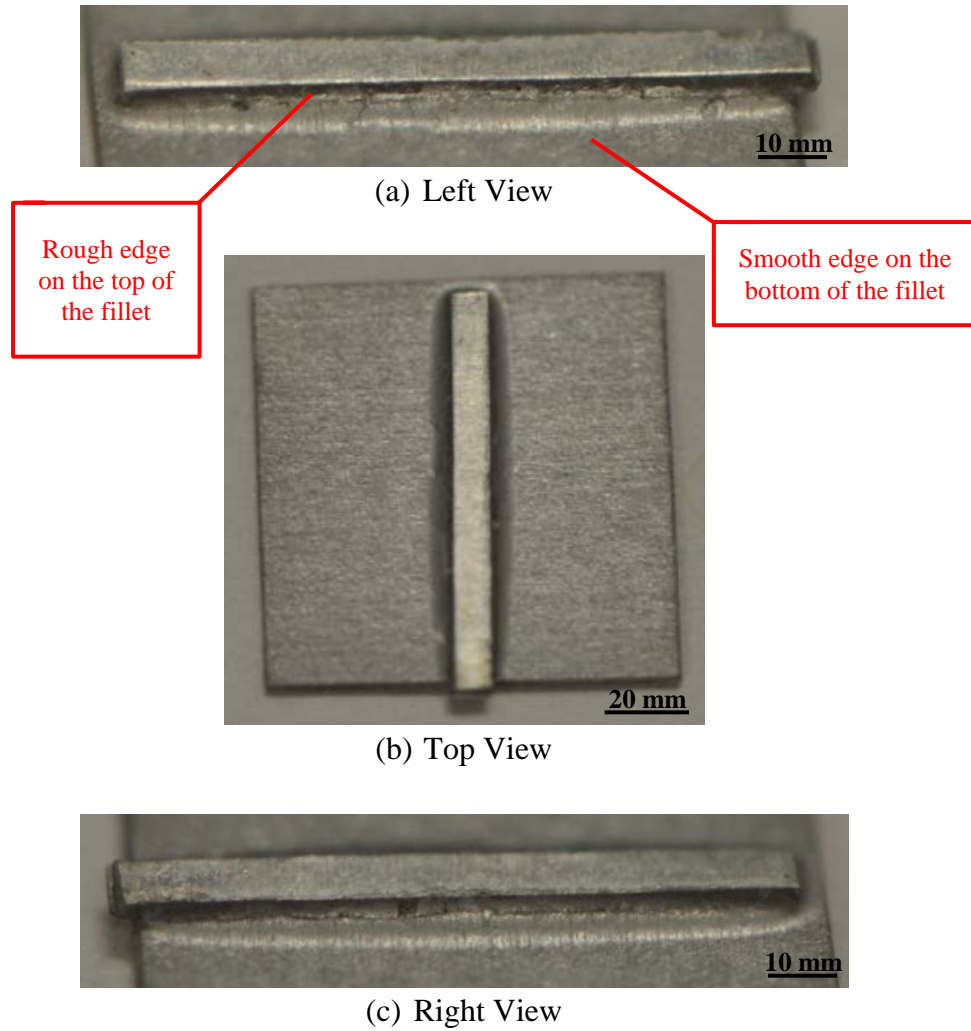
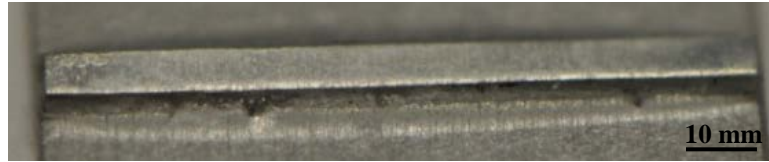
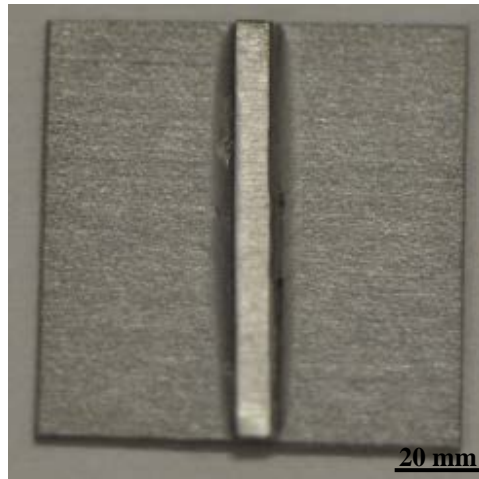


Figure 3-16 Macroscopic Joint Features of Trillium™ Brazing Sample in 200 ppm



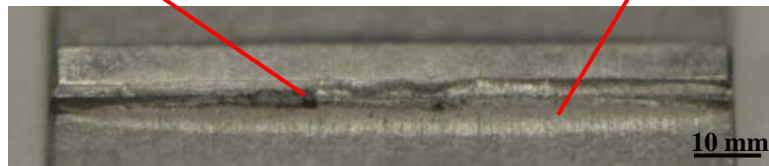
(a) Left View



(b) Top View

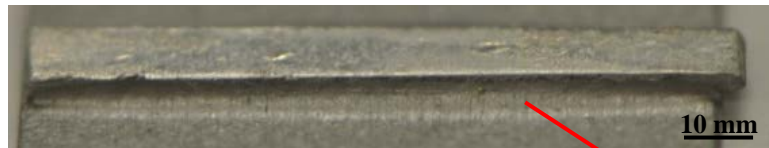
Rough edge
on the top of
the fillet

Smooth edge on
the bottom of
the fillet



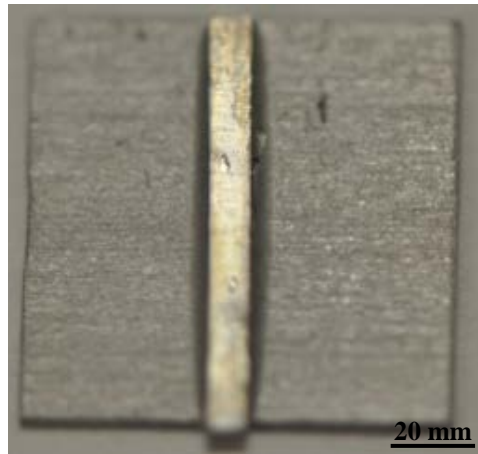
(c) Right View

Figure 3-17 Macroscopic Joint Features of Trillium™ Brazing Sample in 500 ppm



(a) Left View

Smooth meniscus
joint formation



(b) Top View

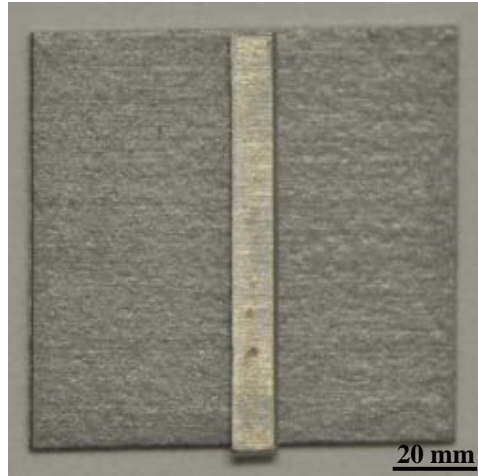


(c) Right View

Figure 3-18 Macroscopic Joint Features of Trillium™ Brazing Sample in 2000 ppm



(a) Left View



(b) Top View



(c) Right View

Unfilled edges of mating surfaces

Figure 3-19 Macroscopic Joint Features of Trillium™ Brazing Sample in Air. Test I.

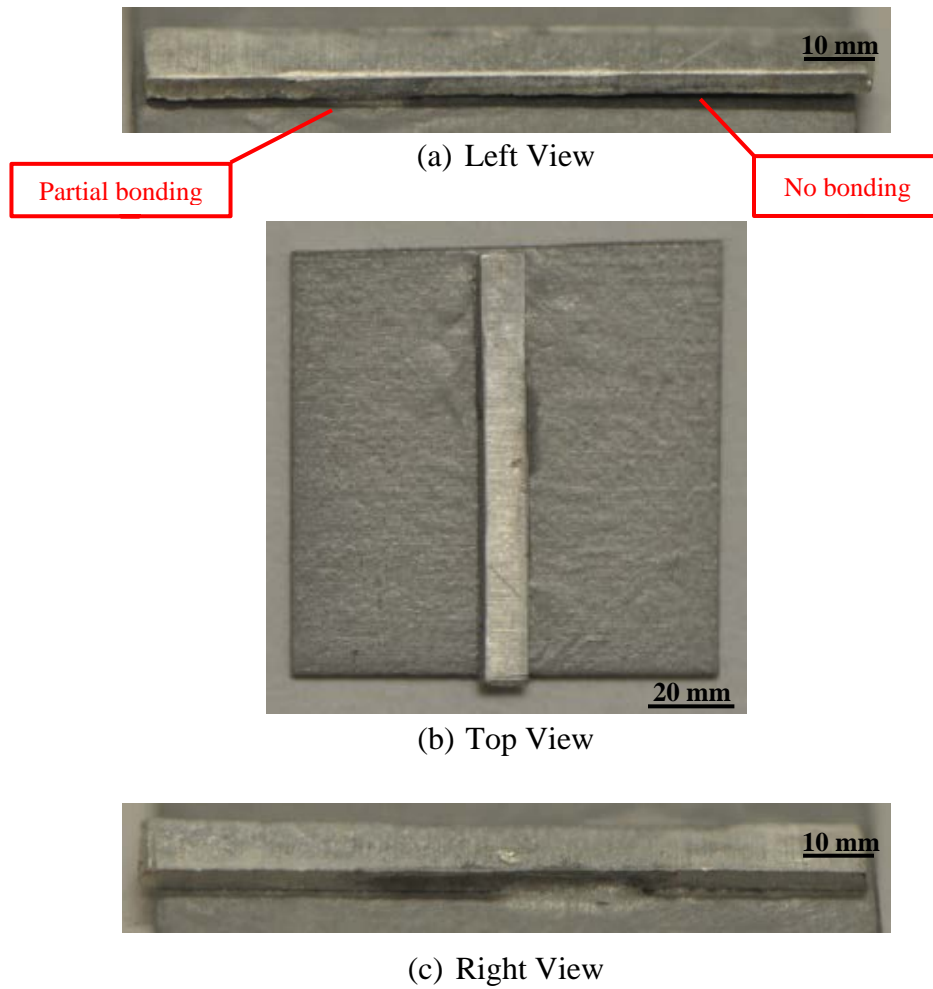


Figure 3-20 Macroscopic Joint Features of Trillium™ Brazing Sample in Air. Test II.

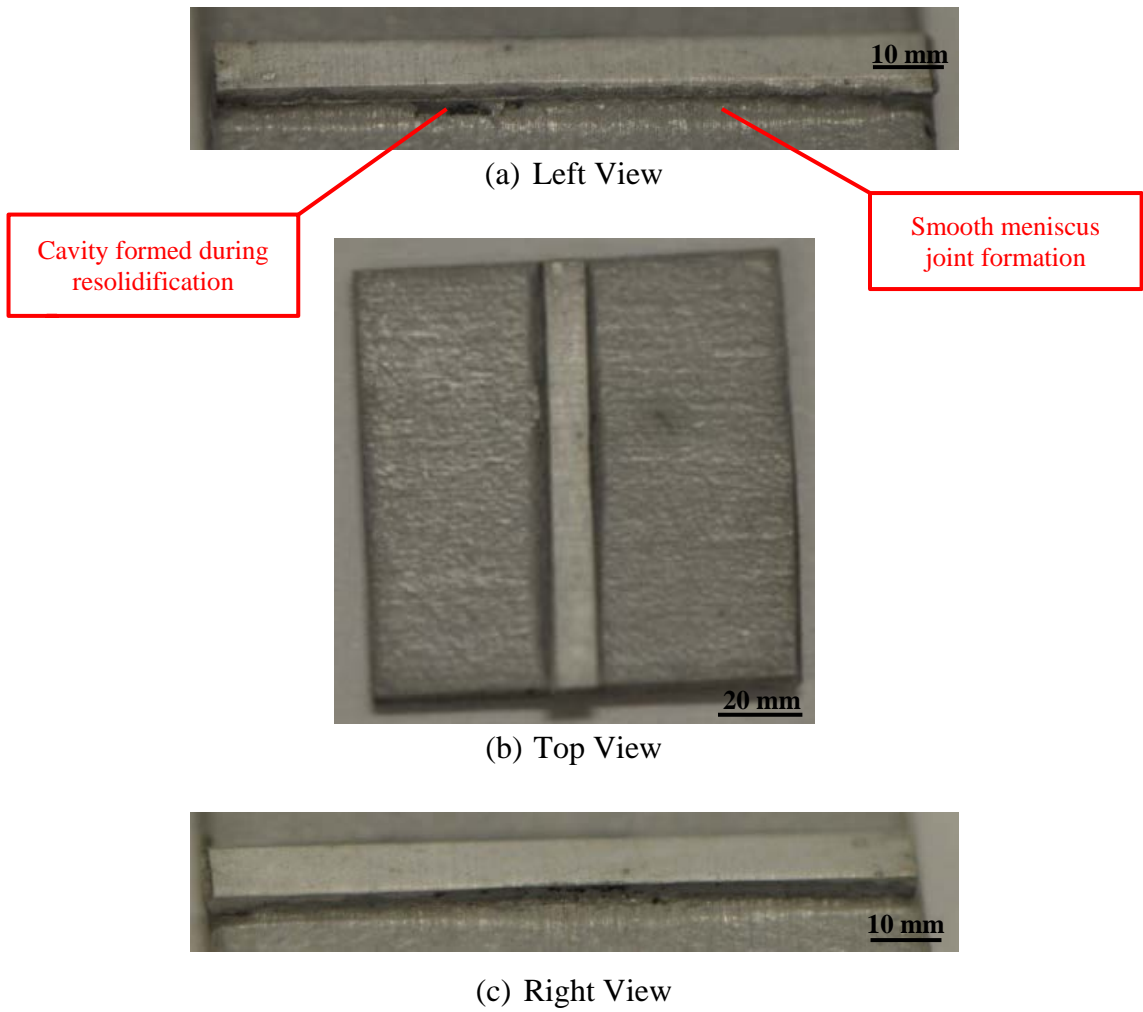


Figure 3-21 Macroscopic Joint Features of Traditional Brazing Sample in 20 ppm

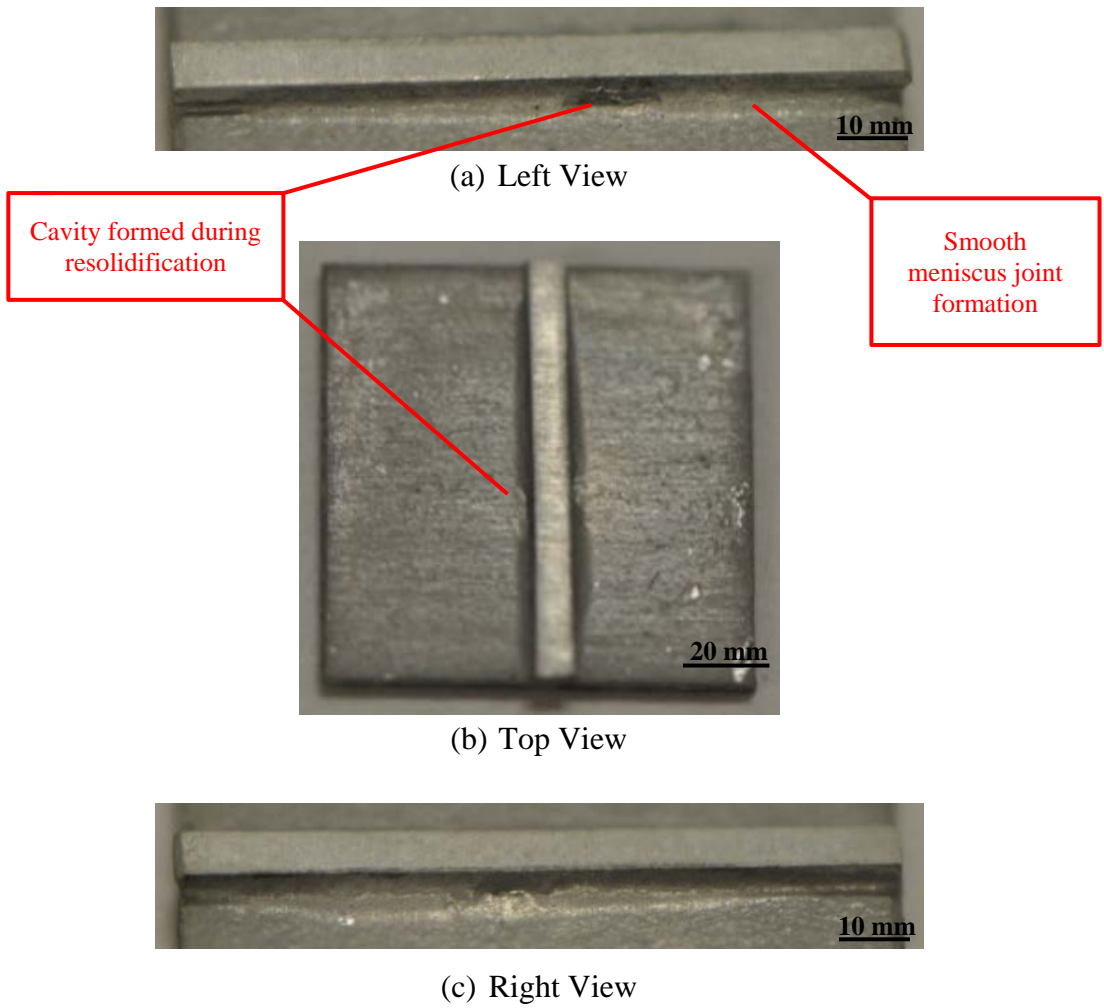
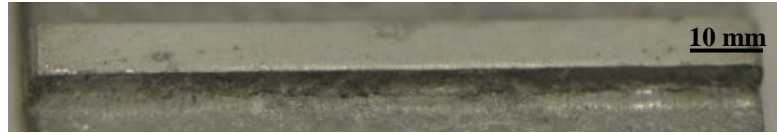
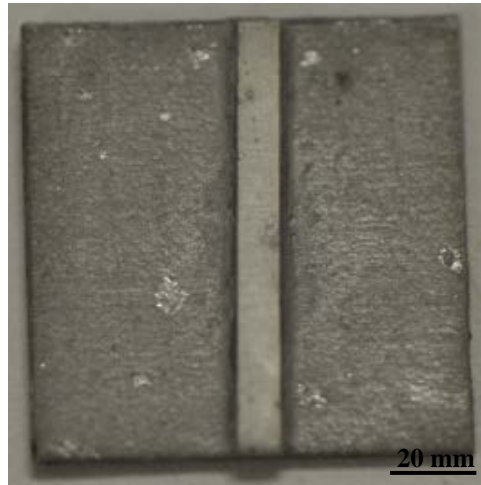


Figure 3-22 Macroscopic Joint Features of Traditional Brazing Sample in 200 ppm

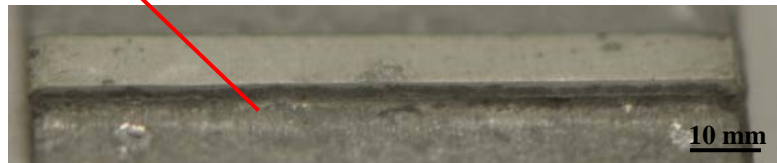


(a) Left View



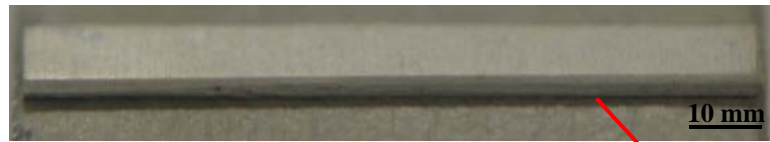
(b) Top View

Successfully
formed fillet



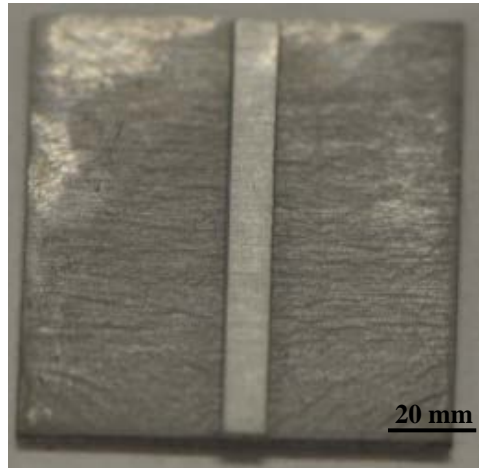
(c) Right View

Figure 3-23 Macroscopic Joint Features of Traditional Brazing Sample in 500 ppm



(a) Left View

Unfilled edges of mating surfaces



(b) Top View



(c) Right View

Figure 3-24 Macroscopic Joint Features of Traditional Brazing Sample in 2000 ppm.
Test I.

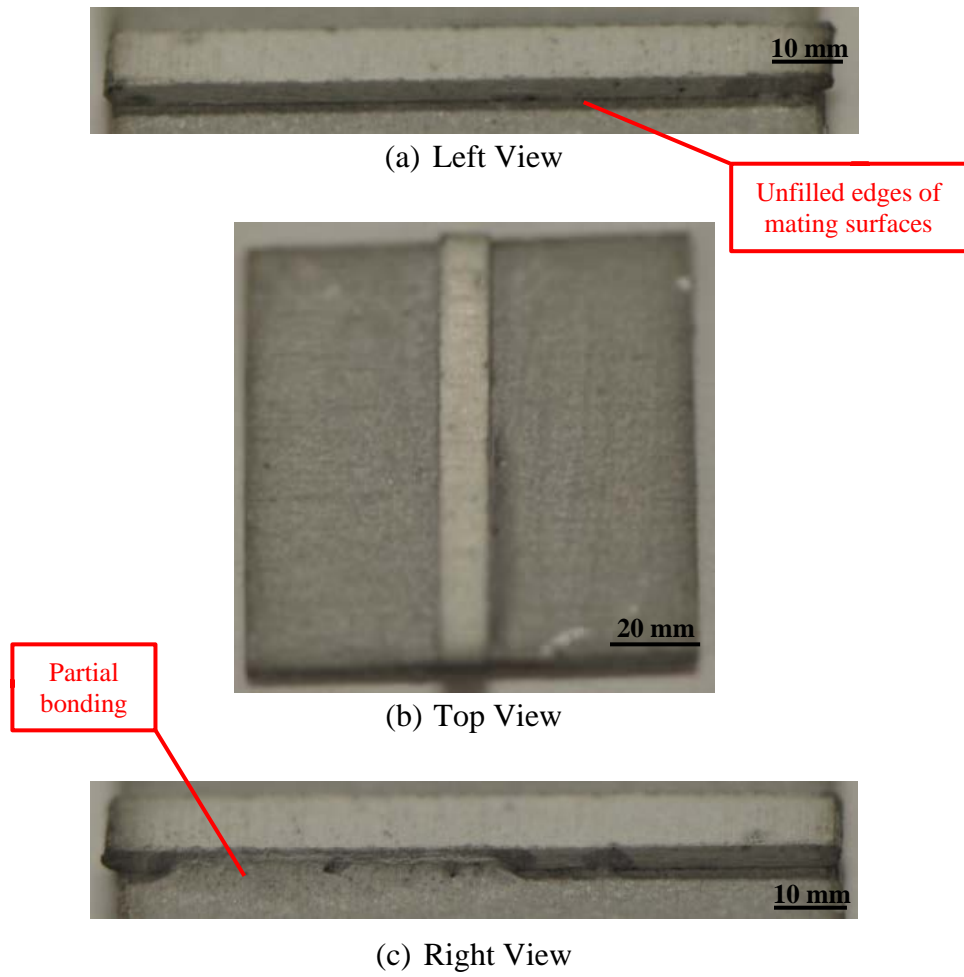


Figure 3-25 Macroscopic Joint Features of Traditional Brazing Sample in 2000 ppm.
Test II.

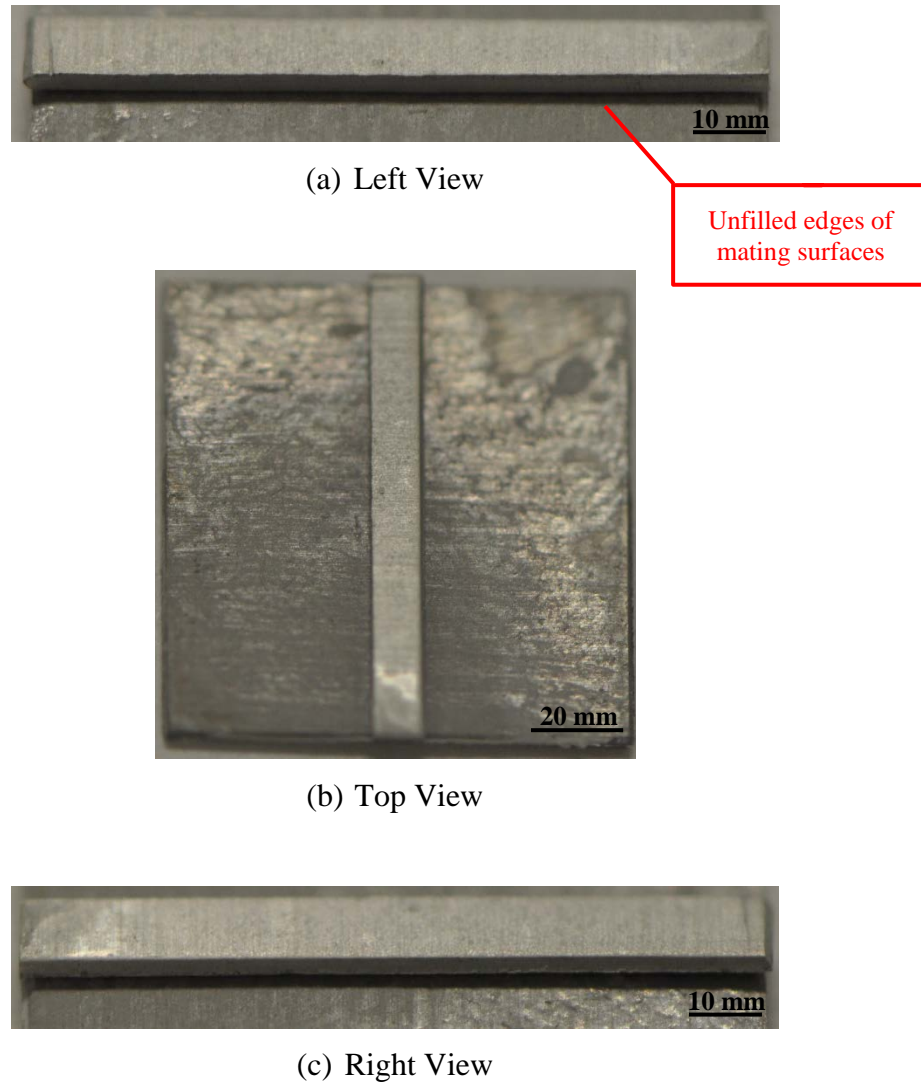


Figure 3-26 Macroscopic Joint Features of Traditional Brazing Sample in Air.

3.4 Microscopic Features of Joint Formation

Selected brazed samples were cut at the location 3 mm away from an edge, as illustrated in Figure 3-27. For obtaining the metallurgical cross-section pictures, brazed pieces were cold mounted to form epoxy samples. Epofix resin with hardener (Struers), by a weight ratio of 25 to 3, was used for cold mounting. Mounted samples were grinded sequentially by SiC#320, #500, #800, and #1000 sand papers. Then 9 μm , 3 μm , and 0.04 μm colloidal silica suspensions were applied for polishing. The automatic grinding/polishing facility is consisted of Struers' RotoPol-22 and RotoForce-3 (grinder/polisher), Multidoser (polishing fluid dispenser), and RotoCom (control unit).

After the polishing process, samples were etched by Keller's reagent, an acid developed for revealing the grain boundary and orientation of aluminum alloys. The solution includes in volume 1% hydrofluoric acid (HF), 2.5% nitric acid (HNO₃), 1.5% hydrochloric acid (HCl), and 95% water (H₂O). The etched time is approximately 10 seconds. Etched samples were photographed using an Olympus BX51M microscope equipped with an imaging system. The left view and right view of joint formation were presented in Figures 3-28 ~ 3-39.

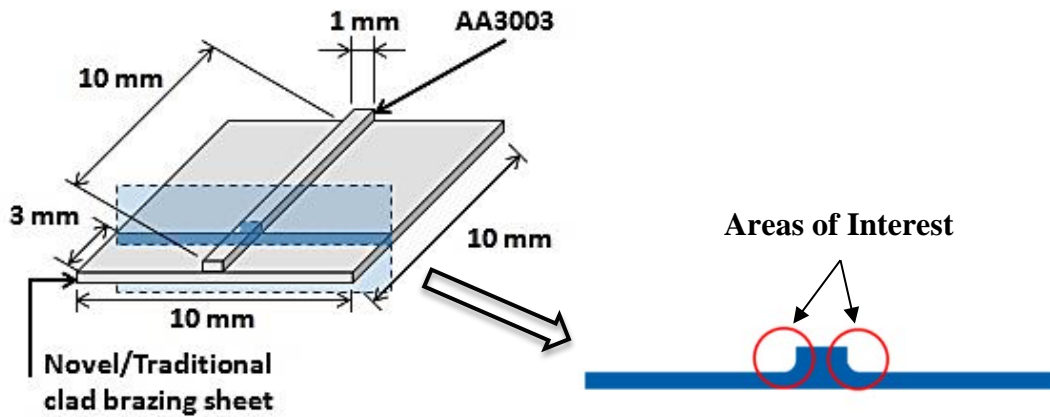


Figure 3-27 Polishing Location

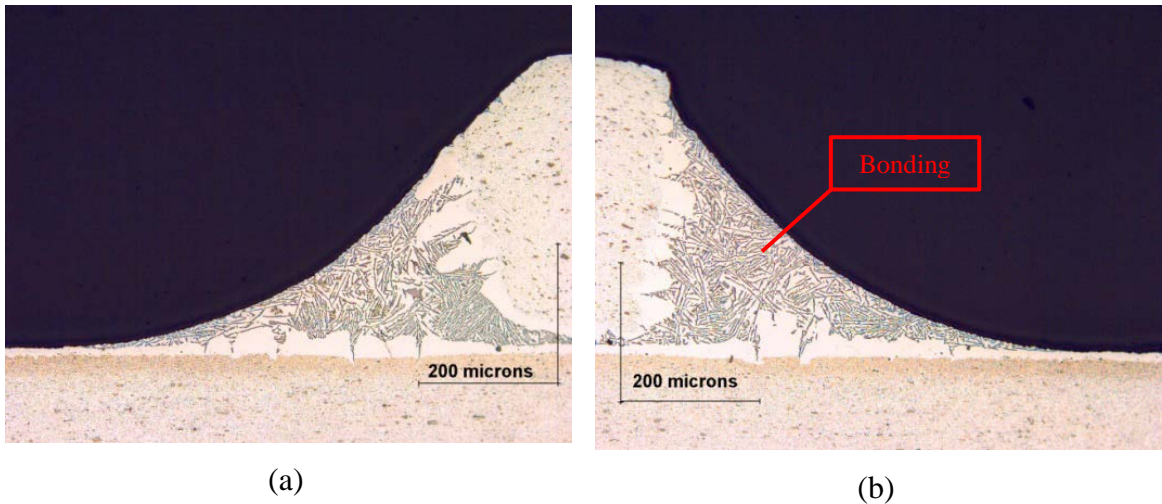
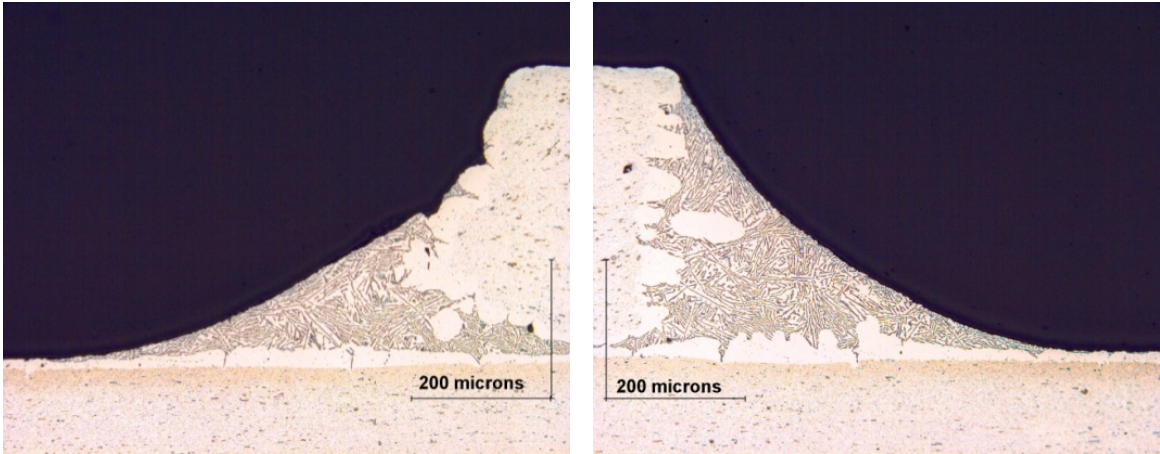
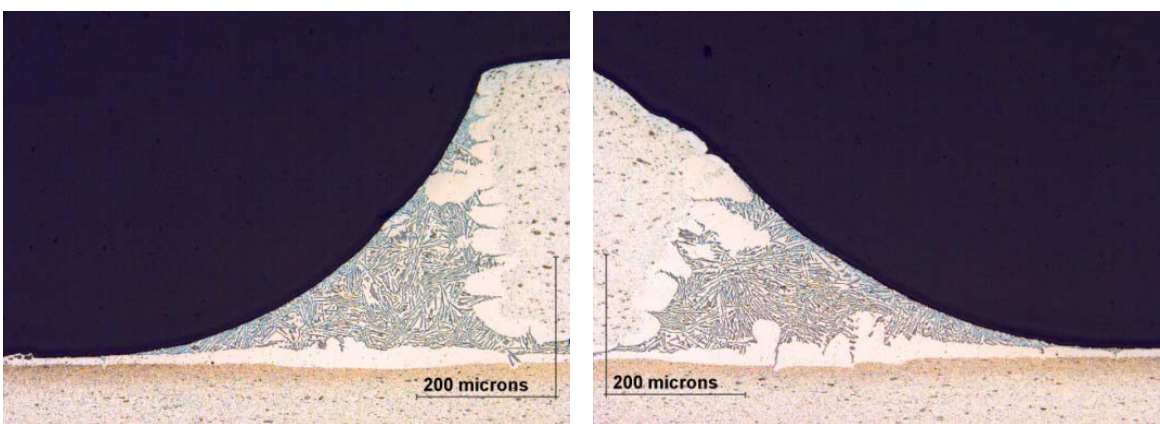


Figure 3-28 Metallurgical Photos of Trillium™ Brazed Sample in 20 ppm (a) Left Joint and (b) Right Joint



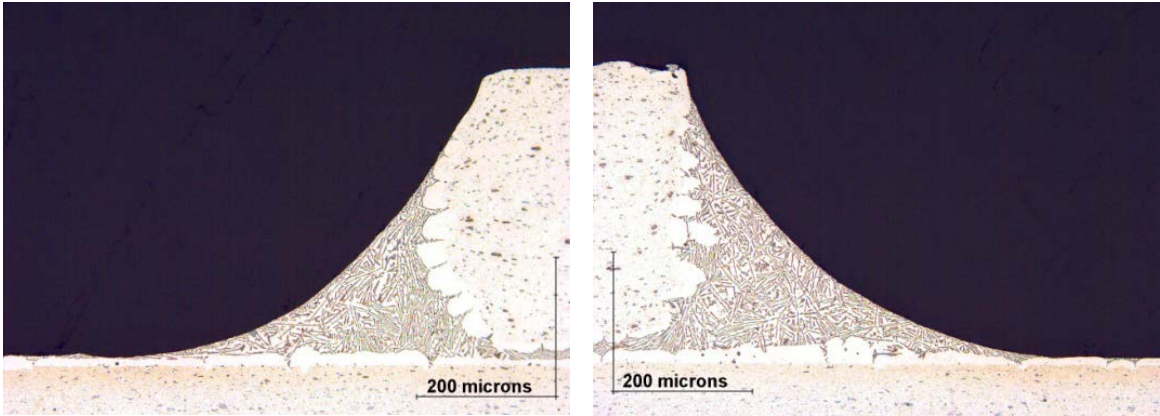
(a) (b)

Figure 3-29 Metallurgical Photos of Trillium™ Brazed Sample in 200 ppm (a) Left Joint and (b) Right Joint



(a) (b)

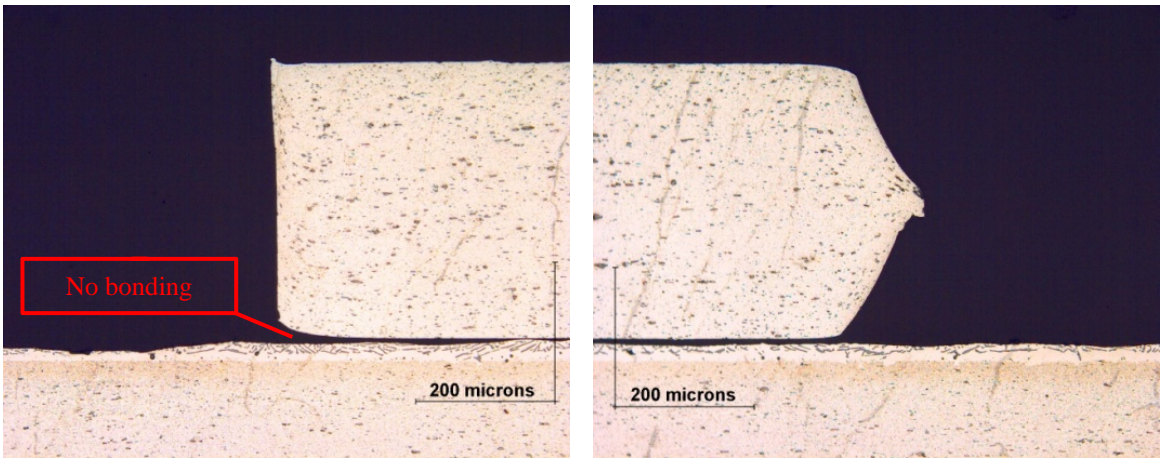
Figure 3-30 Metallurgical Photos of Trillium™ Brazed Sample in 500 ppm (a) Left Joint and (b) Right Joint



(a)

(b)

Figure 3-31 Metallurgical Photos of Trillium™ Brazed Sample in 2000 ppm (a) Left Joint and (b) Right Joint



(a)

(b)

Figure 3-32 Metallurgical Photos of Trillium™ Brazed Sample in Air (a) Left Joint and (b) Right Joint. Test I.

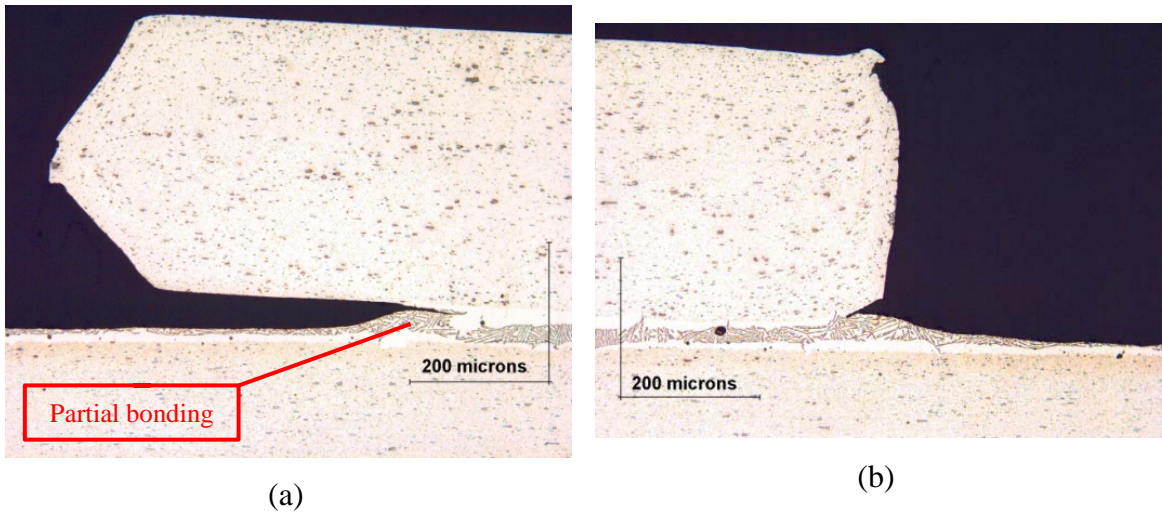


Figure 3-33 Metallurgical Photos of Trillium™ Brazed Sample in Air (a) Left Joint and (b) Right Joint. Test II.

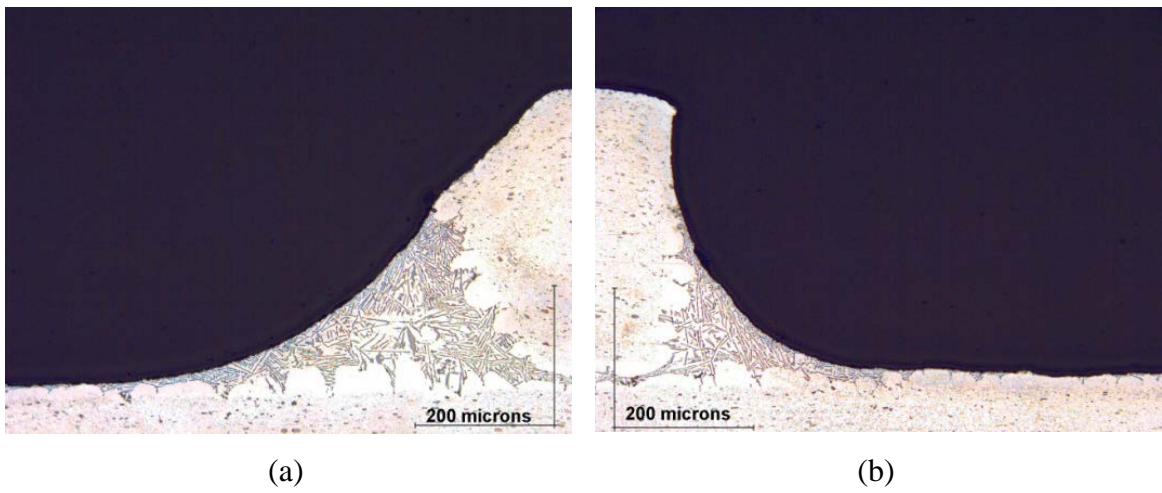


Figure 3-34 Metallurgical Photos of Traditional Brazed Sample in 20 ppm (a) Left Joint and (b) Right Joint.

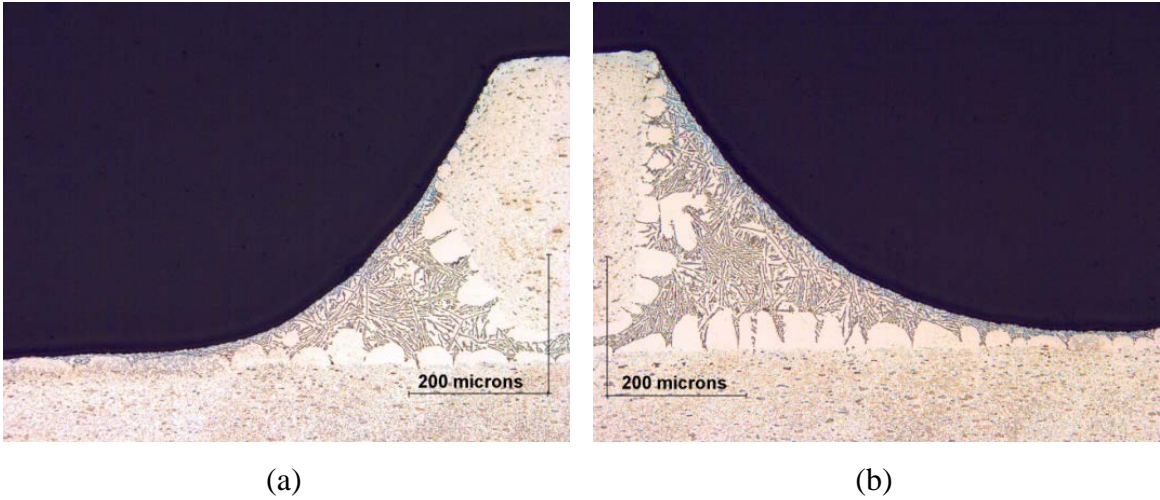


Figure 3-35 Metallurgical Photos of Traditional Brazed Sample in 200 ppm (a) Left Joint and (b) Right Joint.

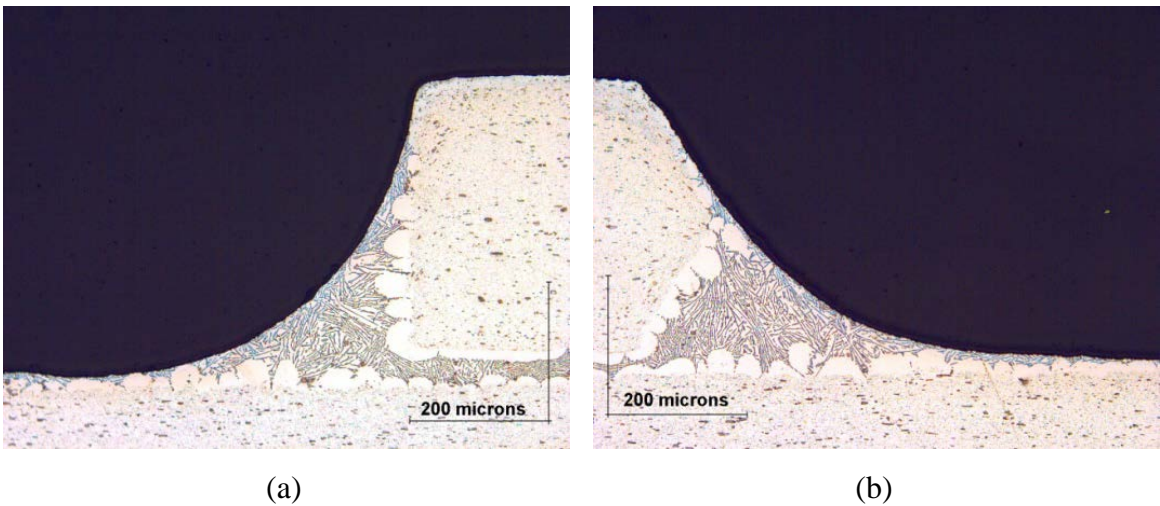


Figure 3-36 Metallurgical Photos of Traditional Brazed Sample in 500 ppm (a) Left Joint and (b) Right Joint.

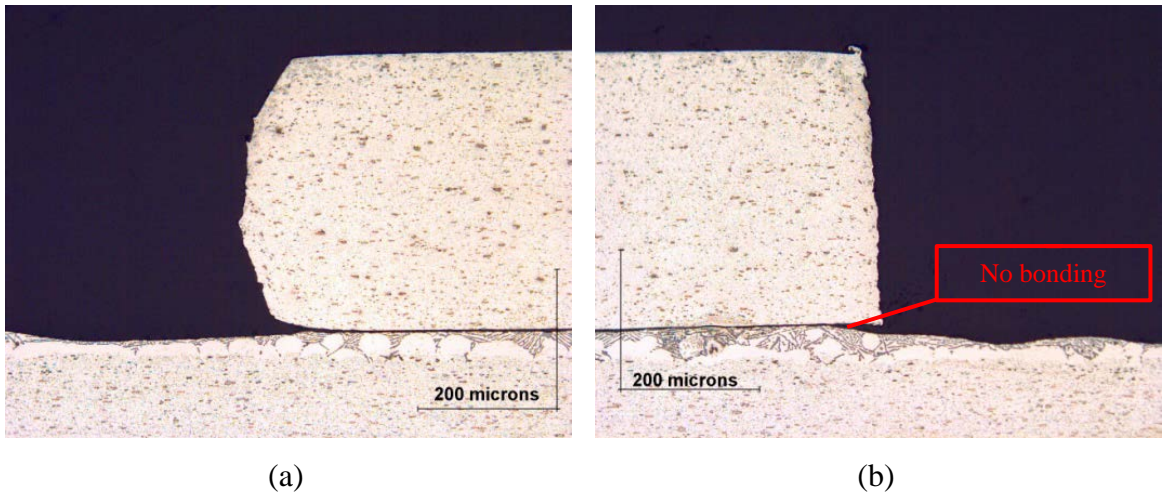


Figure 3-37 Metallurgical Photos of Traditional Brazed Sample in 2000 ppm (a) Left Joint and (b) Right Joint. Test I.

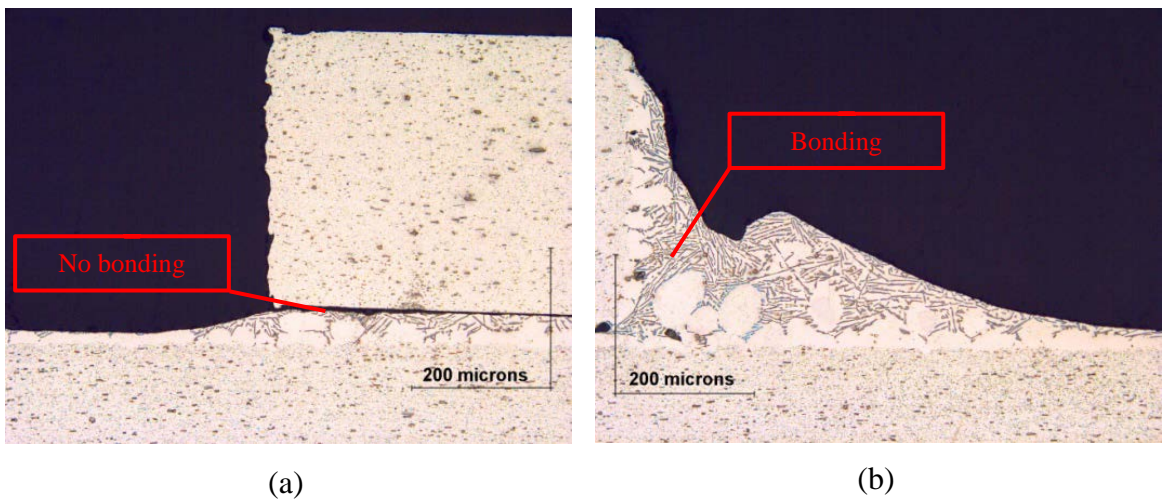


Figure 3-38 Metallurgical Photos of Traditional Brazed Sample in 2000 ppm (a) Left Joint and (b) Right Joint. Test II.

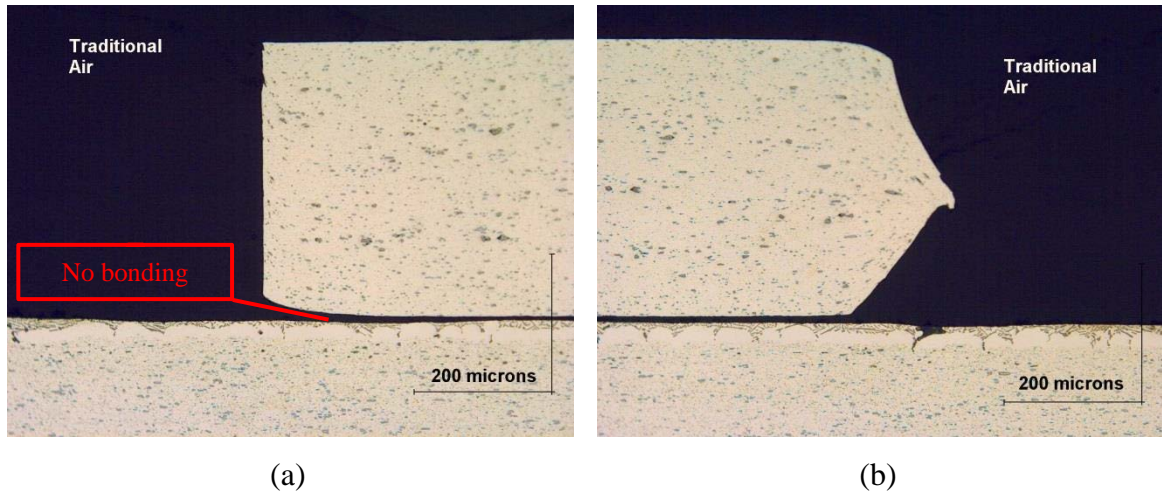


Figure 3-39 Metallurgical Photos of Traditional Brazed Sample in Air (a) Left Joint and (b) Right Joint.

Results showed that even for the oxygen level of up to 2000 ppm, joint clad melting and subsequent joint formation is featured uniform spreading and uniform fillet formation for TrilliumTM samples (Figure 3-31). When a traditional material is used, the same atmosphere condition 2000 ppm severely hampers spreading and joint formation (Figure 3-37). However, if excessive flux loading is applied for traditional material in 2000 ppm, joints may possibly form (Figure 3-38). Brazing in air using a traditional brazing sheet features consistently no bonding (Figure 3-39). In air, TrilliumTM brazing sheet features no spreading in most cases (Figure 3-32) but a partial joint formation was observed in one test (Figure 3-33). In sum, TrilliumTM was proved to feature better fillet formation under severe atmospheric condition than traditional material.

CHAPTER 4: Results and Discussion – Furnace Experiments

In this chapter, the summary of the performances of both Trillium™ and traditional brazing materials under different atmospheric conditions will be presented and discussed. Test at each atmosphere condition was repeated at least three times under all other influential factors kept unchanged. Experiments were performed using the CAB transparent furnace, see Sections 2.2.1 ~ 2.2.5 for details. Collected data are presented in Table 4-2. Joint formations are presented by Figures 4-5 through 4-28. Each Figure consists of either three or four photos of brazed samples, representing a set of repeated experiments. There were 15 different combinations of background atmosphere conditions, see Section 2.2.3 for clarification. Total of 75 sets of experiments were documented.

The uncertainty for the dew point temperature measurements is $\pm 0.2^\circ\text{C}$, by the General Eastern dew point monitoring system: Hygro M4 and 1311DR (General Eastern, 1996). The accuracy for the oxygen measurement is 5% of the full scale by the Teledyne 316RA Oxygen Analyzer (Teledyne, 1995). As an example, the uncertainty is ± 5 ppm for 20 ppm tests since the measuring scale ranges between 0 and 100 ppm. The accuracy is ± 50 ppm for 200 ppm tests because of the 0 through 1000 ppm scale. The uncertainty for the joint fillet length measurement is ± 0.02 mm.

4.1 Brazeability Criteria

Four empirical criteria for brazeability were selected for evaluation, see Table 4-1. The first criterion (C_a) features joint fillet length which correlates with wetting performance, considered as the primary metric and worth 3 points of brazeability score if considered as a sufficient* joint fillet length. This metric is defined by the normalized joint length (L'). As examples, Figure 4-1 illustrates samples with formed fillets and their measured linear dimensions. The measured joint fillet length in Figure 4-1 (a), 26.2 mm, is divided by the maximum length of the clearance, 50 mm, and denoted by L' . Thus the normalized length L' in Figure 4-1 (a) is

* A sufficient joint fillet length is considered as a length equal or larger than a half of the maximum joint fillet length registered in all 75 tests. The maximum length existed in Test #5 and measured 29.6 mm ($L' = 0.59$) so the value of a sufficient normalized joint fillet length in this study is 0.3.

$$L' = \frac{26.2 \text{ mm}}{50 \text{ mm}} = 0.52 > 0.3$$

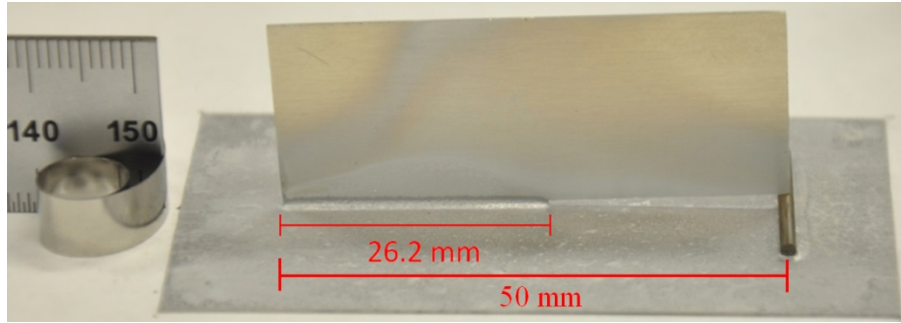
The second example, in Figure 4-1 (b), is

$$L' = \frac{10.5 \text{ mm}}{50 \text{ mm}} = 0.21 < 0.3$$

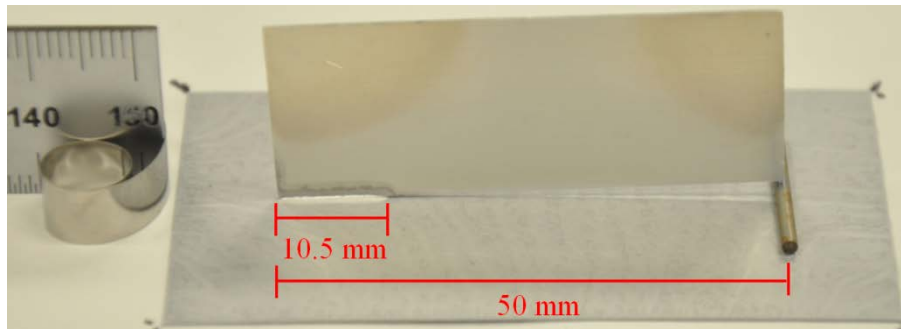
The secondary metrics are related to joint appearance, which are considered as indicators for joint integrity. The metrics include: C_b – absence of a re-solidified clad aggregation (Figure 4-2), C_c – smooth joint appearance (Figure 4-3), and C_d – completed filling at the tip (Figure 4-4). Figure 4-2 (a) presents a uniform joint fillet formation without localized resolidified clad aggregation. In contrast, Figure 4-2 (b) shows that the aggregation appeared on the right end, as marked. Figure 4-3 (a) identifies a smooth/gradual growth of joint fillet from left end to right end. Figure 4-3 (b) features an irregular fillet growth from the left end to the right end. Figure 4-4 (a) presents a covered tip at the left end of the joint fillet, whereas Figure 4-4 (b) features a revealed tip. Each of the secondary metric has 1 point if fulfilled.

Table 4-1 Brazeability Criteria

Category	Metric	Score
Primary	C_a – Joint fillet length	+3
Secondary	C_b – Absence of a re-solidified clad aggregation	+1
	C_c – Smooth joint appearance	+1
	C_d – Completed filling at the tip	+1

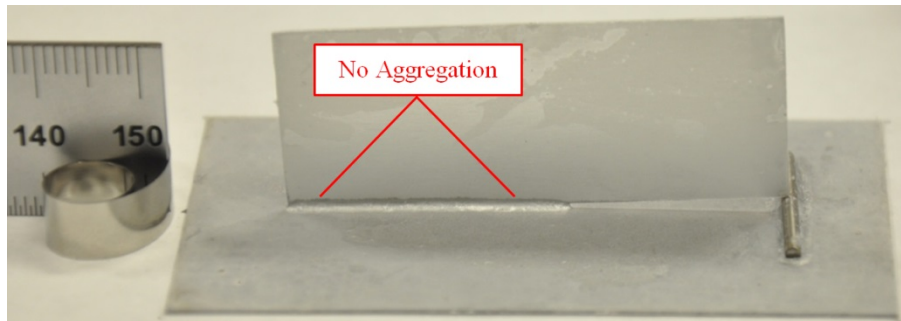


(a)

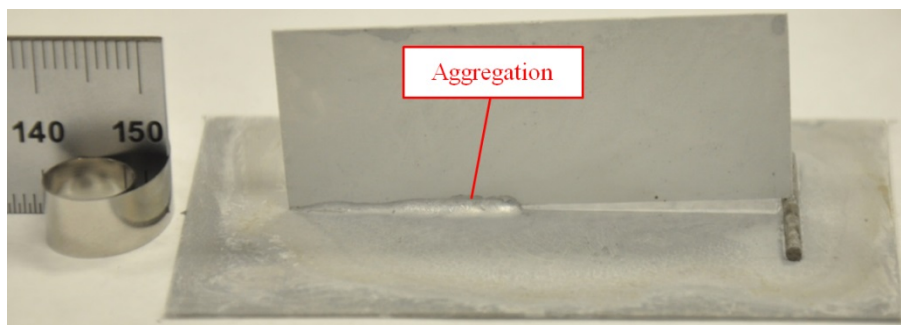


(b)

Figure 4-1 Examples for Metric C_a (a) $L' > 0.3$ (b) $L' < 0.3$

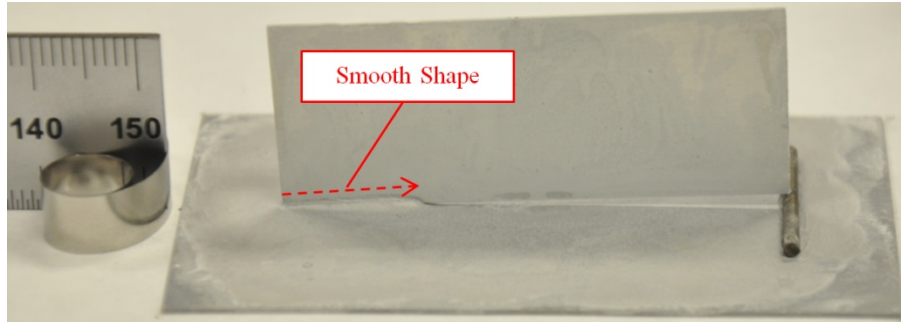


(a)

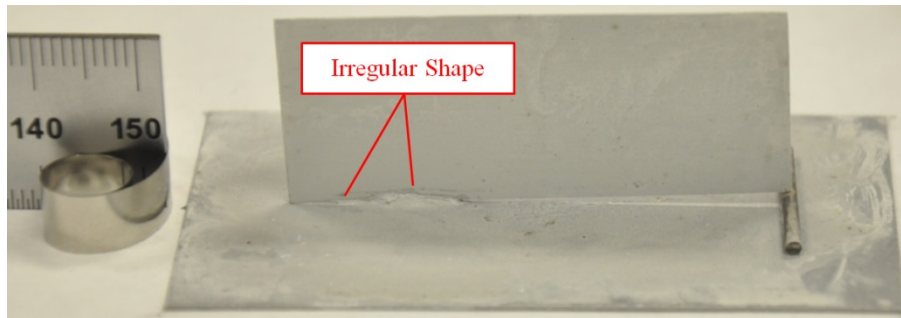


(b)

Figure 4-2 Examples for Metric C_b (a) No Aggregation (b) Aggregation

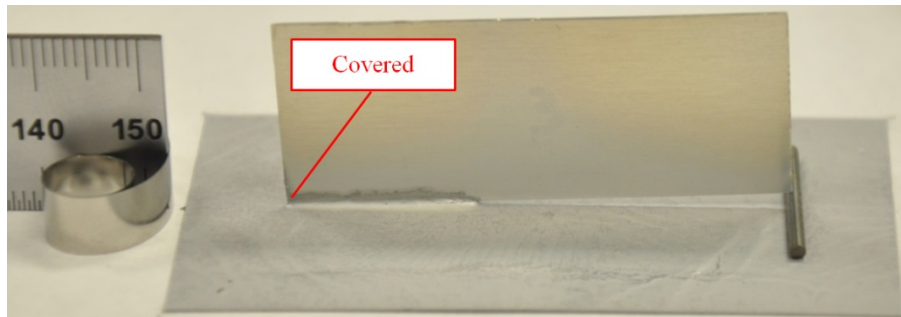


(a)

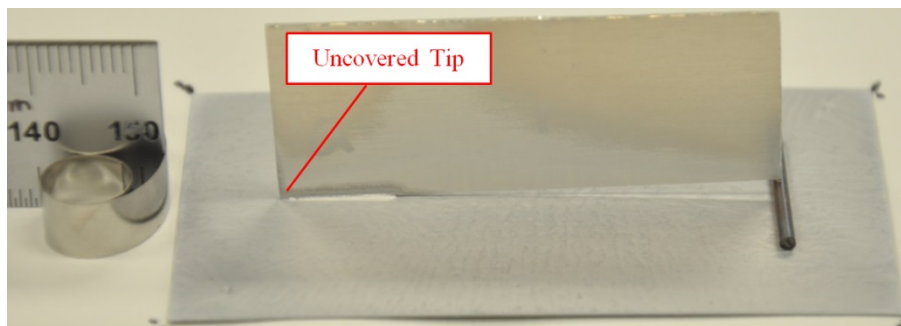


(b)

Figure 4-3 Examples for Metric C_c (a) Smooth Shape (b) Irregular Shape



(a)



(b)

Figure 4-4 Examples for Metric C_d (a) Covered Tip (b) Uncovered Tip

4.2 Results of Furnace Experiments

All test results are summarized in Table 4-2. For each metric, “Y” is marked if fulfilled and “N” if failed to satisfy. The last column of Table 4-2 concludes the total score for each sample. All brazed samples are photo documented and presented by Figures 4-5 ~ 4-28.

Table 4-2 Test Results of Brazed Samples

Test #	Data Entry	Material	T _{dp} (°C)*	O ₂ (ppm)†	L' ‡	C _a (+3)	C _b (+1)	C _c (+1)	C _d (+1)	Score
1	Figure 4-5 (a)	Traditional	-48	2E+1	0.56	Y	Y	Y	Y	6
2	Figure 4-5 (b)	Traditional	-48	2E+1	0.48	Y	Y	Y	Y	6
3	Figure 4-5 (c)	Traditional	-48	2E+1	0.55	Y	Y	Y	Y	6
4	Figure 4-6 (a)	Traditional	-48	2E+2	0.58	Y	Y	Y	Y	6
5	Figure 4-6 (b)	Traditional	-48	2E+2	0.59	Y	Y	Y	Y	6
6	Figure 4-6 (c)	Traditional	-48	2E+2	0.51	Y	Y	Y	Y	6
7	Figure 4-7 (a)	Traditional	-48	2E+3	0.44	Y	N	Y	Y	5
8	Figure 4-7 (b)	Traditional	-48	2E+3	0.48	Y	N	Y	Y	5
9	Figure 4-7 (c)	Traditional	-48	2E+3	0.56	Y	N	N	Y	4
10	Figure 4-8 (a)	Traditional	-18	2E+1	0.58	Y	N	Y	Y	5
11	Figure 4-8 (b)	Traditional	-18	2E+1	0.56	Y	Y	Y	Y	6
12	Figure 4-8 (c)	Traditional	-18	2E+1	0.57	Y	N	Y	Y	5
13	Figure 4-9 (a)	Traditional	-18	2E+2	0.50	Y	N	Y	Y	5
14	Figure 4-9 (b)	Traditional	-18	2E+2	0.58	Y	N	Y	Y	5
15	Figure	Traditional	-18	2E+2	0.46	Y	N	N	Y	4

* Uncertainty for T_{dp} measurement is ± 0.2°C

† Uncertainty for O₂ measurement is ± 0.25 * (value of O₂) ppm

‡ Uncertainty for normalized fillet length is ± 0.0004 (i.e. ± 0.02 mm /50 mm)

	4-9 (c)									
16	Figure 4-10 (a)	Traditional	-18	2E+3	0.28	N	N	Y	Y	2
17	Figure 4-10 (b)	Traditional	-18	2E+3	0.23	N	N	N	Y	1
18	Figure 4-10 (c)	Traditional	-18	2E+3	0.35	Y	N	N	Y	4
19	Figure 4-11 (a)	Traditional	-7	2E+1	0.34	Y	N	N	N	3
20	Figure 4-11 (b)	Traditional	-7	2E+1	0.27	N	N	N	N	0
21	Figure 4-11 (c)	Traditional	-7	2E+1	0.28	N	N	N	N	0
22	Figure 4-12 (a)	Traditional	-7	2E+2	0.00	N	N	N	N	0
23	Figure 4-12 (b)	Traditional	-7	2E+2	0.27	N	N	N	Y	1
24	Figure 4-12 (c)	Traditional	-7	2E+2	0.33	Y	N	N	N	3
25	Figure 4-13 (a)	Traditional	-7	2E+3	0.27	N	N	N	N	0
26	Figure 4-13 (b)	Traditional	-7	2E+3	0.16	N	N	N	N	0
27	Figure 4-13 (c)	Traditional	-7	2E+3	0.16	N	N	N	N	0
28	Figure 4-14 (a)	Trillium™	-48	2E+1	0.52	Y	Y	Y	Y	6
29	Figure 4-14 (b)	Trillium™	-48	2E+1	0.53	Y	Y	Y	Y	6
30	Figure 4-14 (c)	Trillium™	-48	2E+1	0.54	Y	Y	Y	Y	6
31	Figure 4-15 (a)	Trillium™	-48	2E+2	0.59	Y	Y	Y	Y	6
32	Figure 4-15 (b)	Trillium™	-48	2E+2	0.50	Y	Y	Y	Y	6
33	Figure 4-15 (c)	Trillium™	-48	2E+2	0.54	Y	Y	Y	Y	6
34	Figure 4-16 (a)	Trillium™	-48	2E+3	0.40	Y	Y	Y	Y	6
35	Figure 4-16 (b)	Trillium™	-48	2E+3	0.46	Y	N	Y	Y	5
36	Figure 4-16 (c)	Trillium™	-48	2E+3	0.40	Y	Y	Y	Y	6
37	Figure 4-19 (a)	Trillium™	-18	2E+1	0.53	Y	N	Y	Y	5

38	Figure 4-19 (b)	Trillium™	-18	2E+1	0.49	Y	N	Y	Y	5
39	Figure 4-19 (c)	Trillium™	-18	2E+1	0.55	Y	Y	Y	Y	6
40	Figure 4-20 (a)	Trillium™	-18	2E+2	0.38	Y	N	Y	Y	5
41	Figure 4-20 (b)	Trillium™	-18	2E+2	0.51	Y	N	Y	Y	5
42	Figure 4-20 (c)	Trillium™	-18	2E+2	0.44	Y	N	Y	Y	5
43	Figure 4-21 (a)	Trillium™	-18	2E+3	0.43	Y	N	Y	Y	5
44	Figure 4-21 (b)	Trillium™	-18	2E+3	0.35	Y	N	Y	Y	5
45	Figure 4-21 (c)	Trillium™	-18	2E+3	0.41	Y	N	Y	Y	5
46	Figure 4-24 (a)	Trillium™	-7	2E+1	0.39	Y	N	Y	Y	5
47	Figure 4-24 (b)	Trillium™	-7	2E+1	0.33	Y	N	Y	N	4
48	Figure 4-24 (c)	Trillium™	-7	2E+1	0.32	Y	N	Y	N	4
49	Figure 4-25 (a)	Trillium™	-7	2E+2	0.43	Y	N	Y	N	4
50	Figure 4-25 (b)	Trillium™	-7	2E+2	0.34	Y	N	Y	N	4
51	Figure 4-25 (c)	Trillium™	-7	2E+2	0.30	Y	N	Y	N	4
52	Figure 4-26 (a)	Trillium™	-7	2E+3	0.31	Y	N	Y	N	4
53	Figure 4-26 (b)	Trillium™	-7	2E+3	0.29	N	N	Y	N	1
54	Figure 4-26 (c)	Trillium™	-7	2E+3	0.27	N	N	Y	N	1
55	Figure 4-17 (a)	Trillium™	-48	2E+4	0.31	Y	N	Y	N	4
56	Figure 4-17 (b)	Trillium™	-48	2E+4	0.26	N	N	Y	Y	2
57	Figure 4-17 (c)	Trillium™	-48	2E+4	0.21	N	N	Y	Y	2
58	Figure 4-22 (d)	Trillium™	-48	2E+4	0.39	Y	N	Y	Y	5
59	Figure 4-22 (a)	Trillium™	-18	2E+4	0.29	N	N	Y	Y	2
60	Figure 4-22 (b)	Trillium™	-18	2E+4	0.27	N	N	Y	Y	2

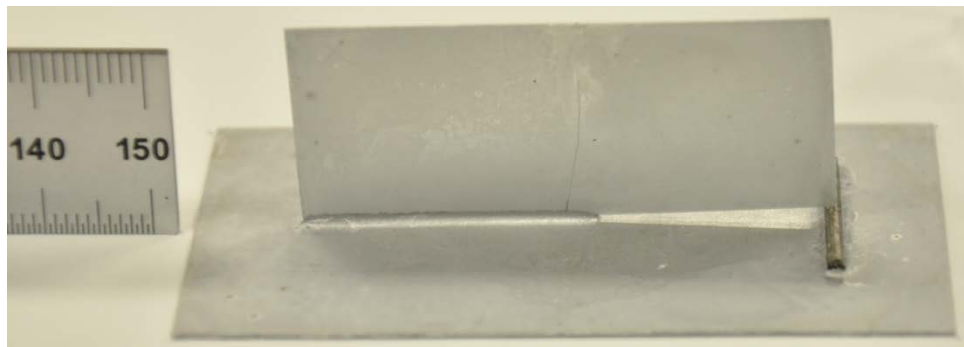
61	Figure 4-22 (c)	Trillium™	-18	2E+4	0.23	N	N	Y	Y	2
62	Figure 4-27 (c)	Trillium™	-7	2E+4	0.00	N	N	N	N	0
63	Figure 4-27 (b)	Trillium™	-7	2E+4	0.22	N	N	Y	N	1
64	---	Trillium™	-7	2E+4	0.23	N	N	Y	N	1
65	Figure 4-18 (a)	Trillium™	-48	2E+5	0.21	N	N	Y	N	1
66	Figure 4-18 (b)	Trillium™	-48	2E+5	0.19	N	N	Y	N	1
67	Figure 4-18 (c)	Trillium™	-48	2E+5	0.20	N	N	Y	Y	2
68	Figure 4-23 (a)	Trillium™	-18	2E+5	0.25	N	N	Y	N	1
69	Figure 4-23 (b)	Trillium™	-18	2E+5	0.23	N	N	Y	N	1
70	Figure 4-23 (c)	Trillium™	-18	2E+5	0.20	N	N	Y	N	1
71	Figure 4-23 (d)	Trillium™	-18	2E+5	0.31	Y	N	Y	N	4
72	Figure 4-28 (a)	Trillium™	-7	2E+5	0.25	N	N	Y	N	1
73	Figure 4-28 (b)	Trillium™	-7	2E+5	0.15	N	N	N	N	0
74	Figure 4-28 (c)	Trillium™	-7	2E+5	0.00	N	N	N	N	0
75	Figure 4-28 (d)	Trillium™	-7	2E+5	0.20	N	N	N	N	0



(a)



(b)

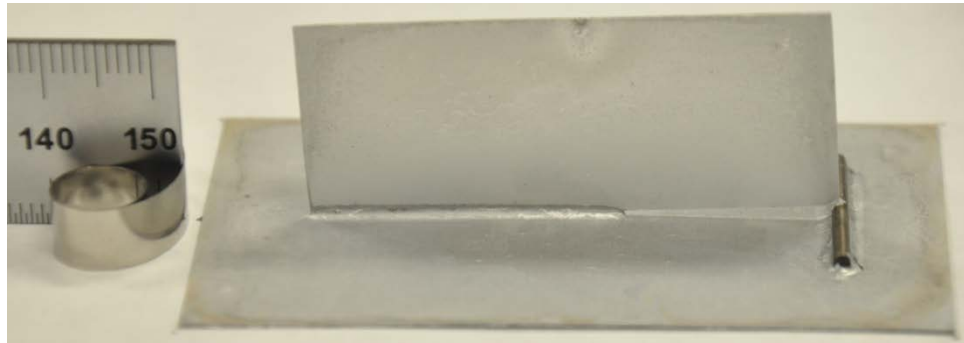


(c)

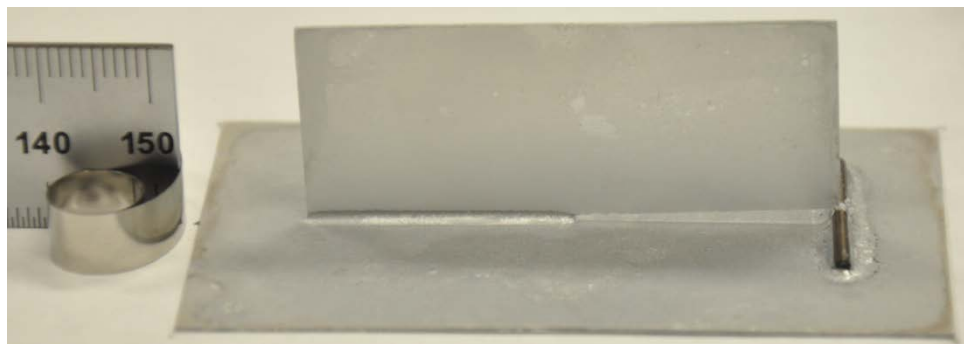
Figure 4-5 Joint Formation of Traditional Brazing Samples at $T_{dp} = -48^{\circ}\text{C}$ and $\text{O}_2 = 20 \text{ ppm}$ (a) Test #1 (b) Test #2 (c) Test #3



(a)

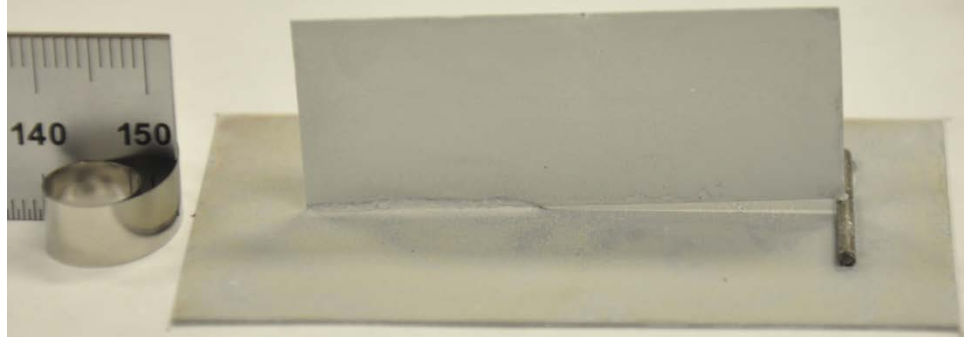


(b)

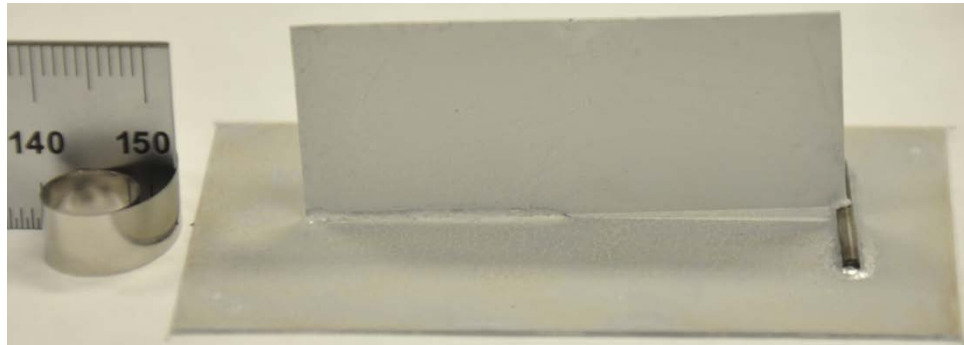


(c)

Figure 4-6 Joint Formation of Traditional Brazing Samples at $T_{dp} = -48^{\circ}\text{C}$ and $\text{O}_2 = 200 \text{ ppm}$ (a) Test #4 (b) Test #5 (c) Test #6



(a)

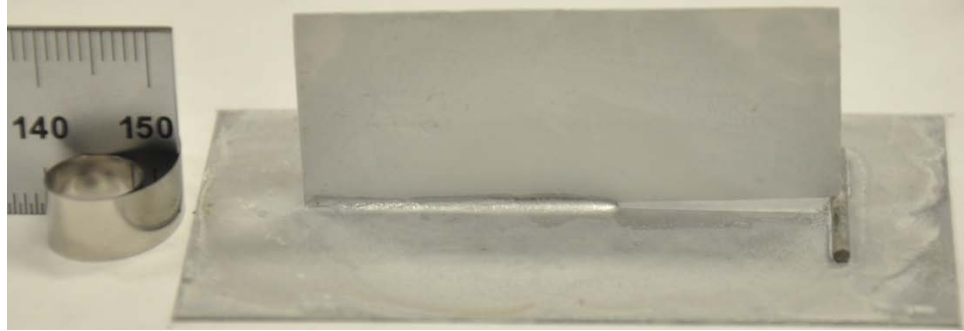


(b)

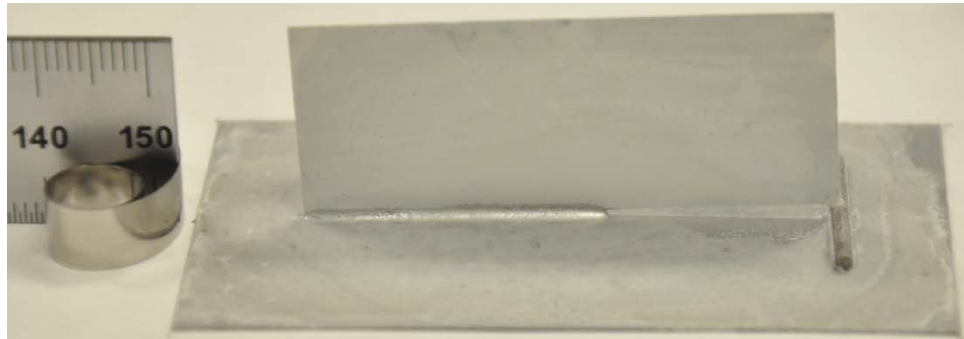


(c)

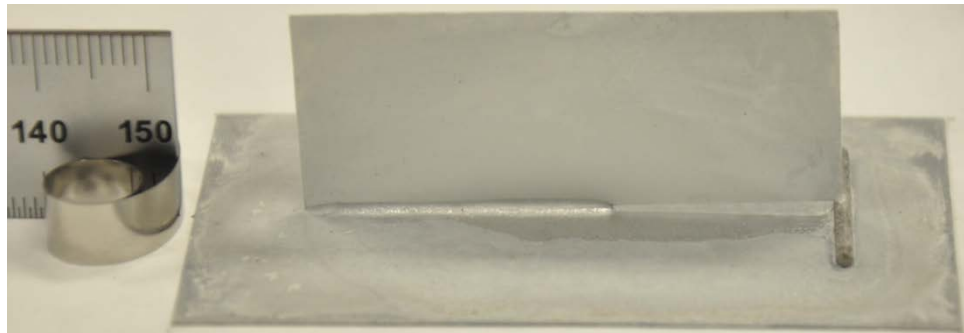
Figure 4-7 Joint Formation of Traditional Brazing Samples at $T_{dp} = -48^{\circ}\text{C}$ and $\text{O}_2 = 2000 \text{ ppm}$ (a) Test #7 (b) Test #8 (c) Test #9



(a)

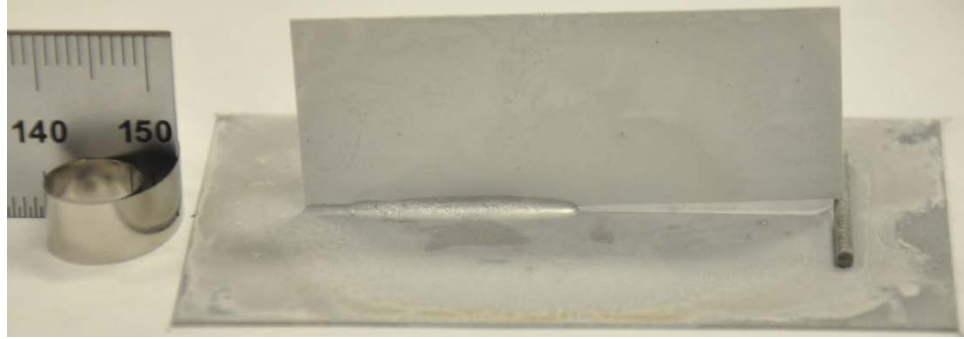


(b)

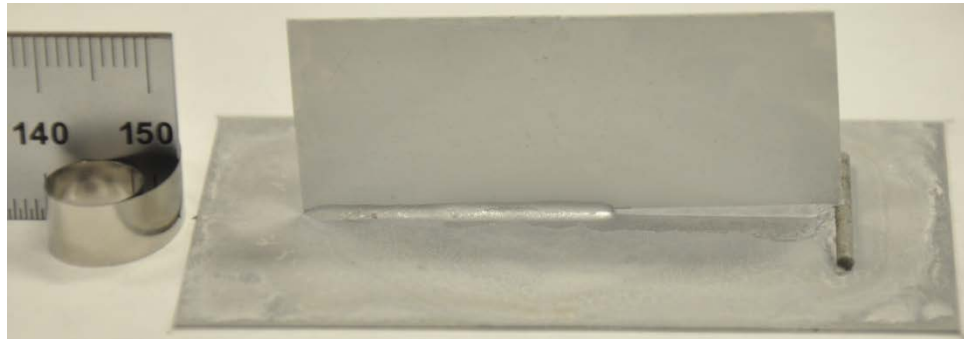


(c)

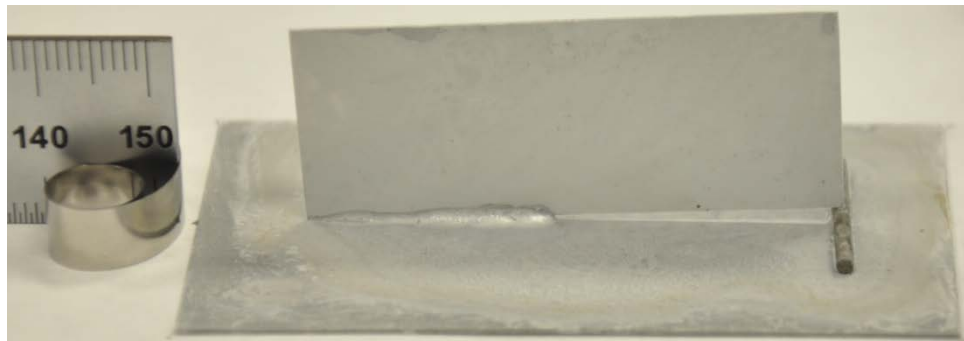
Figure 4-8 Joint Formation of Traditional Brazing Samples at $T_{dp} = -18^{\circ}\text{C}$ and $\text{O}_2 = 20 \text{ ppm}$ (a) Test #10 (b) Test #11 (c) Test #12



(a)

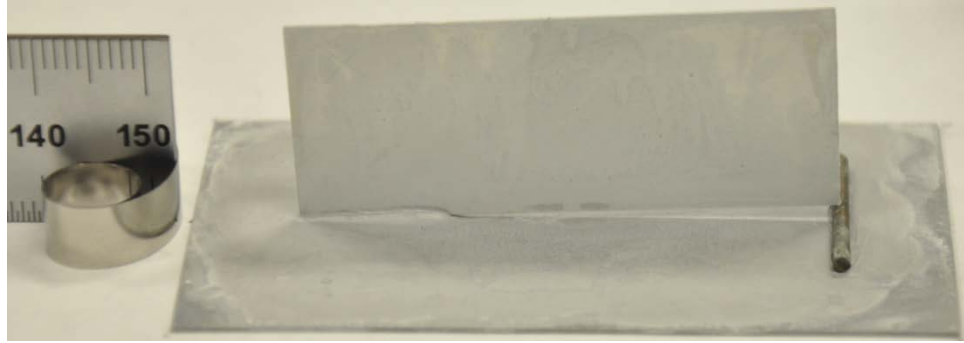


(b)



(c)

Figure 4-9 Joint Formation of Traditional Brazing Samples at $T_{dp} = -18^{\circ}\text{C}$ and $\text{O}_2 = 200 \text{ ppm}$ (a) Test #13 (b) Test #14 (c) Test #15



(a)



(b)

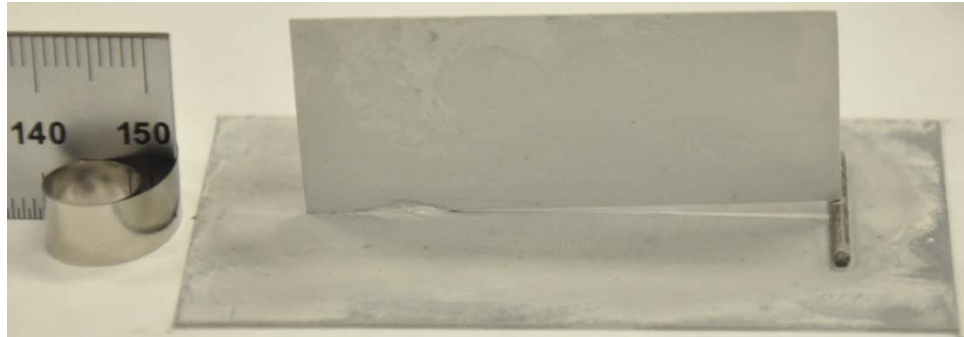


(c)

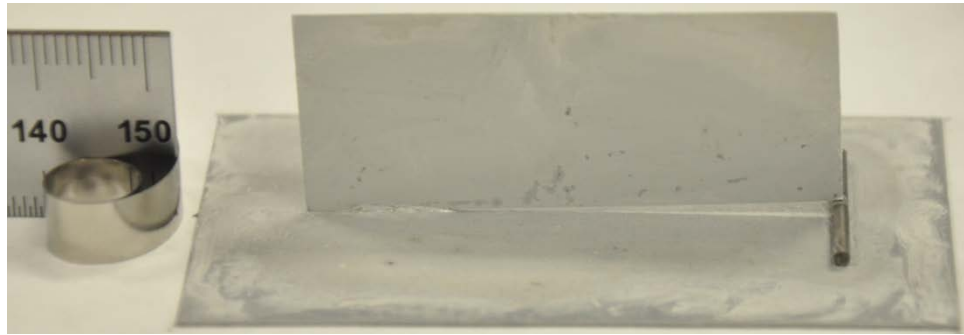
Figure 4-10 Joint Formation of Traditional Brazing Samples at $T_{dp} = -18^{\circ}\text{C}$ and $\text{O}_2 = 2000 \text{ ppm}$ (a) Test #16 (b) Test #17 (c) Test #18



(a)



(b)



(c)

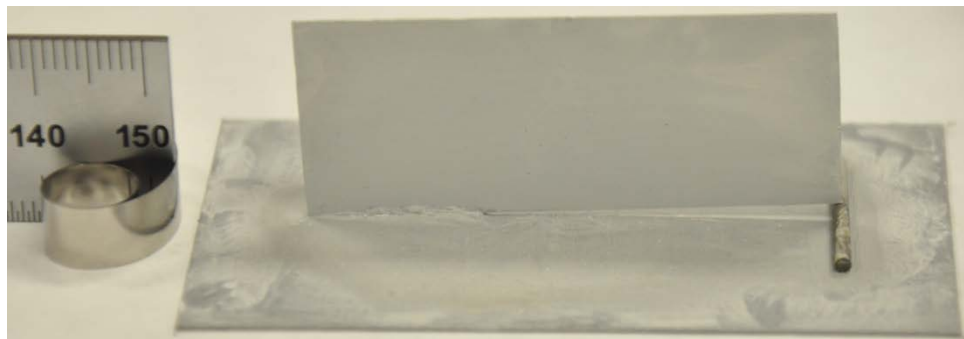
Figure 4-11 Joint Formation of Traditional Brazing Samples at $T_{dp} = -7^{\circ}\text{C}$ and $\text{O}_2 = 20 \text{ ppm}$ (a) Test #19 (b) Test #20 (c) Test #21



(a)



(b)



(c)

Figure 4-12 Joint Formation of Traditional Brazing Samples at $T_{dp} = -7^{\circ}\text{C}$ and $\text{O}_2 = 200 \text{ ppm}$ (a) Test #22 (b) Test #23 (c) Test #24



(a)

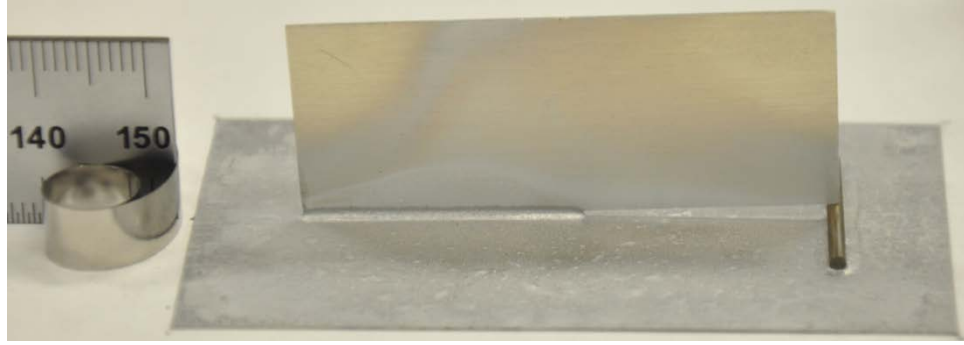


(b)

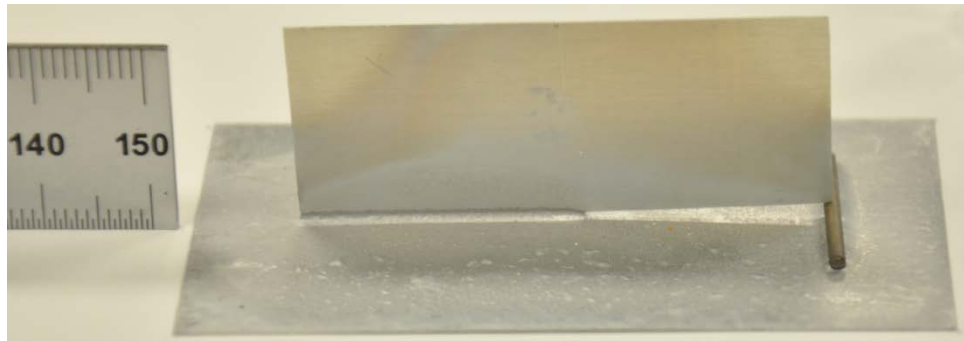


(c)

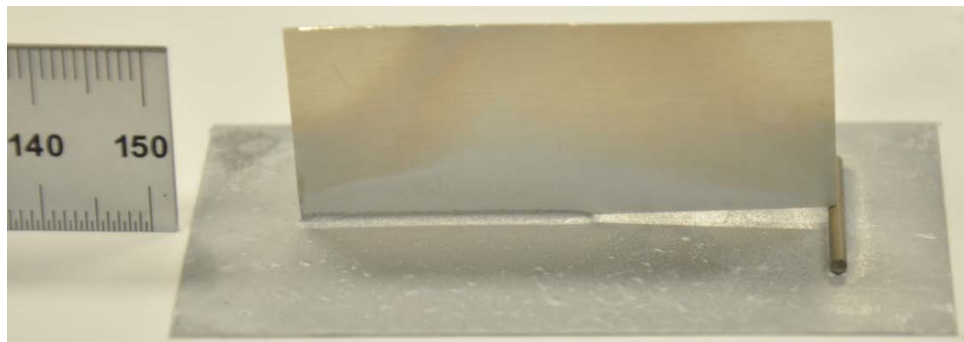
Figure 4-13 Joint Formation of Traditional Brazing Samples at $T_{dp} = -7^{\circ}\text{C}$ and $\text{O}_2 = 2000 \text{ ppm}$ (a) Test #25 (b) Test #26 (c) Test #27



(a)

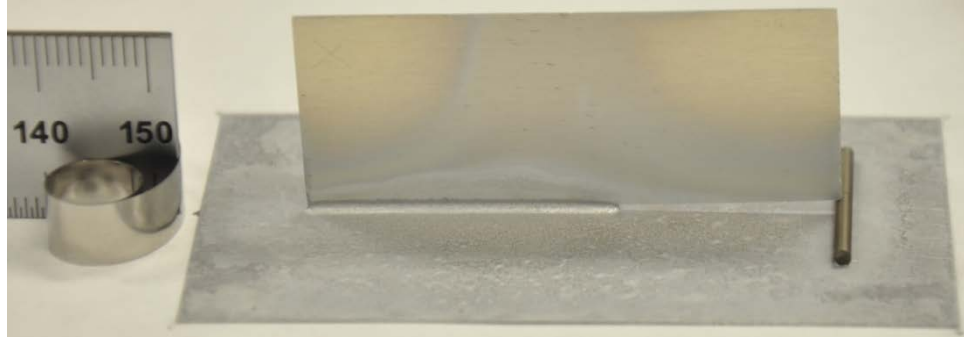


(b)

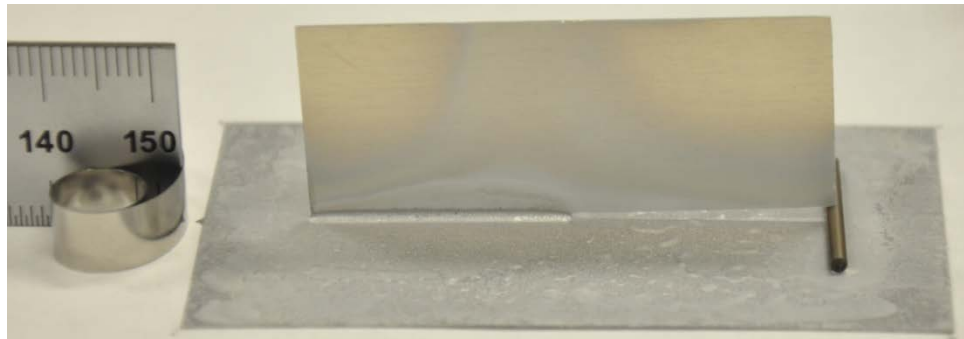


(c)

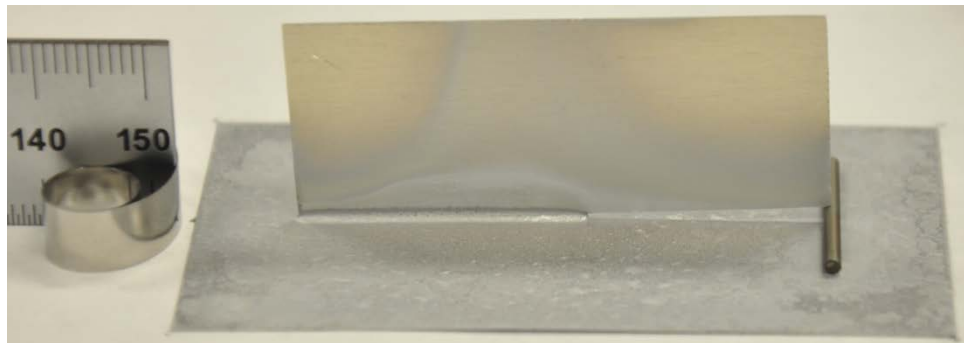
Figure 4-14 Joint Formation of Trillium™ Brazing Samples at $T_{dp} = -48^{\circ}\text{C}$ and $\text{O}_2 = 20$ ppm (a) Test #28 (b) Test #29 (c) Test #30



(a)

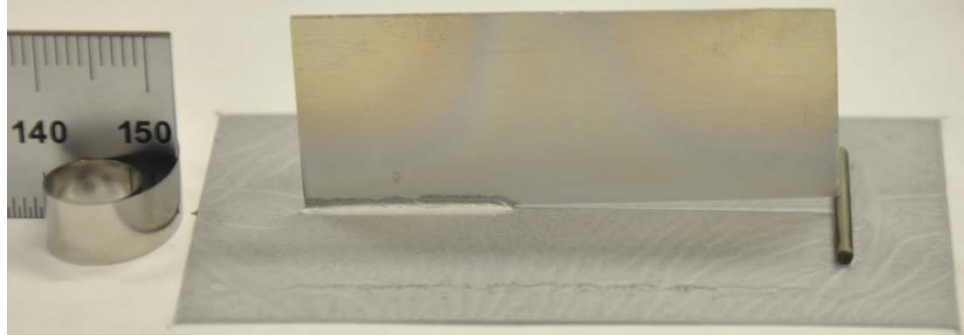


(b)



(c)

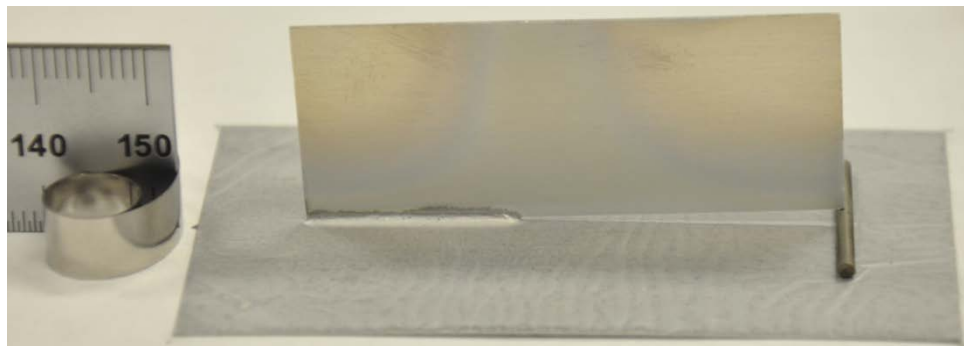
Figure 4-15 Joint Formation of Trillium™ Brazing Samples at $T_{dp} = -48^{\circ}\text{C}$ and $\text{O}_2 = 200 \text{ ppm}$ (a) Test #31 (b) Test #32 (c) Test #33



(a)



(b)

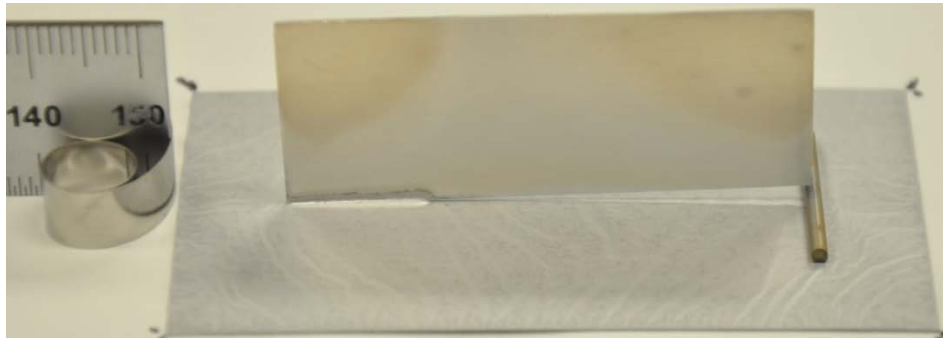


(c)

Figure 4-16 Joint Formation of Trillium™ Brazing Samples at $T_{dp} = -48^{\circ}\text{C}$ and $\text{O}_2 = 2000 \text{ ppm}$ (a) Test #34 (b) Test #35 (c) Test #36



(a)



(b)



(c)

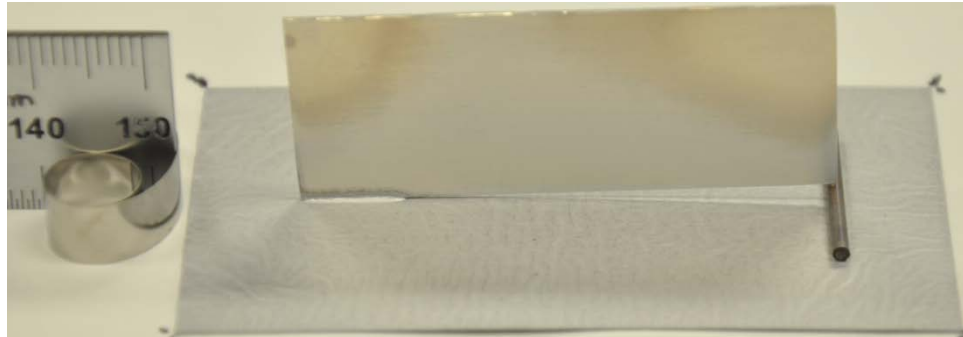


(d)

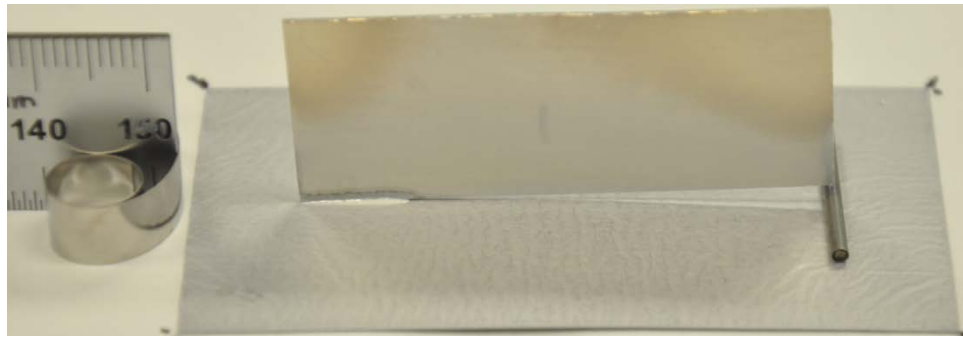
Figure 4-17 Joint Formation of Trillium™ Brazing Samples at $T_{dp} = -48^{\circ}\text{C}$ and $\text{O}_2 = 20000 \text{ ppm}$ (a) Test #55 (b) Test #56 (c) Test #57 (d) Test #58



(a)

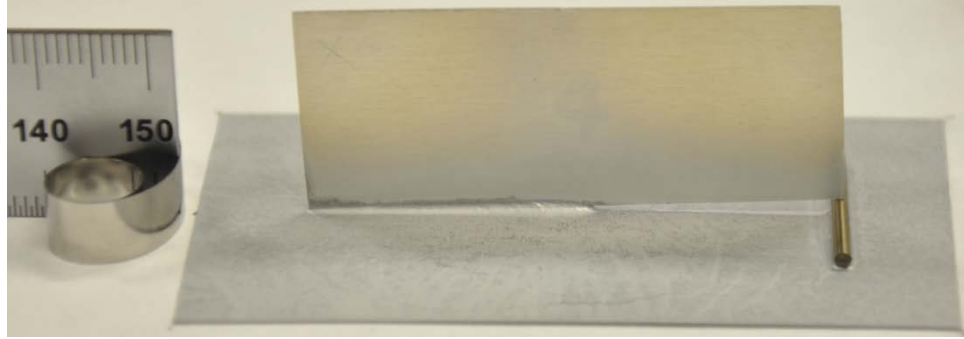


(b)



(c)

Figure 4-18 Joint Formation of Trillium™ Brazing Samples at $T_{dp} = -48^{\circ}\text{C}$ and $\text{O}_2 = 200000 \text{ ppm}$ (a) Test #65 (b) Test #66 (c) Test #67



(a)



(b)



(c)

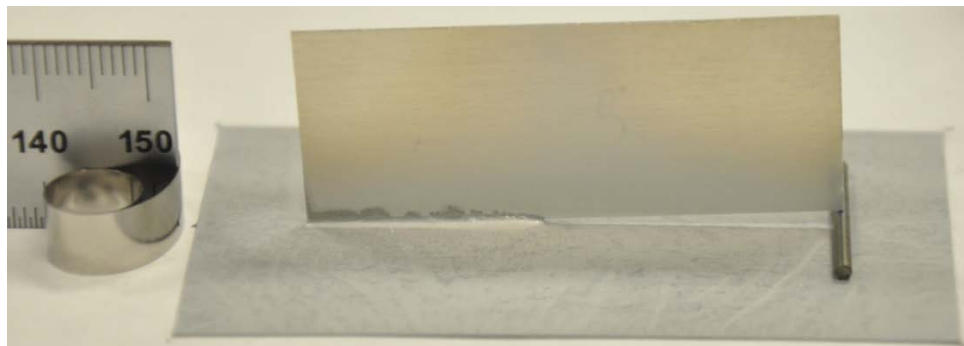
Figure 4-19 Joint Formation of Trillium™ Brazing Samples at $T_{dp} = -18^{\circ}\text{C}$ and $\text{O}_2 = 20 \text{ ppm}$ (a) Test #37 (b) Test #38 (c) Test #39



(a)



(b)



(c)

Figure 4-20 Joint Formation of Trillium™ Brazing Samples at $T_{dp} = -18^{\circ}\text{C}$ and $\text{O}_2 = 200 \text{ ppm}$ (a) Test #40 (b) Test #41 (c) Test #42



(a)

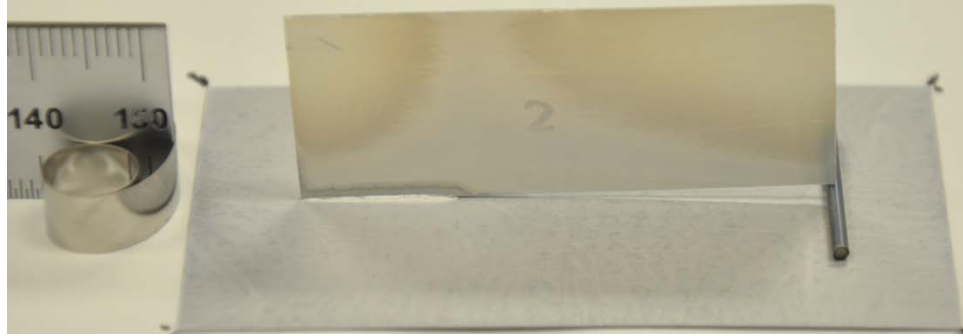


(b)



(c)

Figure 4-21 Joint Formation of Trillium™ Brazing Samples at $T_{dp} = -18^{\circ}\text{C}$ and $\text{O}_2 = 2000 \text{ ppm}$ (a) Test #43 (b) Test #44 (c) Test #45



(a)

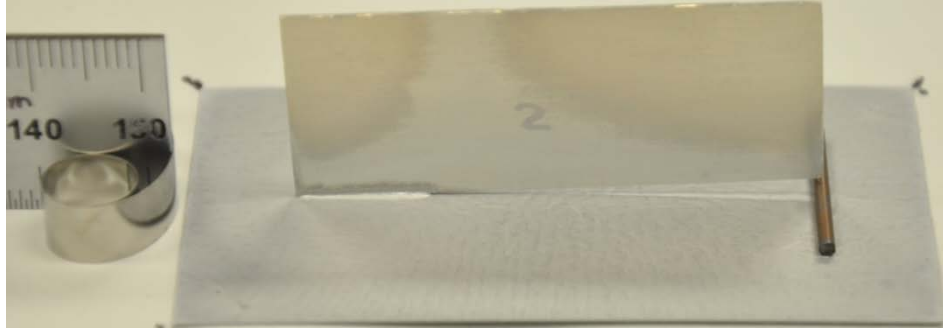


(b)

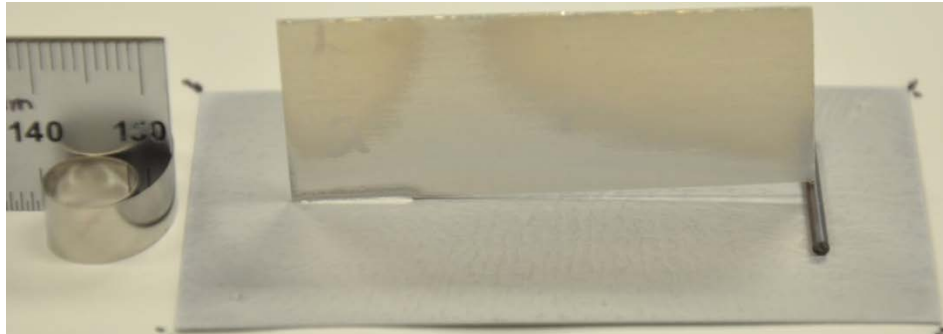


(c)

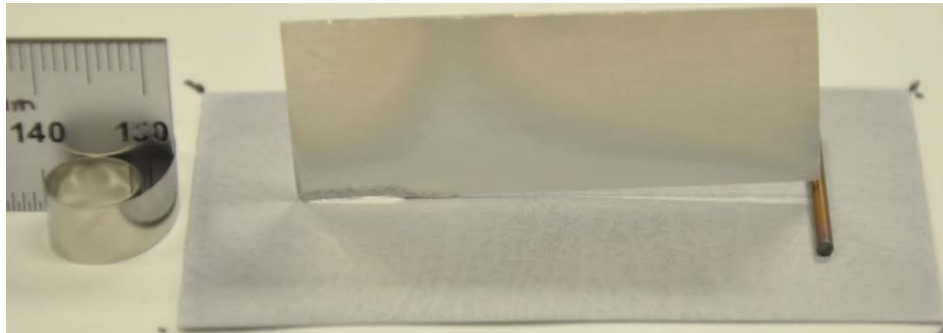
Figure 4-22 Joint Formation of Trillium™ Brazing Samples at $T_{dp} = -18^{\circ}\text{C}$ and $\text{O}_2 = 20000 \text{ ppm}$ (a) Test #59 (b) Test #60 (c) Test #61



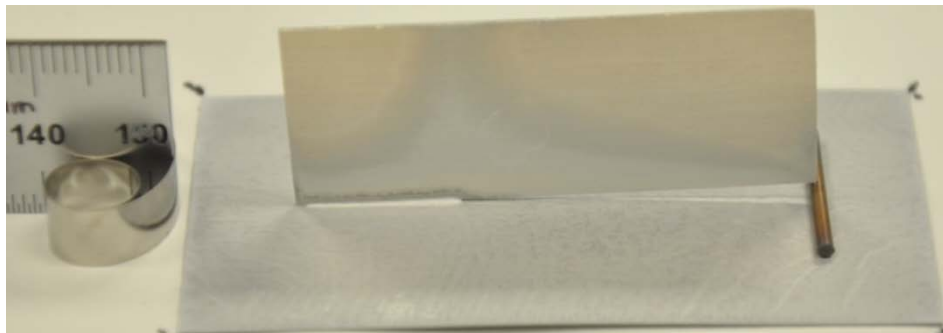
(a)



(b)



(c)



(d)

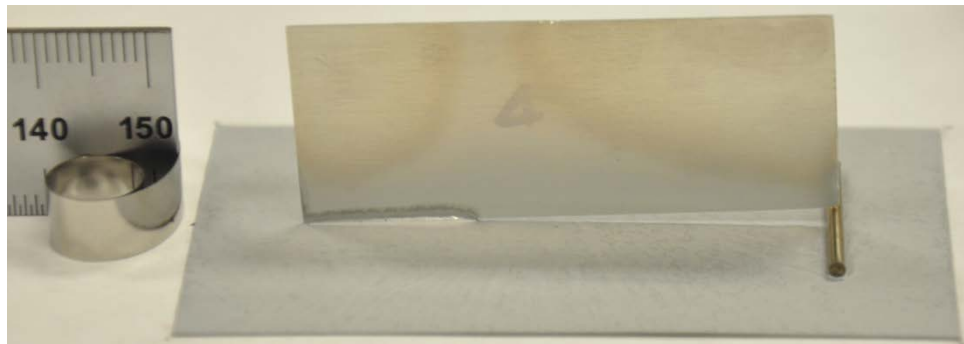
Figure 4-23 Joint Formation of Trillium™ Brazing Samples at $T_{dp} = -18^{\circ}\text{C}$ and $\text{O}_2 = 200000$ ppm (a) Test #68 (b) Test #69 (c) Test #70 (d) Test #71



(a)

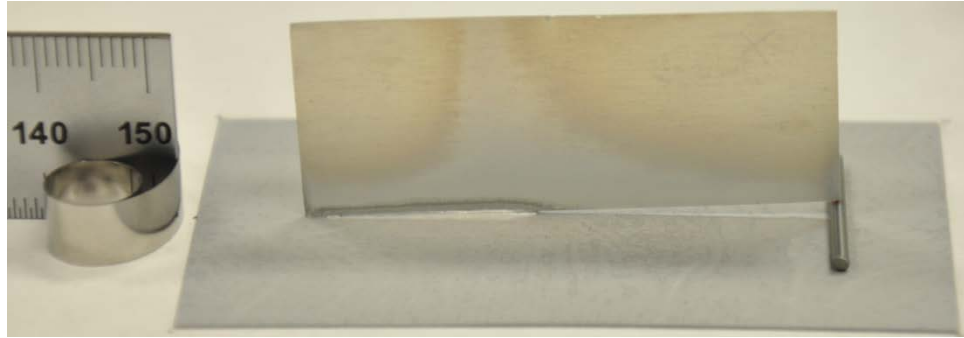


(b)



(c)

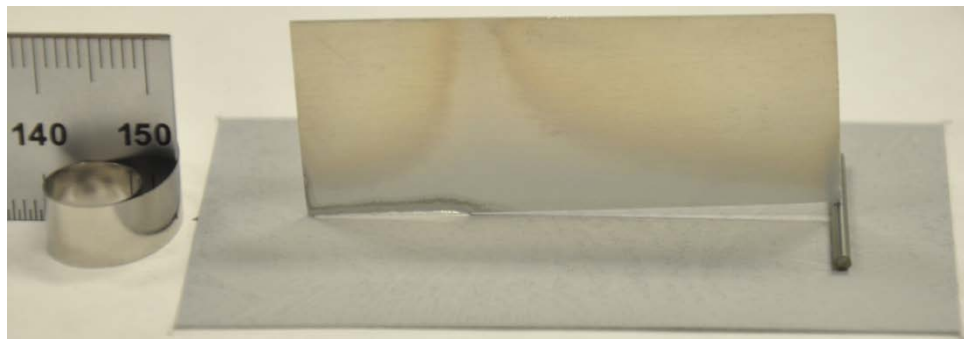
Figure 4-24 Joint Formation of Trillium™ Brazing Samples at $T_{dp} = -7^{\circ}\text{C}$ and $\text{O}_2 = 20 \text{ ppm}$ (a) Test #46 (b) Test #47 (c) Test #48



(a)

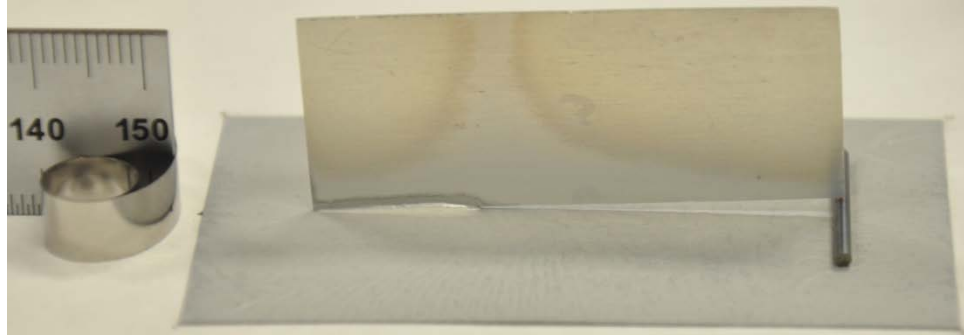


(b)

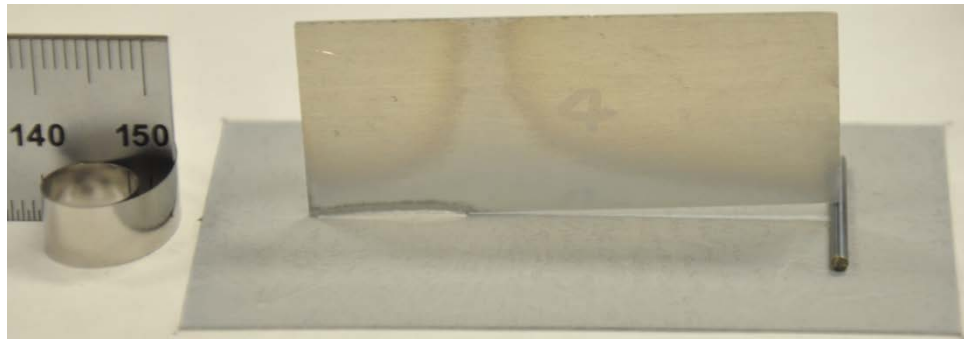


(c)

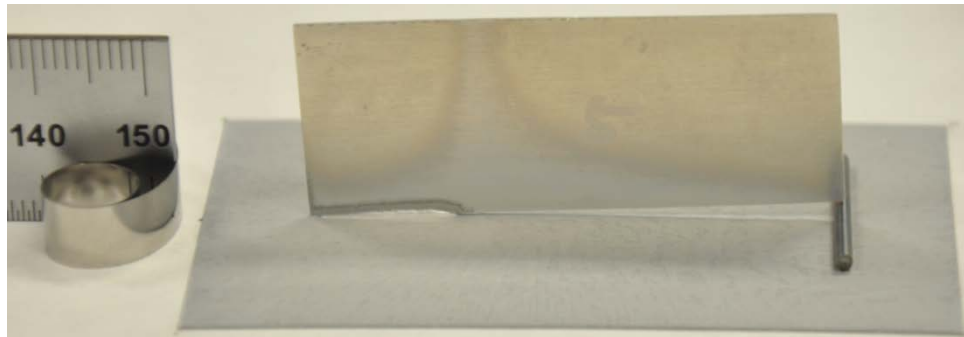
Figure 4-25 Joint Formation of Trillium™ Brazing Samples at $T_{dp} = -7^{\circ}\text{C}$ and $\text{O}_2 = 200 \text{ ppm}$ (a) Test #49 (b) Test #50 (c) Test #51



(a)



(b)

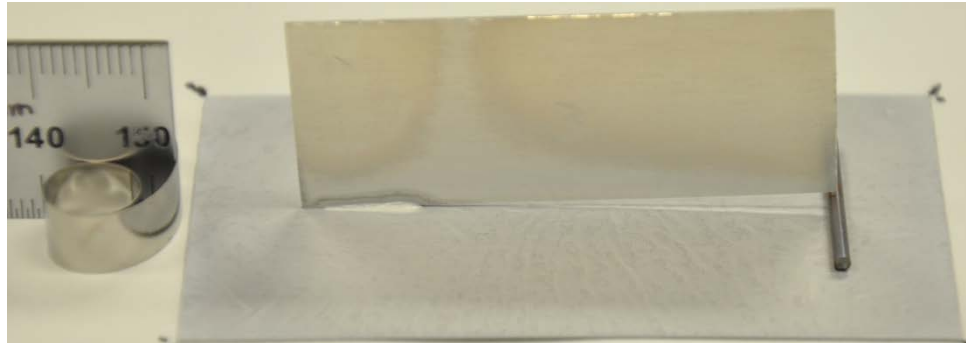


(c)

Figure 4-26 Joint Formation of Trillium™ Brazing Samples at $T_{dp} = -7^{\circ}\text{C}$ and $\text{O}_2 = 2000 \text{ ppm}$ (a) Test #52 (b) Test #53 (c) Test #54



(a)

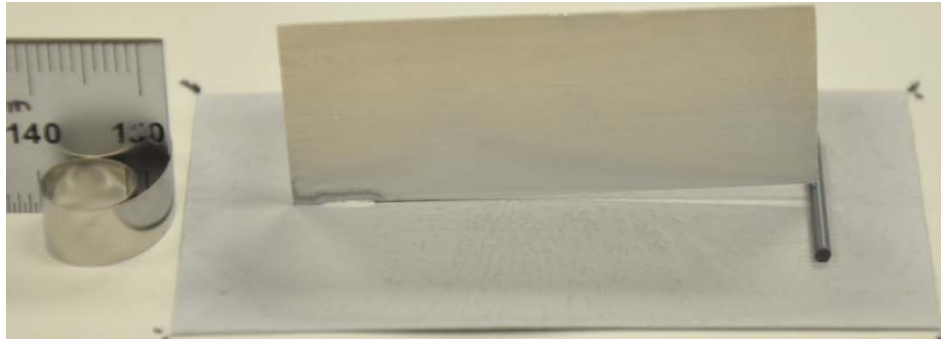


(b)

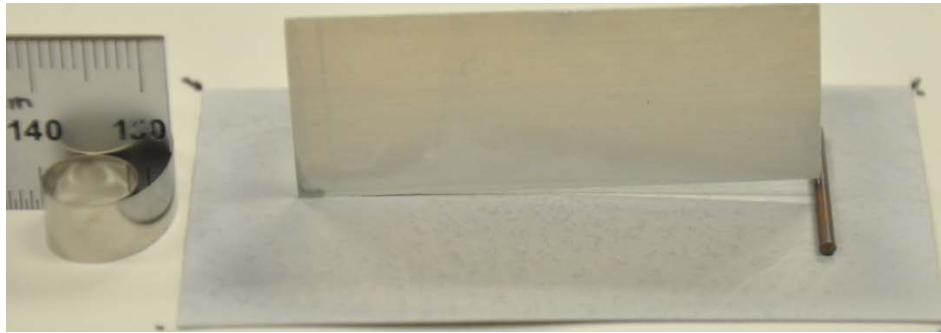
Figure 4-27 Joint Formation of Trillium™ Brazing Samples at $T_{dp} = -7^{\circ}\text{C}$ and $\text{O}_2 = 20000 \text{ ppm}$ (a) Test #62 (b) Test #63



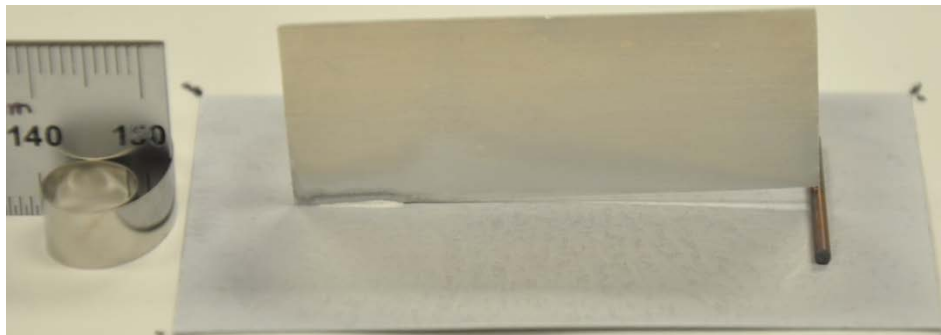
(a)



(b)



(c)



(d)

Figure 4-28 Joint Formation of Trillium™ Brazing Samples at $T_{dp} = -7^{\circ}\text{C}$ and $\text{O}_2 = 200000$ ppm (a) Test #72 (b) Test #73 (c) Test #74 (d) Test #75

4.3 Brazeability vs. Atmospheric Conditions

Table 4-3 Brazeability Symbols

Score	Performance	Symbol for Traditional Material	Symbol for Trillium™ Material
6	Excellent	■	●
5	Good	◼	◐
3 or 4	Fair	▨	◑
1 or 2	Poor	◻	◒
0	Bad	□	○

In Table 4-3 the scores of brazed samples are categorized into five different levels of performance of joint formation and marked with different symbols. A square icon represents a traditional sample and a circular icon denotes a Trillium™ sample. An icon is marked solid if a score of 6 is obtained, considered an excellent joint formation. A half solid icon stands for a score of 5, referring to good joint formation. An icon with multiple diagonal lines is for the score of 3 or 4, representing a fair joint formation. If an icon has a single diagonal line, the score of a sample is evaluated 1 or 2, considered poor joint formation. An empty icon indicates a score of 0 and it is referring to bad or none joint formation.

Figure 4-29 presents a brazeability map based on the brazed data from Table 4-2 with symbols as given in Table 4-3. The horizontal and vertical axes are oxygen concentration and dew point temperature, respectively. Five levels of oxygen concentration and three levels of dew point temperature are included in this plot, in total 15 combinations of brazing background atmosphere conditions. The measured atmospheric conditions and their repeatability are documented in Table D-1, see Appendix D. In the range of 20 ppm through 2000 ppm oxygen concentration and -48°C through -7°C dew point temperatures, each of these 9 atmospheric conditions was repeated three times for both traditional and Trillium™ samples. The other atmospheric conditions were repeated three to four times only for Trillium™ sample because of the limited resources related to available traditional materials. Note that each data point may not represent the exact location on the axes but shifted to the adjacent position for the

purpose of displaying comprehensive data entries. Each set of parentheses with O_2 & T_{dp} values denotes an atmosphere combination for the adjacent data entries.

According to Figure 4-29, one can see that Trillium™ and traditional materials behaved excellently in the lower left region of the map, i.e. under most favorable background atmosphere. The poorest joint formation happens in the top right region of the map, i.e. a condition analogue to air. Gradual deterioration of joint fillet performance can be noticed along with increasing levels of oxygen concentration (X-axis) and dew point temperature (Y-axis). As the atmosphere condition deteriorates, Trillium™ materials features good joint formation at $T_{dp} = -7^\circ C$ & 20 ppm O_2 , $T_{dp} = -18^\circ C$ & 2000 ppm O_2 , and $T_{dp} = -48^\circ C$ & 20000 ppm O_2 , as marked by the dashed line with the notation “Trillium™” in Figure 4-29. On the other hand, traditional materials have good joint formation in the region of $T_{dp} = -18^\circ C$ & 20 ppm O_2 , $T_{dp} = -18^\circ C$ & 200 ppm O_2 , and $T_{dp} = -48^\circ C$ & 2000 ppm O_2 , indicated by the dashed line with the notation “Traditional”. It is concluded that Trillium™ brazing sheet is significantly more resilient vs. traditional brazing sheet under adverse background atmosphere conditions.

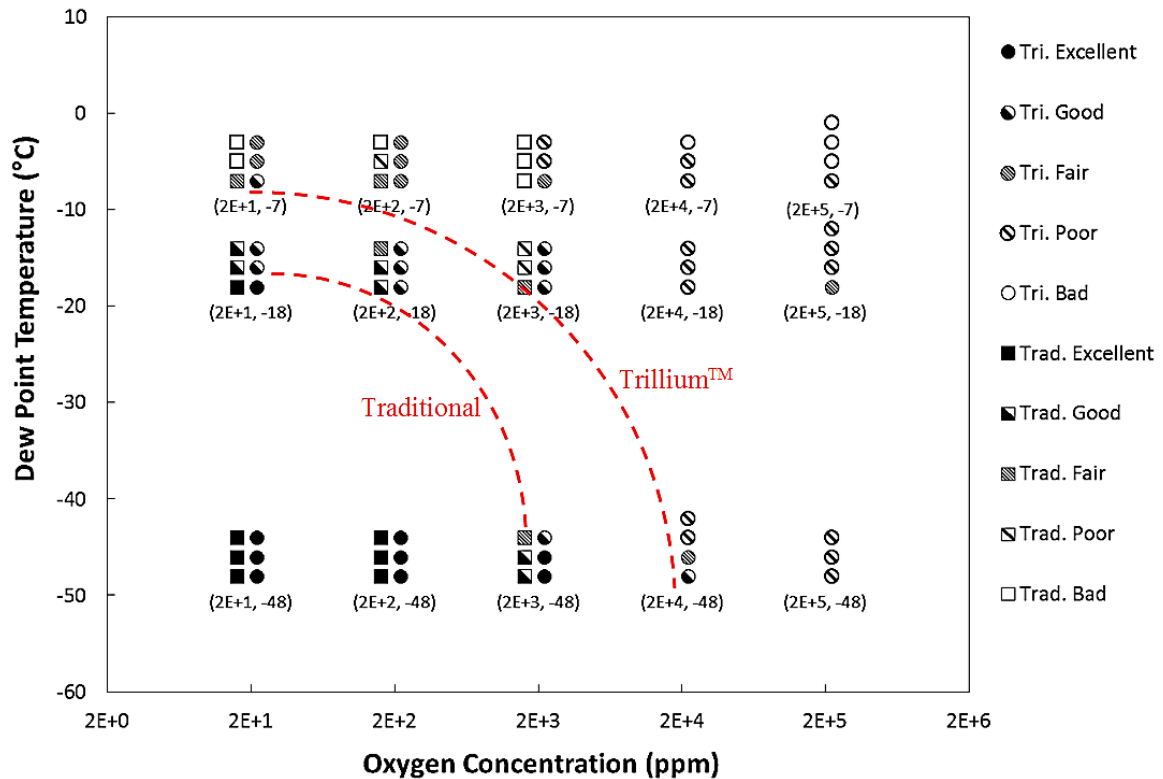


Figure 4-29 Background Atmosphere Condition vs. Brazeability

CHAPTER 5: Conclusion and Future Work

5.1 Conclusion

The impact of the background atmosphere on aluminum brazing has been studied using the hotstage microscopy and the CAB transparent furnace. Both Trillium™ material and the traditional material were tested in parallel. Based on the experimental results, the following conclusions can be formulated:

- Typical outcome of deteriorated joint formation due to adverse background atmosphere are: smaller joint size, non-uniform joint formation, in-completed joining area, or no joint formation.
- The adverse background atmosphere deteriorates the joint formation for both materials, by either increasing the oxygen level, humidity level, or both. At extreme atmosphere conditions, poor or none brazed joint exists.
- Hotstage tests:
 - At high levels of oxygen concentration conditions the filler metal melts with no spreading because the flow was hampered. No joint will form.
 - The traditional clad loaded by $\sim 10 \text{ g/m}^2$ flux does not work under 2000 ppm oxygen level. The acceptable oxygen level registered for the traditional clad was 500 ppm, whereas Trillium™ clad works up to 2000 ppm oxygen level.
- Furnace tests:
 - Low oxygen and humidity levels are considered as a protective brazing atmosphere where a high quality joint fillet forms. However, if the atmosphere condition consists of high oxygen and humidity levels, the situation is quite unfavorable for joint formation, therefore poor or none joint exists.
 - Transitional behavior of deteriorating joint formation has been observed when atmosphere conditions shift due to gradual increases of the oxygen or humidity levels. Worse joints occur when multiple adverse conditions exist at the same time.

- Trillium™ brazing sheet (self-fluxing) is more resilient than the traditional brazing sheet (surface-fluxing) under adverse background atmosphere. Favorable atmosphere conditions (good joint formation) for both materials are shown in Table 5-1.

Table 5-1 Limits for Favorable Combined Background Atmosphere Conditions

Material	Condition	T _{dp} (°C)	O ₂ (ppm)
Trillium™	1	-7	20
	2	-18	2000
	3	-48	20000
Traditional	1	-18	20
	2	-18	200
	3	-48	2000

5.2 Future Work

- Complement experimental data points for the traditional brazing sheet on the adverse atmosphere map (Figure 4-29).
- Characterize aluminum oxidation layer and its effects on brazeability.
- Compare results from vacuum processes and CAB processes.
- Reactive wetting kinetics under various atmospheric conditions.
- Silicon diffusion of brazed samples under different background atmosphere.
- Impacts on joint formation, residue formation, or core dissolution, by the effects of peak temperature, dwell time, and heating speed.
- Uncovering the mechanism of imbedded flux action vs. traditional fluxing.

APPENDICES

Appendix A

Table A-1 Specification of Gas Sources

Desired O ₂ Level	Certified O ₂ Level	Balance
20 ppm [*]	< 2 ppm	N ₂
200 ppm [†]	200 ppm ± 2%	N ₂
500 ppm [‡]	501 ppm ± 2%	N ₂
2000 ppm [§]	2003 ppm	N ₂
20000 ppm ^{**}	20000 ppm	N ₂
200000 ppm ^{††}	215000 ppm ± 2%	N ₂

* Source: PurityPlus 5.0 in the Catalog for PurityPlus Specialty Gases, Scott-Gross Company.

† Source: Certificate of Analysis from Scott-Gross Company.

‡ Source: Certificate of Analysis from Scott-Gross Company.

§ Source: Certificate of Analysis from Scott-Gross Company.

** Source: Certificate of Analysis from Scott-Gross Company.

†† Source: PurityPlus Extra Dry in the Catalog for PurityPlus Specialty Gases, Scott-Gross Company.

Appendix B

Table B-1 Calibration Data for the Dew Point Monitor System

GE Standard Dew Point		Customer Unit Dew Point		Difference		Specficiation of Unit	
(°F)	(°C)	(°F)	(°C)	(°F)	(°C)	(°F)	(°C)
-55.48	-48.60	-55.68	-48.71	0.2	0.11	± 0.5	± 0.3
-0.63	-18.13	-0.78	-18.21	0.15	0.08	± 0.4	± 0.2
19.24	-7.09	19.1	-7.17	0.14	0.08	± 0.4	± 0.2
32.02	0.01	31.89	-0.06	0.13	0.07	± 0.4	± 0.2
42.00	5.56	41.80	5.44	0.2	0.12	± 0.4	± 0.2

Source: As Received Calibration Data from GE Sensing.

Appendix C

Table C-1 offers a summary of hotstage test results and their corresponding Figures in Chapter 3. Documented in-situ in real time videos of hotstage experiments are available upon request (Please contact the Brazing, Soldering, and Heat Exchangers Research Laboratory in the University of Kentucky).

Table C-1 List of Hotstage Test Results and Corresponding Figures in Chapter 3

#	Material	Chamber Oxygen Concentration (ppm)	Spreading Temperature (°C)	Resolidification Temperature (°C)	Corresponding Figure
1	Trillium™	20	595	582	Figure 3-1 Figure 3-13 Figure 3-15 Figure 3-28
2	Trillium™	200	591	580	Figure 3-2 Figure 3-16 Figure 3-29
3	Trillium™	500	588	579	Figure 3-3 Figure 3-17 Figure 3-30
4	Trillium™	2000	594	586	Figure 3-4 Figure 3-18 Figure 3-31
5	Trillium™ Test I	200000 (air)	None	600	Figure 3-5 Figure 3-19 Figure 3-32
6	Trillium™ Test II	200000 (air)	592	585	Figure 3-6 Figure 3-20 Figure 3-33
7	Traditional	20	591	586	Figure 3-7 Figure 3-14 Figure 3-21 Figure 3-34
8	Traditional	200	592	583	Figure 3-8 Figure 3-22 Figure 3-35
9	Traditional	500	595	594	Figure 3-9 Figure 3-23 Figure 3-36

10	Traditional Test I	2000	None	588	Figure 3-10 Figure 3-24 Figure 3-37
11	Traditional Test II	2000	594	600	Figure 3-11 Figure 3-25 Figure 3-38
12	Traditional	200000 (air)	None	587	Figure 3-12 Figure 3-26 Figure 3-39

Appendix D

Table D-1 Repeatability of Atmospheric Conditions

#	Target T _{dp} (°C)	Measured T _{dp} (°C)	STD of T _{dp} (°C)	Target O ₂ (ppm)	Measured O ₂ (ppm)	STD of O ₂ (ppm)
1	-48	-47.8	0.2	2E+1	1.3E+1	1.6
2	-48	-48.2		2E+1	1.1E+1	
3	-48	-47.9		2E+1	1.5E+1	
4	-48	-47.9	0.1	2E+2	NA	NA
5	-48	-48.0		2E+2	NA	
6	-48	-48.3		2E+2	NA	
7	-48	-47.8	0.0	2E+3	NA	NA
8	-48	-47.9		2E+3	NA	
9	-48	-47.9		2E+3	2.0E+3	
10	-18	-17.9	0.1	2E+1	2.1E+1	4.7
11	-18	-18.1		2E+1	1.1E+1	
12	-18	-18.2		2E+1	1.1E+1	
13	-18	-18.0	0.2	2E+2	2.3E+2	9.4
14	-18	-18.2		2E+2	2.3E+2	
15	-18	-17.8		2E+2	2.1E+2	
16	-18	-18.0	0.1	2E+3	2.0E+3	81.6
17	-18	-18.2		2E+3	1.9E+3	
18	-18	-17.9		2E+3	2.1E+3	
19	-7	-6.8	0.1	2E+1	9.8E+0	7.2
20	-7	-6.7		2E+1	9.8E+0	
21	-7	-6.9		2E+1	2.5E+1	
22	-7	-6.9	0.3	2E+2	2.0E+2	4.7
23	-7	-7.2		2E+2	1.9E+2	
24	-7	-6.5		2E+2	2.0E+2	
25	-7	-7.3	0.3	2E+3	1.8E+3	0.0
26	-7	-6.5		2E+3	1.8E+3	
27	-7	-6.8		2E+3	1.8E+3	
28	-48	-48.1	0.1	2E+1	2.0E+1	3.3
29	-48	-47.8		2E+1	2.0E+1	
30	-48	-48.2		2E+1	1.3E+1	
31	-48	-48.1	0.1	2E+2	2.1E+2	8.2
32	-48	-47.9		2E+2	2.2E+2	
33	-48	-48.1		2E+2	2.3E+2	
34	-48	-48.4	0.2	2E+3	NA	NA
35	-48	-47.8		2E+3	NA	

36	-48	-48.3		2E+3	NA	
37	-18	-17.7	0.0	2E+1	1.9E+1	1.7
38	-18	-17.7		2E+1	2.0E+1	
39	-18	-17.6		2E+1	1.6E+1	
40	-18	-17.6	0.3	2E+2	1.9E+2	4.7
41	-18	-18.2		2E+2	2.0E+2	
42	-18	-17.8		2E+2	2.0E+2	
43	-18	-17.8	0.2	2E+3	1.8E+3	81.6
44	-18	-17.9		2E+3	1.9E+3	
45	-18	-18.3		2E+3	2.0E+3	
46	-7	-6.6	0.1	2E+1	9.3E+0	5.9
47	-7	-6.5		2E+1	1.2E+1	
48	-7	-6.7		2E+1	2.3E+1	
49	-7	-6.8	0.2	2E+2	2.0E+2	4.7
50	-7	-6.5		2E+2	2.0E+2	
51	-7	-6.9		2E+2	2.1E+2	
52	-7	-7.1	0.2	2E+3	1.8E+3	0.0
53	-7	-7.2		2E+3	1.8E+3	
54	-7	-6.8		2E+3	1.8E+3	
55	-48	-47.8	0.0	2E+4	NA	NA
56	-48	-47.8		2E+4	NA	
57	-48	-47.8		2E+4	NA	
58	-48	-47.8		2E+4	NA	
59	-18	-18.4	0.2	2E+4	NA	NA
60	-18	-18.7		2E+4	NA	
61	-18	-18.7		2E+4	NA	
62	-7	-5.8	0.7	2E+4	NA	NA
63	-7	-7.4		2E+4	NA	
64	-7	-5.9		2E+4	NA	
65	-48	-47.8	0.4	2E+5	NA	NA
66	-48	-48.6		2E+5	NA	
67	-48	-48.7		2E+5	NA	
68	-18	-17.8	0.2	2E+5	NA	NA
69	-18	-17.6		2E+5	NA	
70	-18	-17.7		2E+5	NA	
71	-18	-18.2		2E+5	NA	
72	-7	-7.0	0.1	2E+5	NA	NA
73	-7	-7.0		2E+5	NA	
74	-7	-7.2		2E+5	NA	
75	-7	-7.1		2E+5	NA	

REFERENCES

- ALTENPOHL, D. 1965. *Aluminium und aluminiumlegierungen*, Berlin; New York, Springer-Verlag.
- BASKIN, Y. & BEMIS, L. 2003. Effective brazing using safer fluxes. *Welding Design & Fabrication, Including Welding Engineer*, 76, 29-29.
- BRANDON, D. G. & KAPLAN, W. D. 1997. *Joining Processes : An Introduction*, Chichester, New York, United States, Wiley.
- CLAESSON, E., ENGSTROM, H., HOLM, T. & SCHOLIN, K. 1995. Nitrogen flow optimization system for CAB (NOCOLOK) furnaces. *VTMS Conference*. England.
- CONN, P. J. & SCHRAMECK, W. J. 1995. *Flux composition for aluminum brazing*. United States patent application US5450666 A.
- COOKE, W. E. 1976. *Method of brazing aluminum*. United States patent application US3971501 A.
- COOKE, W. E., WRIGHT, T. E. & HIRSCHFIELD, J. A. 1978. Furnace brazing of aluminum with a non-corrosive flux. *Welding Journal*, 57, 23-28.
- DOCKUS, K. F. 1978. Fluxless Bonding Method for Aluminum Components. *Welding Journal*, 57, 36-42.
- EISENBEIS, C. 2011. Soldering and brazing of aluminium and its alloys. *International Aluminium Journal*, 54-56.
- FIELD, D. J. 1989. Oxidation of Aluminum and Its Alloys. *In: A.K, V. & R.D, D. (eds.) Treatise on Materials Science & Technology*. Elsevier.
- FIELD, D. J. & STEWARD, N. I. Mechanistic aspects of the NOCOLOK flux brazing process. SAE International Congress and Exposition, 1987 Detroit, MI, United States. SAE, 870186.
- GE 2006. General Eastern Dew Point Analyzer Operator's Manual. GE Sensing.
- GROOVER, M. P. 1996. *Fundamentals of modern manufacturing : materials, processes, and systems*, Upper Saddle River, New Jersey, Prentice Hall.
- HAWKSWORTH, D. K., WESTERGARD, R. G. J. & OGILVY, A. J. W. 2012. Trillium technology - aluminium brazing with a composite liner. *7th International Congress of Aluminium Brazing*. Germany.
- HUMPSTON, G. & JACOBSON, D. M. 1993. *Principles of soldering and brazing*, Materials Park, Ohio, ASM International.
- HUNTER, M. S. & FOWLE, P. 1956. Natural and thermally formed oxide films on aluminum. *Journal of the Electrochemical Society*, 103, 482-485.
- JEURGENS, L. P. H., SLOOF, W. G., TICHELAAAR, F. D. & MITTEMEIJER, E. J. 2002. Growth kinetics and mechanisms of aluminum-oxide films formed by thermal oxidation of aluminum. *Journal of Applied Physics*, 92, 1649-1656.
- KAWASE, H., SHINTANI, H. & MIYAMOTO, M. 1986. *Flux for brazing the aluminum parts and preparing method of the same*. United States patent application US4579605 A.
- KAWASE, H., TAKEMOTO, T., ASANO, M., KAWAKATSU, I. & LIU, K. 1989. Study of a method for evaluating the brazeability of aluminum sheet. *Welding Journal, Research Supplement*, 68, 396-s to 403-s.

- KAWASE, H. & YAMAGUCHI, M. 1980. Effect of the oxide film thickness on aluminium vacuum brazeability. *Journal of the Light Metal Welding & Construction*, 18, 149-156.
- KILMER, R. J. & EYE, J. B. 2002. *Method of depositing flux or flux and metal onto a metal brazing substrate*. United States patent application US6344237 B1.
- KOEHLER, S. & REINHARD, G. 2011. Corrosion behaviour of aluminium materials in aqueous cleaning solutions. *International Aluminium Journal*, 50-53.
- KUMAR, G. & PRABHU, K. 2007. Review of non-reactive and reactive wetting of liquids on surfaces. *Advances in Colloid and Interface Science Advances in Colloid and Interface Science*, 133, 61-89.
- LAUZON, D. C., BELT, H. J. & BENTRUP, U. HF generation in NOCOLOK flux brazing furnaces. Therm Alliance International Invitational Brazing Seminar, 1998 Detroit, MI, United States.
- LAUZON, D. C. & SWIDERSKY, H.-W. 2002. Myths about aluminum brazing with non-corrosive fluxes.
- LINKAM 2015. Online source: Linkam THMS 600 Specifications, Linkam Official Website (<http://www.linkam.co.uk/>). Accessed in October 2015.
- LIU, J. NOCOLOK flux and aluminum brazing. SAE International Congress & Exposition, Feb. 26-29 1996 Detroit, MI, United states. SAE Special Publications 960244.
- NARAYANASWAMY, R. 2006. *Influence of flux deposition non-uniformity on molten metal spreading in aluminum joining by brazing*. Thesis, University of Kentucky.
- OGILVY, A. J. W., HAWKSWORTH, D. K. & ABOM, E. 2008. *A brazing piece, a method of making a brazing piece, and a method of brazing and components made from said brazing piece*. WO2008110808 A1.
- OGILVY, A. J. W., HAWKSWORTH, D. K. & ABOM, E. 2010. *A Brazing Piece, a Method of Making a Brazing Piece, and a Method of Brazing and Components Made From Said Brazing Piece*. USA patent application US20100206529 A1.
- OLYMPUS 2015. Online Source: Olympus BX51M Specifications, Olympus Office Website (<http://www.olympus-ims.com/>) Accessed in October 2015.
- ONO, M., HATTORI, M., ITAYA, E. & YANAGAWA, Y. 2000. *Flux for brazing aluminum members*. United States patent application US6010578 A.
- PAN, C. X. & SEKULIC, D. P. 2002. Microstructural characteristics of AA4343/AA3003 Al-alloy sheet brazed joints. *Chinese Journal of Nonferrous Metals*, 12, 481-485.
- SCHWARTZ, M. M. 1987. *Brazing*, Metals Park, Ohio, ASM International.
- SCIENTECH 2015. Online Source: Scientech SA310 Electronic Balance Specifications, Office Scientech Website (<http://scientech-inc.com/>). Accessed in Oct 2015.
- SEKULIC, D. P. 2013. *Advances in Brazing Science, Technology and Applications*, Woodhead Pub Ltd.
- SHAPIRO, A. E. & SEKULIC, D. P. 2008. A New Approach to Quantitative Evaluation of a Design for Braze Structures. *Welding Journal*, 87, 1s-10s.
- STENQVIST, T., SCHOLIN, K. & ENGSTROM, H. British Association for Brazing & Soldering Conference in Joining Technology, October 1994 Solihull.
- SUGIYAMA, Y. 1989. Brazing of aluminum alloys. *Welding International*, 3, 700-710.

- SWIDERSKY, H.-W. Comparison of flux characteristics and flux transfer systems in electrostatic Nocolok flux application for aluminum brazing. Therm Alliance International Invitational Aluminum Brazing Seminar, Oct 1999 Detroit, MI, United States.
- SWIDERSKY, H.-W. 2001. Aluminium brazing with non-corrosive fluxes - state of the art and trends in NOCOLOK flux technology. *DVS-Berichte*, 212, 164-169.
- T'JOEN, C., DE JAEGER, P., HUISSEUNE, H., VAN HERZEELE, S., VORST, N. & DE PAEPE, M. 2010. Thermo-hydraulic study of a single row heat exchanger consisting of metal foam covered round tubes. *International Journal of Heat and Mass Transfer*, 53, 3262-3274.
- TAKEMOTO, T., UJIE, T., CHAKI, H. & MATSUNAWA, A. 1996. Influence of oxygen content on brazeability of a powder aluminum braze filler metal. *Welding Journal*, 75, 372-378.
- TAKIGAWA, J. & OKAMOTO, T. 1993. Materials and process factors in non-corrosive flux brazing for aluminum automobile heat exchangers. *Kobelco Technology Review*, 34-38.
- TELEDYNE 1995. Model 316RA/RB/RAD/RBD trace oxygen analyzer instructional manual. Teledyne Analytical Instruments.
- THOMPSON, W. T. & GOAD, D. G. W. 1976. Some Thermodynamic Properties of K3AlF6-KAlF4 Melts. *Canadian Journal of Chemistry*, 54, 3342-3349.
- VAN EVANS, T., ZALUZEC, M. J., GRAB, G. A., MEHRABAN, H., BURT, R. P., UYEDA, S. Y. & EYE, J. B. 2000. *Method of making a braze sheet*. United States patent application US6120848 A.
- WALLACE, E. R. & DEWING, E. W. 1976. *Joining of metal surfaces*. United States patent application US3951328 A.
- WEFERS, K. & MISRA, C. 1987. Oxides and Hydroxides of Aluminum. *Alcoa Technical Paper*.
- WITTEBROOD, A. J. 2004. *Composite sheet material for brazing*. United States patent application US6753094 B1.
- YU, C.-N., HAWKSWORTH, D. & SEKULIC, D. 2013. Impact of the Background Atmosphere on the Aluminum Brazing Joint Formation. *2013 International Mechanical Engineering Congress & Exposition (ASME-IMECE), November 15 - November 21*. San Diego, California, United States: ASME.
- YU, C. N., HAWKSWORTH, D., LIU, W. & SEKULIC, D. P. 2012. Al brazing under severe alterations of the background atmosphere: A new vs. traditional brazing sheet. *5th International Brazing and Soldering Conference, IBSC 2012, April 22, 2012 - April 25, 2012*. Las Vegas, Nevada, United States: ASM International.
- ZAHR, J., HOFMANN, E., ULLRICH, H. J., FUSSEL, U., TURPE, M. & OSWALD, S. Correlations between the atmosphere conditions on the natural aluminum oxide layer and the brazeability. *5th International Brazing and Soldering Conference, April 22-25 2012a Las Vegas, NV, United states*. ASM International, 275-280.
- ZAHR, J., OSWALD, S., TUERPE, M., ULLRICH, H. J. & FUESSEL, U. 2011. Influence of the natural aluminium oxide layer on brazeability. *International Aluminium Journal*, 57-59.

- ZAHR, J., OSWALD, S., TUERPE, M., ULLRICH, H. J. & FUESSEL, U. 2012b. Characterisation of oxide and hydroxide layers on technical aluminum materials using XPS. *Vacuum*, 86, 1216-1219.
- ZHAO, H., SALAZAR, A. J. & SEKULIC, D. P. 2009. Analysis of Fin-Tube Joints in a Compact Heat Exchanger. *Heat Transfer Engineering*, 30, 931-940.
- ZIMMER, A. T. & BISWAS, P. 2000. Mechanistic Understanding of Aerosol Emissions from a Brazing Operation. *American Industrial Hygiene Association Journal*, 61, 351-361.

VITA

Name

Cheng-Nien Yu (Brian)

Place of Birth

Kaohsiung, Taiwan

Education

- Bachelor of Science in Mechanical Engineering
Yuan Ze University, Taiwan.
- Research Assistant
Brazing, Soldering, and Heat Exchangers Research Laboratory,
Institute for Sustainable Manufacturing, University of Kentucky, USA.
- Teaching Assistant
Elements of Heat Transfer
Department of Mechanical Engineering, University of Kentucky, USA.

Honor

- NSF Graduate Student Award,
ASME-IMECE at San Diego, CA, USA.
- Excellent Work Award, National Student Paper Competition,
Chinese Institute of Engineers, Taiwan.
- Best Paper Award, Student Engineering Paper Competition,
College of Engineering, Yuan Ze University, Taiwan.
- Academic Silver Medal Award,
College of Engineering, Yuan Ze University, Taiwan.
- Champion of the Mechanical Structural Design Competition,
Department of Mechanical Engineering, Yuan Ze University, Taiwan.

Peer-Reviewed Publication

- Doug K. Hawkworth, Dusan P. Sekulic, Cheng-Nien Yu, Hai Fu, Richard G.J. Westergard, “*A mechanistic study of aluminium controlled atmosphere brazing processes.*”, the 12th Vehicle Thermal Management Systems (VTMS) Conference and Exhibition, Nottingham, U.K., May 10-13, 2015.
- Dusan P. Sekulic, Rahul Nehete, Cheng-Nien Yu, Hai Fu, “*An energy sustainability metric*”, *Energy*, v.74, pp.37-44, 2014.

- Cheng-Nien Yu, Doug K. Hawksworth, and Dusan P. Sekulic, “*Impact of the Background Atmosphere on the Aluminum Brazing Joint Formation*”, Proceedings of the ASME 2013 International Mechanical Engineering Congress & Exposition, November 15-21 2013 San Diego, CA, USA. [Paper#IMECE2013-64776]
- Rahul Nehete, Cheng-Nien Yu, and Dusan P. Sekulic, “*Limits of Energy Resources Use in Traditional Technological Processes – A General Approach and a Metal Bonding Case Study*”, Proceedings of the International Symposium on Sustainable Systems & Technologies, May 15-17 2013 Cincinnati, OH, USA.
- Rahul Nehete, Cheng-Nien Yu, Hai Fu, and Dusan P. Sekulic, “*Energy Resource Use: Sustainability Metric of a Manufacturing Process*”, International Conference on Efficiency, Cost, Optimization, Simulation and Environmental Impact of Energy System, July 16-19 2013 Guilin, China. [Session: Energy and manufacturing: new routes to sustainability, Paper PO12]
- Cheng-Nien Yu, Doug K. Hawksworth, Wen Liu, and Dusan P. Sekulic, 2012, “*Al Brazing Under Severe Alternations of the Background Atmosphere: A New vs. Traditional Brazing Sheet*”, International Brazing and Soldering Conference, April 22-25 2012 Las Vegas, NV, USA.
- Hsuan-Han Lin, Cheng-Nien Yu, and Yur-Tsai Lin, 2005, “*Optimization of Heat Sink Module Using Genetic Algorithms*”, Proceedings of the 29th National Conference on Theoretical and Applied Mechanics, pp.A020-1~A020-8.